ASSESSMENT OF GROUND FILTERING ALGORITHMS OF POINT CLOUDS IN COMPLEX ARTIFICIAL TERRAINS

Czech University of Life Sciences Prague

Faculty of Environmental Sciences

DISSERTATION THESIS

PETR KLÁPŠTĚ

Czech University of Life Sciences Prague

Faculty of Environmental Sciences

Assessment of Ground Filtering Algorithms of Point Clouds in Complex Artificial Terrains

Petr Klápště

This dissertation thesis is submitted for the degree *Doctor of Philosophy* at the Department of Spatial Sciences.

Prague   June 2021

Assessment of Ground Filtering Algorithms of Point Clouds in Complex Artificial Terrains

Dissertation Thesis

Author:	Petr Klápště
Supervisor:	Assoc. Prof. Vítězslav Moudrý
	Czech University of Life Sciences Prague

Acknowledgements

Abstract

Digital Elevation Models (DEMs) play an important role in a wide range of environmental applications. Nowadays, remote sensing constitutes the most common source of data for the generation of elevation models. One of the techniques widely used in remote sensing, airborne photogrammetry, is a standard method for the acquisition of such data. Especially with the current boom of unmanned aerial vehicles (UAVs), the potential of this method is growing. Still, laser altimetry, commonly referred to as airborne laser scanning (ALS) or light detection and ranging (LiDAR) remains the most popular technique. Both ALS and airborne photogrammetry result in the point clouds that need to be further processed to obtain DEMs. The first step of point cloud processing is called ground filtering – a process separating points that represent bare ground from non-ground points. Ground filtering represents an essential step of point cloud processing. The aim of this thesis is to evaluate the performance of commonly used ground filtering algorithms of point clouds in a complex artificial terrain for the purpose of creating an accurate digital terrain model. Specifically, in this thesis was assessed: 1) the effect of vegetation and terrain characteristics on the performance of individual algorithms in a complex non-natural terrain overgrown with forest, steppe, and grass vegetation; 2) sensitivity of parameters and differences in performance between algorithms applied to both types of point clouds (i.e., derived from both ALS and UAV photogrammetry); and 3) we evaluated whether DEMs accuracy can be improved by acquisition of images under leaf-off conditions and, hence, potentially used in combination with leaf-on conditions to estimate vegetation cover characteristics. The results of this thesis showed a

great potential of ground filtering of point cloud data. All tested algorithms behaved consistently when filtering LiDAR point clouds, with problems typically more common when filtering low vegetation and/or with increasing slope; however, when filtering photogrammetric point clouds, this was not completely true; hence, caution is needed when choosing algorithms for ground filtering of photogrammetric data. Some algorithms were more susceptible to Type I error while others tended rather to the Type II error; future research should evaluate whether these tendencies are universal and how they relate to the vegetation and terrain character. In addition, the combination of UAV imagery from leaf-off and leaf-on conditions have a potential to replace expensive airborne LiDAR surveys for applications requiring information on vegetation cover or vegetation height.

Abstrakt (Czech)

Digitální výškové modely hrají důležitou roli v široké škále environmentálních aplikací. V dnešní době je dálkový průzkum Země nejběžnějším zdrojem dat pro tvorbu digitálních výškových modelů. Jedna z široce využívaných technik v dálkovém průzkumu Země, letecká fotogrammetrie, je standardní metodou pro získávání těchto dat. Zejména se současným rozmachem bezpilotních leteckých prostředků (UAV) potenciál této metody roste. Nejvíce využívanou technikou však stále zůstává laserová altimetrie, běžně označována jako letecké laserové skenování (LLS) nebo LiDAR. Výsledkem LLS i letecké fotogrammetrie jsou mračna bodů, jež je třeba pro získání digitálních výškových modelů dále zpracovat. Prvním krokem ve zpracovávání bodových mračen je tzv. ground filtering – proces, při kterém se filtrují body reprezentující zemský povrch od bodů, které představují objekty nad ním. Ground filtetring je základním procesem v analyzování bodových mračen. Cílem této práce je vyhodnotit výkonnost běžně používaných filtračních algoritmů bodových mračen v komplexním terénu post-těžebních oblastí za účelem vytvoření přesného digitálního modelu reliéfu (DMR). Konkrétně se tato disertační práce zabývá: 1) hodnocením vlivu vegetačních a terénních charakteristik na výkonnost jednotlivých algoritmů v komplexním nepřírodním terénu porostlém lesní, stepní a travnatou vegetací; 2) citlivostní analýzou parametrů a rozdílností ve výkonnosti algoritmů aplikovaných na oba typy bodových mračen (tj. získaných z LLS i UAV fotogrammetrie); 3) vyhodnocením, zda lze přesnost digitálních výškových modelů zlepšit při pořizování UAV snímků v období bez olistění a tudíž potenciálně využít syntézu s daty z olistěného obdobím k následnému odhadu charakteristik vegetačního krytu. Výsledky této práce ukázaly

velký potenciál ground filtering procesu při zpracování bodových mračen. Všechny testované algoritmy se při filtrování bodových mračen získaných z LLS chovaly konzistentně, přičemž docházelo častěji k problémům při filtraci nízké vegetace a/nebo rostoucí sklonitosti terénu, nicméně při filtraci fotogrammetrických mračen bodů tento jev zcela neplatil. Proto je nezbytné postupovat obezřetně při výběru algoritmů pro ground filtering fotogrammetrických dat. Z výsledků dále plyne, že některé algoritmy byly náchylnější k chybě I. druhu, zatímco jiné inklinovaly spíše k chybě II. druhu. Následný výzkum by měl proto zhodnotit, zda jsou tyto tendence univerzální a jakou mají souvislost s charakterem vegetace a terénu. Kombinace snímkování bezpilotními leteckými prostředky v období bez olistění a s olistěním má navíc potenciál nahradit nákladné LLS pro aplikace vyžadující informace o vegetačním krytu nebo výšce vegetace.

Contents

II Research 41

Part I

Introduction and Theory

Chapter 1

Thesis Preface

1.1 Foreword

Digital Elevation Models (DEMs) play an important role in a wide range of environmental applications. Historically, ground surveys and digitizing of existing topographic maps constituted the most common source of data for generation of elevation models. Nowadays, however, their place was taken by remote sensing. One of the popular techniques widely used in remote sensing, photogrammetry, is a standard method that has been used for several decades and keeps improving. Radar is another often used remote sensing technique for DEM acquisition. Last but not least, laser altimetry, commonly referred to as light detection and ranging (LiDAR) or airborne laser scanning (ALS), has become increasingly available since mid-nineties. ALS uses laser to collect height information. Laser is an active sensor capable of penetrating through gaps in vegetation, allowing acquisition of information about the ground even under the vegetation canopy, which used to be extremely difficult with aerial photogrammetry or radar. This, along with the fact that it provides very accurate information about terrain elevation, caused the boom of its popularity.

The use of ALS-derived accurate elevation models in various fields such as landscape modeling, forest inventory, city modeling, visualization applications, flood or drainage modeling, landslides monitoring,

land-use studies, and geological applications (to name but a few) keeps increasing. ALS is undoubtedly an excellent method for any applications requiring accurate models of areas from tens up to tens of thousands of square kilometers. However, relatively high acquisition costs of ALS have nourished the interest to find alternative techniques for obtaining surface elevation and, therefore, left the door open for photogrammetry. Current advances in computer processing and algorithm development powered the progress in photogrammetric techniques facilitating faster data processing and higher accuracy of elevation models than twenty years ago.

Both ALS and airborne photogrammetry produce point clouds that need to be further processed. The first step of point cloud processing is called ground filtering – a process separating points that represent bare ground from non-ground points representing objects above it, such as trees. Dozens of algorithms automatically distinguishing the bare earth in point clouds have been developed, generally referred to as filtering algorithms. However, despite the large efforts invested into the development of filtering algorithms, accurate filtering remains a challenge, particularly in landscapes with dense vegetation and rugged terrain. In this thesis, I assess the performance of several filtering algorithms in complex terrain and provide guidelines for their use.

1.2   Research Motivation

I work as a pilot of unmanned aerial vehicles (UAVs). It is, therefore, not surprising that my PhD research is in a related field, mainly focusing on the use of various point cloud data and their processing to obtain DEMs. At the end of the last century, the availability of DEMs was limited due to their difficult acquisition. However, techniques and technologies are evolving every day and I am personally interested in how to use them and what progress can be made in acquiring information about

the environment and the Earth. Airborne laser scanning may be at present the preferred way of obtaining point clouds; nevertheless, photogrammetry, especially in combination with UAVs, can undoubtedly be considered a modern method of obtaining information about the Earth's surface.

Ground filtering is the most crucial and critical step of point cloud data processing. Indeed, countless algorithms based on different principles were developed for ALS point clouds filtering. I have been always curious to learn how they work and to look for ways to improve their performance. When I saw a point cloud from the UAV aerial photogrammetry for the first time, several questions occurred to me. Firstly, whether ground filtering algorithms designed for point clouds obtained from ALS are able to work with photogrammetry-derived point clouds; secondly, how the filtering will be affected by environmental characteristics such as the vegetation cover or terrain slope that are well known to affect ALS point clouds filtering. Motivated by curiosity and (being a UAV pilot) frequent queries by users on how to generate bare earth models for various applications, I immersed myself in this issue.

1.3 Thesis Structure

The thesis consists of three published studies and is divided into two parts and seven chapters. The **Part I** contains a preface and general introduction into the field of ground filtering algorithms of point clouds. The **Part II** consists of individual published studies:

- **Study I:** Assessment of LiDAR ground filtering algorithms for determining ground surface of non-natural terrain overgrown with forest and steppe vegetation.

- **Study II:** Sensitivity analysis of parameters and contrasting performance of ground filtering algorithms with UAV photogrammetry-based and LiDAR point clouds.

- **Study III:** Comparison of leaf-off and leaf-on combined UAV imagery and airborne LiDAR for assessment of a post-mining site terrain and vegetation structure: Prospects for monitoring hazards and restoration success.

Chapter 2

Objectives of the Thesis

The aim of this thesis is to evaluate the performance of commonly used ground filtering algorithms of point clouds in complex artificial terrains for the purpose of creating an accurate digital terrain model. Specifically, we assessed: **1)** the effect of vegetation and terrain characteristics on the performance of individual algorithms in a complex non-natural terrain overgrown with forest, steppe, and grass vegetation; **2)** sensitivity of parameters and differences in performance between algorithms applied on both types of point clouds (i.e., derived from both ALS and UAV photogrammetry); and **3)** we evaluated whether DEMs accuracy can be improved by the acquisition of images under leaf-off conditions and, hence, potentially used in combination with leaf-on conditions to estimate vegetation cover characteristics.

Chapter 3

Theoretical Background

3.1 Introduction

Many definitions of remote sensing can be found in the literature; in general, it can be defined as a method of obtaining information about objects without physical contact with them (Fischer et al. 1976). A more specific definition is provided in the UN General Assembly Resolutions(UN General Assembly 1986), where remote sensing is described as sensing the Earth's surface from space using the properties of electromagnetic waves emitted, reflected, or refracted by the scanned objects for the purpose of improving the use of terrestrial resources, land use, and environmental protection. The term "remote sensing" describes the complete process from data acquisition, processing to the final visualization and interpretation.

Elevation data are a critical element in any geoscience application, from the fundamentals of landscape mapping to more advanced three-dimensional (3D) environmental modeling. A large amount of digital elevation data exist, from large-scale global datasets to smaller-scale regional datasets. For each application, a decision must be made on the suitability of particular elevation datasets. This depends on many factors, in particular the cost, resolution, and accuracy of the data. The most common representation of the mapped Earth structure for research applications comes in the form of products such as Digital Terrain Models (DTMs) or Digital Surface Models (DSMs).

3.2 Digital Terrain and Surface Models

Digital elevation models are a superset of both digital terrain and surface models, which constitute the most important spatial datasets in many geographical information systems (GIS). If both of them are available, other products, such as normalized digital surface models (nDSM) or canopy height models (CHMs) can be derived. The above-mentioned terms are defined as follows (Figure 3.1).

- A **DSM** is an elevation model that includes the uppermost layer of the Earth's surface including the buildings, vegetation/trees, and ground (where it is empty of both vegetation and other objects).

- A **DTM** is a "bare ground" surface model, which is supposedly free of trees, buildings, or other non-ground objects.

- An **nDSM** is the difference between the DSM and DTM describing all off-terrain objects.

- A **CHM** is an nDSM showing a certain distinguishable strata of the vegetation.

3.3 Point Cloud Data and Processing

Point cloud data constitute an important source for the assessment of the 3D structure of the environment. Point clouds are extensive, disordered sets of points with X, Y, Z coordinates (and, possibly with other properties, such as the color of the point). A point cloud is typically a product of laser scanning or photogrammetry and becomes a commonplace data source for DTMs production. Data is most commonly acquired by aircraft equipped with LiDAR and UAVs equipped with RGB cameras. Raw point cloud data need to be further processed, the most critical part of which is, again, the identification of ground points (i.e., points representing bare ground; Figure 3.2).
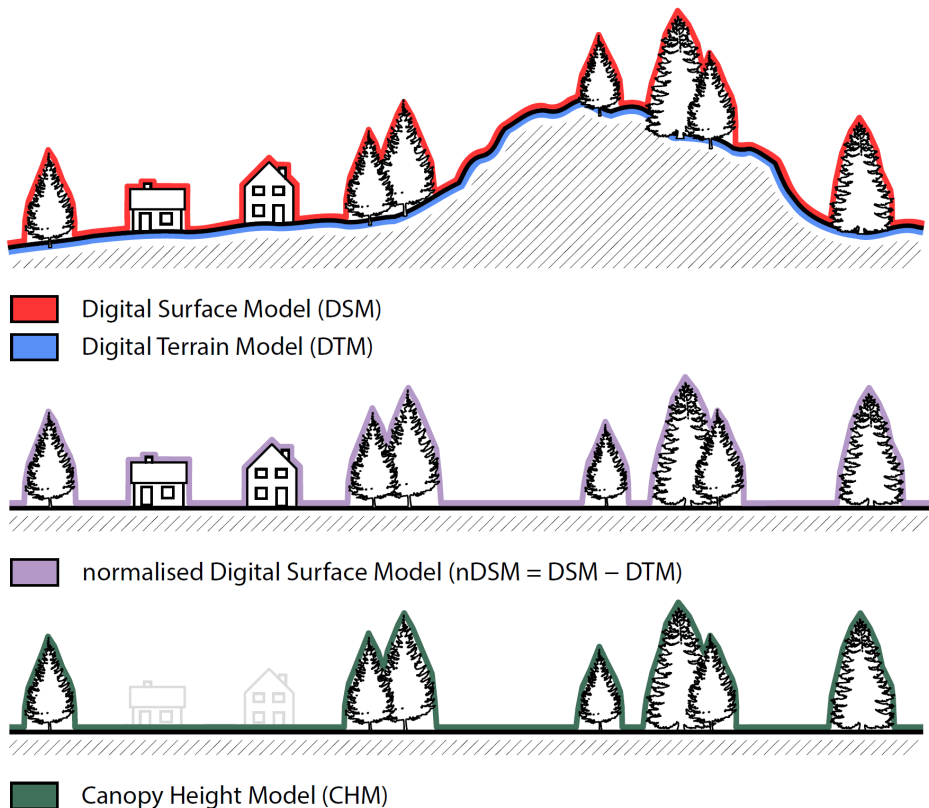
Figure 3.1: A schematic illustration of the most common elevation (DSM, DTM) and height (nDSM, CHM) datasets derived from the LiDAR point clouds.

3.3.1 Aircraft Equipped With LiDAR

The word "laser" is an acronym in itself, standing for Light Amplification by Stimulated Emission of Radiation. A laser is an optical device producing, upon activation by an external energy source, monochromatic radiation – a laser beam. Laser is used for measurement of distances due to its unique characteristics such as the coherence and capability of emitting a huge number of photons in a defined direction in very short pulses of a pre-defined wavelength (Heritage and Large 2009).

A LiDAR system uses laser beams to measure distances between the sensor and a target surface and, in effect, to determine the positions

Classification Value

	1	Unclassified
	2	Ground
	5	High Vegetation
	6	Building
	14	Wire – Conductor
	16	Transmission Tower
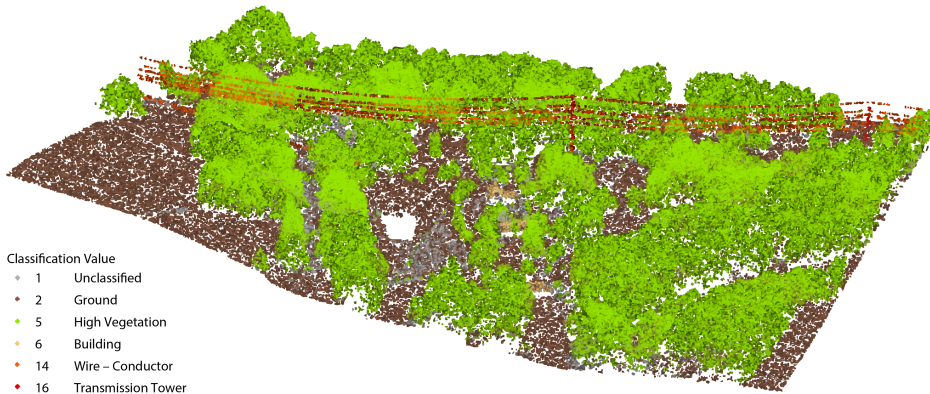
Figure 3.2: An example of a point cloud classified into several different classes.

of objects (Wehr and Lohr 1999). Typically, LiDAR system mounted on the aircraft (airborne LiDAR) is a complex multisensory system consisting most importantly of the control, monitoring and recording units, position and orientation system, and laser scanner (May and Toth 2007). The laser scanner produces a wide swath of pulses and thanks to the known speed of transmission of these pulses, it is possible to calculate the distance of the scanner from the point that caused the reflection of the beam. The distances are computed from the time delay between the laser pulse transmission and detection. The onboard Global Navigation Satellite System (GNSS) components provide the position and orientation of the aircraft movement. Subsequently, all these data are used in post-processing to calculate the coordinates of each point in the point cloud (Vosselman and Mass 2010). In order to calculate the geographical coordinates of the reflected beam, it is necessary to know, in addition to the distance itself, the direction in which the beam was sent from the scanner, the angles of rotation of the scanning device, and the position of that device in the required coordinates. Changing the scanning direction in a plane perpendicular to the direction of flight of the carrier is most commonly provided by a rotating mirror or prism, but other devices - such as optical fibers -

can also be used. The resulting point tracing on the Earth's surface varies, depending on the mechanism used (Slatton et al. 2007). The angles of rotation of the scanning device in three axes are measured by an inertial measurement unit (IMU) and, as mentioned above, the position of the whole system is obtained by the device receiving the GNSS signal (Wehr and Lohr 1999). A typical LiDAR scanning output is represented by an irregular distribution of the returns (e.g., echoes, points) in the three-dimensional space, commonly referred to as a point cloud. Point clouds contain reflections from various features such as ground, vegetation, and buildings (see Figure 3.3).
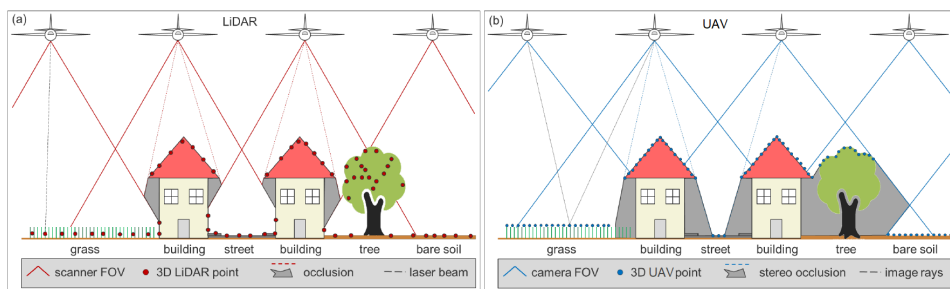
Figure 3.3: A schematic drawing of data acquisition based on the aircraft equipped with LiDAR (a) and UAV equipped with RGB camera (b). Grey areas indicate occlusion, i.e., areas where the respective technique cannot provide reliable data (Mandlburger et al. 2017).

3.3.2 Unmanned Aerial Vehicle Equipped With RGB Camera

UAV is generally defined as an aircraft without an onboard crew that can be operated remotely or fly alone using pre-programmed flight plans or more complex dynamic autonomous systems. The Civil Aviation Authority (CAA) defines it as "aircraft intended to operate without a pilot" (CAA 2017).

The current greater availability of UAVs has led to their use in a wide range of disciplines. The main advantage of UAVs, compared

to traditional airborne methods, is the relatively affordable price, the ability to obtain spatial data of detailed scales, and, most importantly, the fact that anyone can fly them (following certain rules). They are usually used in combination with digital cameras and acquired images are processed using a combination of Structure from Motion (SfM) and Multi-View Stereo (MVS) approaches (Westoby et al. 2012, Javernick et al. 2014), which facilitates the extraction of 3D point clouds similar to those produced by laser scanning (Nex and Remondino 2014). UAVs introduced new possibilities for photogrammetric projects thanks to their flexibility of flight planning, onboard GNSS navigation devices, and inertial data synchronization with photo shooting. Various UAV platforms can be used for data acquisition, such as kites, balloons, airships, helicopters, multi-rotor systems, fixed-wing aircraft, and other devices. Individual unmanned aerial vehicles differ in their capabilities and their performance often depends on the quality of used components and payload (Ritter 2014). In recent years, however, fixed-wing aircraft is clearly the most widely used type. Fixed-wing aircraft are an excellent tool with a relatively long flight time, enabling the acquisition of high-quality photogrammetric data for a larger area (tens of hectares or even more) during a single flight mission. Easy handling with a pre-programmed flight path, stability, wind resistance, etc., count among its principal advantages. The eBee fixed-wing by the Swiss company SenseFly is a typical present-day representative of this technology. It is able to map up to 12 km^2 per one flight while acquiring data with the highest possible resolution (Ground sample distance, GSD) of approx. 1.5 cm. The pixel size of GSD and the resulting size of the scanned area are determined by the selected flight level (altitude above ground) and camera chip size (Mesas-Carrascosa et al. 2016).

3.4 Structure from Motion

The Structure from Motion (SfM) method is widely used in photogrammetric data processing and for efficient management of imagery captured by sensors onboard the UAVs (Figure 3.4). It is, for example, used by commercial software such as Pix4Dmapper (Pix4D S.A., Switzerland) and Agisoft Metashape (Agisoft LLC, Russia), with the latter being, due to its simplicity, the most widely used SfM software (Smith et al. 2016). Besides, it is implemented in several free open source software solutions such as VisualSFM (Wu 2011) or MicMac (Rupnik et al. 2017).
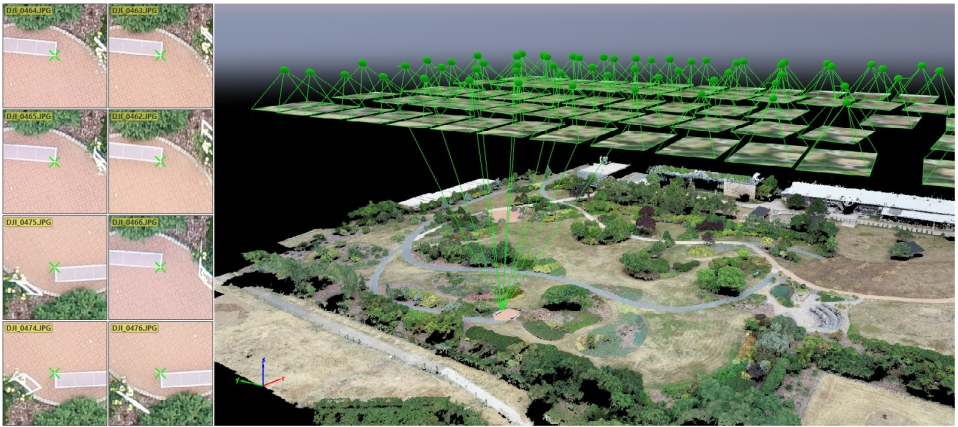
Figure 3.4: Point cloud data processing in Pix4Dmapper software.

It is based on the principle of the photogrammetric intersection. The object is photographed from multiple positions and angles so that the characteristics of the object are captured in several images simultaneously (Figure 3.5). The software mainly uses the SIFT algorithm (Scale Invariant Feature Transform) to find significant points (so-called Features) based on the determination of local extremes in the image (Lowe 2004). From these points, located in several images, the algorithm automatically calculates the parameters and relative positions of the camera, i.e., parameters of the internal orientation. In the next step, the Bundle Adjustment method is used to balance all parameters,

i.e., coordinates of points, position, and rotation of cameras, so-called parameters of the external orientation. Thanks to the obtained geometric relationships between images, it is then possible to estimate the structure of the surfaces present in the images, and thus to create a 3D representation of identical points with coordinates in the relative coordinate system, which are referred to as sparse point clouds (Snavely et al. 2008, Smith et al. 2016).
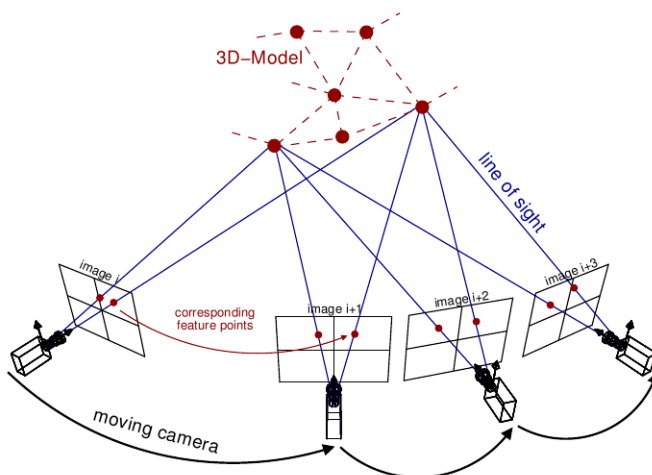
Figure 3.5: Structure from Motion (SfM) photogrammetric principle (Sweeney 2016).

The parameters of internal orientation are directly related to the captured image; they define the geometry of the bundle inside the camera or the position of the projection center in the image coordinate system. These parameters are the key to image alignment and are usually given in the form of three parameters, namely the camera constant (focal length), the position of the main point, and the radial (and tangential) distortion parameters (Bao and Savarese 2011). All images entering SfM processing must have identical internal orientation parameters. This basically means that the focal length must not be changed, the camera must have the motion blur reduction systems turned off (either by moving the chip or by moving the lens internals). Ideally, neither the focusing distance nor the aperture value should change,

either; in addition, the images must not be subsequently cropped or geometrically adjusted (e.g., sharpened). In the case of metric cameras, these internal parameters are known in advance and enter the image alignment process. In the case of conventional UAV cameras, these parameters are usually estimated during alignment. The parameters of UAV cameras can be determined by calibration in special software (Civera et al. 2009, Toldo et al. 2015). Most SfM software solutions support entering parameters determined in this way. It is also recommended to keep identical lighting conditions on all images that enter the alignment. Optimally, the photos should be taken in diffused lighting, i.e., under continuous cloud cover to ensure equal lighting conditions for the entire recorded area. When obtaining images in direct sunlight, the entire campaign should be managed to avoid shifts in the lighting angle, and no part of the captured area should be temporarily obscured (e.g., by trees or clouds) (Tonkin and Midgley 2016). The best option is to use a lens with a fixed focal length which, in addition, usually also provides better image quality than a zoom lens. The type of camera does not determine the accuracy of the result as long as it is able to provide sufficient resolution (e.g., exceeding 10 Mpx). More modern cameras and cameras with larger chips have the advantage of lower noise at higher ISO values and are therefore usable even in poor lighting conditions. Ideally, calibration of the scanning assembly providing basic information about the achievable accuracy of the photogrammetric output should be performed before the acquisition itself.

The parameters of external orientation are related to the platform that captures the images, i.e., carries a sensor. The position of the bundle is usually expressed by six parameters – three coordinates of the center of the optical system x, y, z, and the orientation of the sensor in three rotations ω, φ, κ (see Figure 3.6). External orientation elements may be unknown before image alignment but often enter the alignment process as parameters acquired automatically by GNSS and IMU units onboard the UAV.
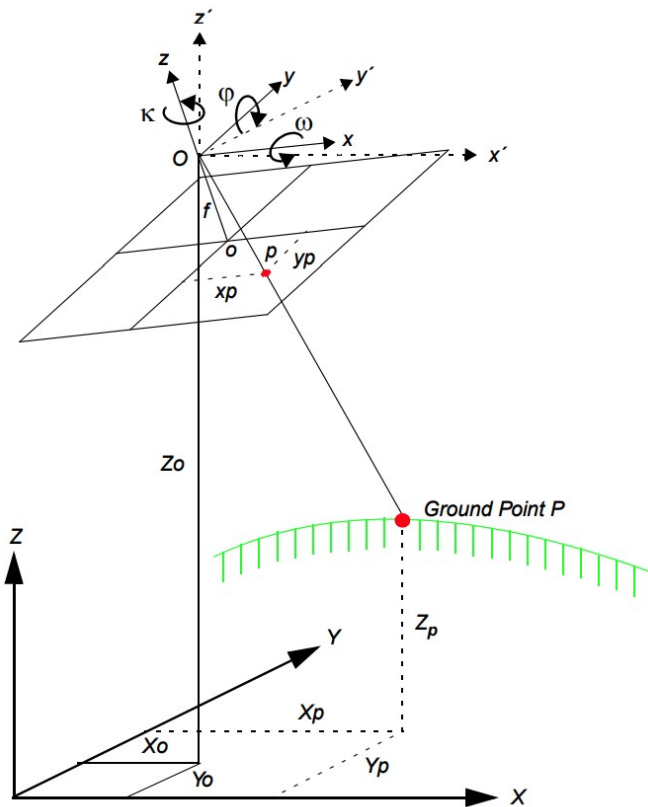
Figure 3.6: Elements of the external orientation (Leica Geosystems 2003).

3.5   Multi-View Stereo

Multi-View Stereo (MVS) technique is used for sparse point cloud densification. Unlike other stereo approaches, MVS has been designed to handle a very large number of images and images taken from different angles. However, this requires an ability to scale the input data (i.e., the ability to switch between image scales). The aim of MVS is to reconstruct a complete scene of the object of interest using input images of a known position. In contrast to SfM, the formation of a point cloud using MVS presupposes the already known internal and external orientation of the input images. MVS generally works poorly for Lambert surfaces, i.e., those with perfect light scattering without

specular reflection. In such a case, it is difficult for MVS to reconstruct the scene (typically interiors, reflective materials, homogeneous patterns). The geometry of the scene can be reconstructed, for example, using depth maps, sparse point clouds, or triangular meshes.

The whole MVS process usually consists of several sub-algorithms, and the principle is always similar. The surface of the object is reconstructed through expansion from a sparse point cloud, where new points are iteratively added to those already existing, and this process is repeated until complete coverage of the captured scene is achieved (Fuhrmann et al. 2014). The resulting surfaces are then subjected to filtering, which removes incorrectly placed points and increases the continuity of the resulting surface (Yang et al. 2013). The algorithms proposed by Furukawa and Ponce (2010) known as CMVS-PMVS are typical examples of this step. Clustering Views for Multi-View Stereo (CMVS) builds upon the output from SfM and mediates the selection of images with similar scenes, creating a multi-stereo projection into clusters. This step is mainly used to reduce computing capacity requirements. Subsequently, Patch-based Multi-View Stereo (PMVS) generates additional points, adding them into the point cloud. The advantage of that algorithm is that it reconstructs only rigid objects; it filters out obscure, e.g., moving, objects. Filtering non-rigid objects out is usually referred to as ghost-filtering.

3.6 Filtering Methods

As already mentioned, the filtering algorithms separate points that represent bare ground from non-ground points representing above-ground objects, such as trees and buildings. The accurate classification provides the basis for the generation of high-quality DTMs. There are dozens of different types of filters; however, the main ones can be classified into the slope-based, morphology-based, and interpolation-

based categories. Each category uses different assumptions of filtering, resulting in the strengths and weaknesses of each category (Favorskaya and Jain 2017).

3.6.1 Slope-Based Filtering Methods

In the slope-based approaches, the slope value for each point is computed using its adjacent points. Points with high slope value are potentially non-ground. Hence, considering the slope value in a constant distance can be a suitable criterion for detecting the non-ground points (Vosselman 2000). However, specifying the slope threshold in these approaches is a challenging issue because the use of a single constant threshold is not appropriate in complex regions (Meng et al. 2010). In other words, the threshold should be slope-adaptive and should be set individually, taking the slope range of the area into account (Susaki 2012). As the height differences even between neighboring ground points can sometimes be similar to those of non-ground points, employing only the slope parameter in the steep and complex terrain with dense coverage is not enough and does not lead to acceptable results (Sithole and Vosselman 2004).

3.6.2 Morphology-Based Filtering Methods

The morphology-based approaches assume that the ground points are associated with the relatively lower points of the point cloud, while the non-ground objects are described by points that are relatively higher. Mathematical morphology is a technique for geometrical structure processing based on the set theory. It is widely used to process digital images but can be also utilized in graphs, surface meshes, and many other spatial structures. Morphology-based filters transform the point cloud data into digital images before performing actual filtering (Zhang et al. 2003). The main idea of this approach is based on the approxi-

mation of a terrain surface using the opening and closing operations built on the dilation and erosion operators (Mongus et al. 2014, Hui et al. 2016).

3.6.3 Interpolation-Based Filtering Methods

The interpolation-based approaches are based on iterative algorithms which work by fitting a surface on the data and iteratively filtering points based on their residuals from the fitted surface. In the first iteration, an averaging surface is fit onto the data and the residuals of the data points relative to the surface are computed. Ground points are more likely to have negative residuals, so they are given more weight in subsequent iterations. The procedure of generating the surface, computing the residuals, weighing the points, and updating the surface is repeated until the surface does not change and remains stable (Kraus and Pfeifer 1998). For example, this approach is used in the algorithm developed by Axelsson (2000) who used a Triangulated Irregular Network (TIN) to generate a surface with the lowest points and, subsequently, gradually increased the number of terrain points based on their angles and distances to the generated surface. In each iteration, the points that met the specified criteria are added to the ground points.

Part II

Research

Chapter 4

Assessment of LiDAR Ground Filtering Algorithms for Determining Ground Surface of Non-Natural Terrain Overgrown With Forest and Steppe Vegetation

Vítězslav Moudrý, **Petr Klápště**, Michal Fogl, Kateřina Gdulová, Vojtěch Barták, Rudolf Urban

Author's contribution: 40%

Abstract

Ground filtering is an inevitable step of processing the Light detection and ranging-acquired point clouds. Our objective was to evaluate the performance of six filtering algorithms. The point clouds filtering and vertical accuracy were evaluated qualitatively, quantitatively and by comparison with a GNSS survey. All tested algorithms achieved good results but their performance was affected by the terrain slope and vegetation cover. Algorithms performed better in forests than in steppes with a high density of low vegetation. The performance of all algorithms decreased with slopes over 15°. Our results show that some algorithms tended to cause Type I error while others tended more to the Type II error. Furthermore, for some algorithms this tendency depended on the vegetation and terrain character. The Progressive Triangulated Irregular Network algorithm provided overall well-balanced results in all environments. We propose that software developers should provide users with recommendations of optimal parameters for individual environments.

4.1 Introduction

Creating an accurate representation of the Earth surface has been a fundamental goal of researchers in many environmental disciplines (Moore et al. 1991). The most widely used representations of the Earth's surface are the Digital Surface Models (DSMs) and Digital Terrain Models (DTMs). DSMs represent the Earth surface including vegetation, buildings and other natural or man-made objects and can be used, for example, for viewshed analyses (Klouček et al. 2015, Lagner et al. 2018), solar potential estimates (Fogl and Moudrý 2016, Moudrý et al. 2019a), or improvement of vegetation classification (Komárek et al. 2018, Prošek and Šímová 2019). In contrast, DTMs provide a bare earth representation of terrain topography and are frequently used for hydrological modelling (Sangireddy et al. 2016), species distribution modelling (Bazzichetto et al. 2018, Moudrý et al. 2018, 2019c), digital soil mapping (Penížek et al. 2016, Baltensweiler et al. 2017), or yield prediction (Kumhálová and Moudrý 2014).

The ways of acquisition of accurate information on the 3D structure of the environment have greatly expanded over the past two decades. In particular, laser altimetry, commonly referred to as light detection and ranging (LiDAR) or airborne laser scanning (ALS) has revolutionized the quality of 3D representation of the environment and has become the primary method for acquisition of accurate terrain information (Wehr and Lohr 1999). LiDAR pulses can penetrate through gaps in vegetation canopies and register multiple returns representing both above ground objects and terrain. The point clouds generated in this way hence contain reflections from various features (e.g., ground, vegetation, buildings). The acquisition costs of LiDAR data per unit area have decreased considerably over the last decades and the use of LiDAR is therefore on the rise, especially for large scale projects (Johansen et al. 2010). Furthermore, ALS data are increasingly available and provided free of charge through government agencies in many

countries (e.g., Denmark, Poland, Estonia, Finland, Slovenia), which in turn leads to a greater use of the data in many disciplines such as forestry (Chen et al. 2017a), hydrology (Yang et al. 2014), geomorphology (Chalupa et al. 2018), and ecology (Bakx et al. 2019).

Regardless of the application and a final product needed, an inevitable and the most critical step of the point cloud processing is ground filtering (i.e., the process when points that represent bare ground are separated from non-ground points representing objects above the bare ground such as trees). The correct filtering (sometimes referred to as classification) of ground points is essential to the subsequent creation of DSMs, DTMs or other derived products (Jakubowski et al. 2013, Guo et al. 2017, Indirabai et al. 2019, Szostak et al. 2019).

The point cloud filtering, besides being a crucial component of any LiDAR dedicated software, is also available in some more complex geographic information systems (GIS) software solutions such as ArcGIS (Esri, CA, USA). An overwhelming number of choices of algorithms and their implementations in various software solutions can easily leave an inexperienced practitioner daunted. On the other hand, most software products implement only a single algorithm, which can lead users to select a solution that is readily available but sub-optimal for a particular environment. Furthermore, some algorithms require cautious tuning of parameters, giving the users an option to influence the results while on the other hand posing higher demands on their experience. In contrast, other algorithms try to be as simple as possible and require minimal number of input parameters or allow only a few predefined options (Wan et al. 2018, Cai et al. 2019).

4.1.1 Related Works

Algorithms for ground filtering of ALS data are usually designed with some specific environment in mind (e.g., forests, steppes, or urban areas) and their efficiency varies across environments as each environment

poses specific challenges (Shan and Aparajithan 2005, Meng et al. 2009, Tinkham et al. 2011, Susaki 2012, Maguya et al. 2014, Rashidi and Rastiveis 2017). For example, a dense forest canopy tends to block LiDAR pulses and therefore to introduce gaps in the data. On the other hand, low vegetation can confound ground filtering algorithms and be misclassified as a ground surface. In addition, ground filtering tends to be challenging in regions with a complex topography (Sithole and Vosselman 2004, Leitold et al. 2015). The first comparison of ground filtering algorithms was performed by Sithole and Vosselman (2004). More recently, Meng et al. (2010) reviewed critical issues of ground filtering algorithms and criteria for their selection. With the increasing availability of ALS data and consequent implementations of ground filtering algorithms in various software solutions, the attention focused on the performance of individual algorithms has increased (see Table 7.1 in Chapter 7 for overview of existing comparative studies; Gonçalves and Pereira 2010, Tinkham et al. 2011, Julge et al. 2014, Korzeniowska et al. 2014, Montealegre et al. 2015, Polat and Uysal 2015, Silva et al. 2018).

Existing comparative studies used collections of different algorithms (Sithole and Vosselman 2004) or focused on the implementation of multiple algorithms into an open source software (Montealegre et al. 2015). Several authors evaluated algorithms implemented to commercial software (Korzeniowska et al. 2014). For such evaluations, some studies used datasets prepared solely for such purposes by the International Society for Photogrammetry and Remote Sensing (ISPRS) (Sithole and Vosselman 2004, Meng et al. 2009, Pingel et al. 2013, Zhang et al. 2016), others used their own datasets (Korzeniowska et al. 2014, Montealegre et al. 2015, Stereńczak et al. 2016). The ISPRS data consist of several LiDAR datasets with varying degree of vegetation, terrain character and density and the nature of man-made structures (e.g., buildings, bridges). The undisputed advantage of the use of the same input data in all experiments and a consequent creation of a

large database of results lies in a better comparability of results among individual studies. This is particularly beneficial when a new algorithm is developed and an assessment of its performance, together with its comparison with existing algorithms, is needed (Pingel et al. 2013). On the other hand, many studies tested existing algorithms with their own data, particularly due to the fact that landscapes are often very specific in their terrain, presence of man-made objects and vegetation character and such individual approach is therefore necessary (Stereńczak et al. 2016). Such studies can be motivated by the need of accurate DTMs for specific purposes (e.g., application in forestry; Montealegre et al. 2015) and expand our understanding of behaviour of filtering algorithms in different environments. Similarly, our study was motivated by a project that required accurate terrain models for analysis of post-mining sites, the character of which is very specific with respect to both terrain and vegetation (Moudrý et al. 2019b,d).

4.1.2 Study goals

With the ongoing development of new algorithms (Pingel et al. 2013, Zhang et al. 2016, Tan et al. 2018) evaluation of their performance in a variety of terrains and vegetation conditions is needed. The presented study evaluated the performance of six ground filtering algorithms contained in five frequently used software solutions. In particular, we: (1) evaluated the filtering error; (2) assessed the accuracy of generated DTMs using field measurements as reference data; and (3) assessed the effect of vegetation and terrain characteristics on the performance of individual algorithms in a complex non-natural terrain (i.e., a spoil heap) overgrown with forest, steppe and grass vegetation.

4.2 Material and Methods

4.2.1 Study Area

The study area is located at Hornojiřetínská spoil heap (north-west Bohemia, Czech Republic, 50°34'N, 13°34'E) covering an area of approximately 450 ha. The spoil heap served as a deposit of the overburden from brown coal mining. It has never been technically reclaimed and the terrain morphology thus remained rugged, with areas of steep slopes
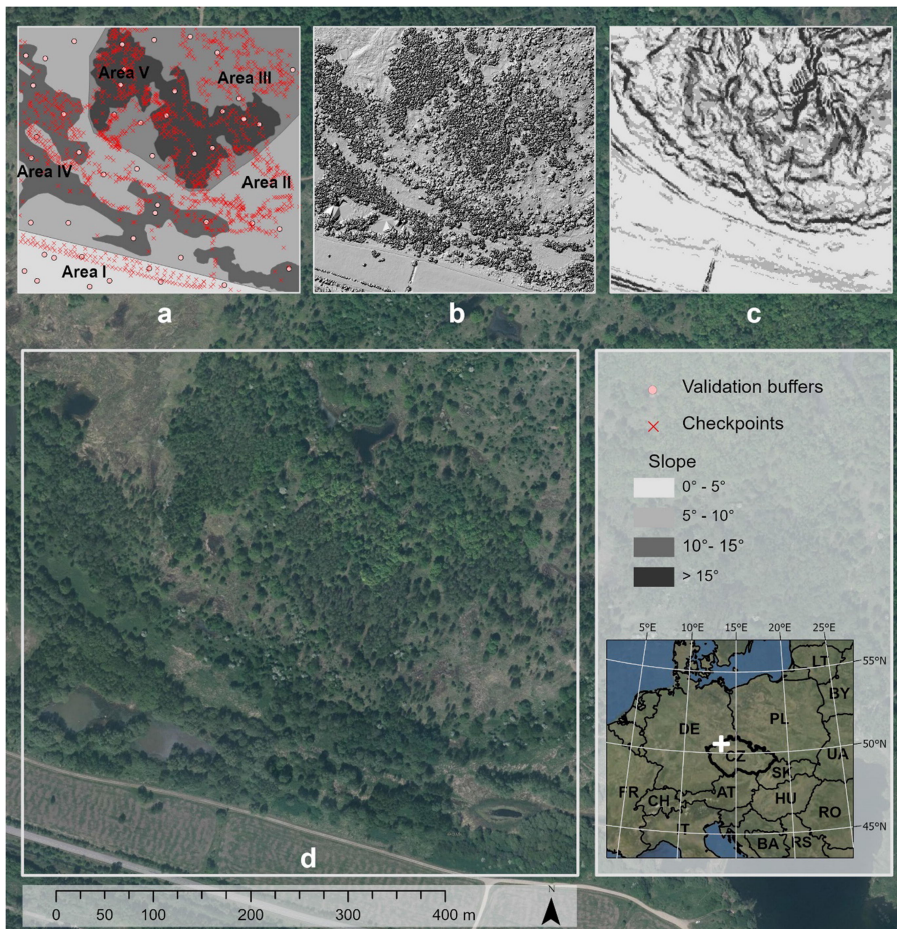
Figure 4.1: Details of the study area. Five areas with different character of vegetation and terrain including the location of validation buffers and checkpoints (a); Hillshaded model (b); Slope (c); Ortophoto (d).

resulting from heaping and with developing successional heterogeneous vegetation (Vymazal and Sklenicka 2012, Frouz et al. 2018). To be able to cover the entire study area with reference GNSS measurements (see below), we limited the study area to a fraction of the spoil heap – 30 ha representative of different conditions on the spoil heap (Figure 4.1). In general, the terrain in the study area changes especially in the south-north direction, from a flat area outside of the spoil heap to slopes and the rugged terrain of the actual spoil heap (Figure 4.1). The vegetation includes grass, aquatic vegetation, steppes and forests. Five areas with different vegetation and terrain character were manually vectorised over an orthophoto, combining the orthophoto with our knowledge of the area (Figure 4.1, Table 4.1). Area I is outside the actual spoil heap and is dominated by low grass with only a few scattered trees. The terrain is flat with ditches alongside the gravel roads. Areas II and III are dominated by low vegetation, especially bush grass *Calamagrostis epigejos* and tall oat grass *Arrhenatherum elatius*, with dense shrubs and scattered trees such as elder *Sambucus*, rosehip *Rosa*, common snowberry *Symphoricarpos albus*, birch *Betula*, or hawthorn *Crataegus*. Area II also includes several terrain depressions overgrown with common reed *Phragmites australis* and common cattail *Typha latifolia*. Area IV is a forest dominated by willow (*Salix spp.*) and alder (*Alnus spp.*) while Area V is a forest dominated by birch *Betula pendula*. All Areas (except Area I) have undulated terrain with steep slopes, small depressions and ridges (Figure 4.1, Table 4.1).

4.2.2 LiDAR and Reference Data Acquisition

4.2.2.1 ALS Data Acquisition

A Riegl full-waveform laser scanner (LMS-Q780) was used for ALS data acquisition over the study area. The data were acquired by the Flying Laboratory of Imaging Spectroscopy (FLIS) in May 2017. The

aircraft flight altitude was 1030 m above the ground level with a ground speed of 110 knots. The scanner is based on a rotating mirror and scans in parallel lines with a field of view of 60°, the wavelength is 1064 nm. The point density of the resulting point cloud was 8 points per square meter. ALS data were processed using a proprietary software of the CAS Global Change Research Institute (CzechGlobe), referenced to the European Terrestrial Reference System, Universal Transverse Mercator projection (ETRS UTM33N), and provided with elevations as ellipsoidal heights.

Table 4.1: General characteristics of the study area.

	Area [ha]	Num. of checkpoints	Slope [°] Mean ± S.D.	Height [m] Mean ± S.D.	Maximum height [m]
Area I *grass*	3.3	107	2.6 ± 3.6	5.9 ± 3.0	18.1
Area II *shrub*	10.9	437	4.8 ± 4.1	6.9 ± 4.0	24.2
Area III *shrub*	6.5	395	8.9 ± 5.4	5.8 ± 3.2	19.4
Area IV *forest*	5.2	170	5.7 ± 4.8	10.3 ± 4.3	23.8
Area V *forest*	5.0	330	9.6 ± 4.6	9.8 ± 3.6	21.5
	Canopy cover [%]	Dens. of ground & low veg. [%] (< 0.3 m)	Density of shrubs [%] (0.3–3 m)	Density of low trees [%] (3–15 m)	Density of high trees [%] (> 15 m)
Area I *grass*	5.8	92.3	2.7	4.8	0.1
Area II *shrub*	22.8	72.7	8.3	18.0	0.9
Area III *shrub*	31.6	64.5	11.4	23.9	0.2
Area IV *forest*	70.4	29.1	6.5	54.9	9.5
Area V *forest*	60.2	40.5	3.1	52.8	3.7

Maximum, mean and standard deviations of height are calculated from a pit free Canopy Height Model. Other characteristics are calculated directly from the LiDAR point cloud. Canopy cover is calculated as the number of first returns above breast height (1.37 m) divided by the number of all first returns. Densities of ground, shrubs and trees are derived as numbers of returns in each height interval divided by a total number of returns. Slope is represented by a mean value ± standard deviation.

4.2.2.2 Manual Classification of Point Clouds and Survey of Checkpoints

A perfect assessment of filtering accuracy would require comparison of all individual points. This would be however impractical due to a large number of points recorded; a frequently utilized approach using randomly sampled points was therefore used in our study (Montealegre et al. 2015). To properly assess classification success, reference data are necessary. We randomly generated 50 point locations (10 point locations in each of the Areas I-V); all points within a 5 mdistance (hereafter buffers) from those locations were selected as test points and manually classified as ground and non-ground, which resulted in 14,102 non-ground and 16,683 ground points used for the validation, respectively.

Compared to pre-existing studies, the areas manually classified in our study for assessment of the filtering performance are relatively large (Montealegre et al. 2015); this on the one hand improves the overall validity of the study, it however on the other hand also increases the risk of manual filtering errors that can still be present in our evaluation dataset. Therefore, we also evaluated the vertical accuracy of DTMs using independent data obtained through a RTK GNSS survey. The RTK GNSS survey was conducted during early spring under leaf-off conditions in 2017 and 2018 using Leica GPS1200 system. In total, 1439 checkpoints distributed throughout the study area (Table 4.1,Figure 4.1) were used. All checkpoints were measured in ETRS89 with ellipsoidal heights and projected to UTM33N.

4.2.3 Ground Point Classification Algorithms

In this study, we compared six algorithms implemented in two open source and three commercial software products that have been increasingly used for ground point classification (Table 4.2).

Table 4.2: List of evaluated software solutions, algorithms and parameters fine-tuned in this study.

Software	Algorithm	Author	Number of evaluated settings	Parameters modified in individual algorithms
CloudCompare	CSF	Zhang et al. (2016)	12	
General settings: Steep slope, Relief, Flat; Cloth res.; Slope processing: enabled/disabled				
LAStools	PTIN	Isenburg (2018)	38	
				Step; Spike; Offset
ArcGIS	ARC	Esri Inc., USA	3	
		Predefined options: Aggressive, Standard, Conservative		
PDAL	PMF	Zhang et al. (2003)	30	
		Initial distance; Max distance; Max window size; Slope		
	SMRF	Pingel et al. (2013)	36	
				Scalar; Slope; Threshold; Window
RealWorks	RW	Trimble Inc., USA	1	–

CSF – Cloth Simulation Filter; PTIN – Progressive Triangulated Irregular Network; PMF – Progressive Morphological Filter; SMRF – Simple Morphological Filter; Note that ARC and RW are only abbreviations used for black-box algorithms implemented in ArcGIS, and RealWorks, respectively. While other abbreviations are commonly used.

One of the currently most popular software solutions for point cloud processing is Rapidlasso LAStools (rapidlasso.com), which has a unique position among the tested programs – it is a commercial software but the limitations of its free version are kept to a minimum. Open source programs CloudCompare (danielgm.net/cc) and PDAL (pdal.io) have also become quite popular. Of the commercial software, we tested the ground classification algorithms implemented in the widely used programs ArcGIS (esri.com) and Trimble Realworks (geospatial.trimble.com). In each software, we started from default settings and through expert tuning of the parameters (based on our experience with the tested algorithms and our knowledge of the terrain and vegetation in the study area) progressed to the best achievable results for each individual algorithm. The algorithms implemented in ArcGIS (hereafter ARC) and Trimble Realworks (hereafter RW) are grey-box

algorithms with default settings only. The basic principles underlying the remaining algorithms evaluated in this study are briefly described below.

CloudCompare (danielgm.net/cc) uses a newly proposed algorithm based on the cloth simulation filter (CSF; Zhang et al. 2016). In this technique, the original point cloud is at first rotated by 180° (upside-down) and a simulated cloth is subsequently "dropped" on the inverted surface. Before running the algorithm itself, the outliers have to be removed. The resolution of the initiating grid (Cloth resolution) determines the number of cloth particles that are placed above the highest point of inverted point cloud. Subsequently, the position of each particle (shape of the cloth) is calculated analysing interactions between the cloth particles and corresponding points in the cloud under the influence of simulated gravity, intersections and internal forces. The simulation is terminated when it exceeds the maximum iteration number (default 500). Finally, distances between the cloth particles and points in the cloud are computed and points with distance lower than specified threshold (default 0.5 m) are classified as ground. We tested all options available for different terrain characters (Steep slope, Relief and Flat) in combination with several values of an initial grid resolution. We also tested the post-processing method for a sharply changing terrain (Zhang et al. 2016).

Rapidlasso LAStools (rapidlasso.com/lastools) uses a progressive triangulated irregular network (PTIN) densification algorithm (Axelsson 2000). This algorithm identifies the ground points with respect to the distance between each point and a generated triangulated irregular network of the lowest points. We used a *LASground new* tool allowing modification of several settings. In addition to the initial Step parameter, we also modified Spike (the vertical threshold at which spikes are removed) and Offset (the maximum offset up to which points above the ground are included). First, the point cloud is overlapped with a user-defined grid (Step parameter), the lowest points in each grid cell

are then selected and serve as initial ground points. Subsequently, a triangulated irregular network (TIN) is built from these selected ground points (reference surface) and the remaining points are used iteratively for a TIN densification. In the next iteration, suitable selected points are used as ground points of TIN and iteration continues until all points are classified as ground or non-ground (Axelsson 2000, Isenburg 2018).

Two morphological filters are available in PDAL (pdal.io). The Progressive Morphological Filter (PMF; Zhang et al. 2003) generates an initial elevation grid from the point cloud by selecting the points with minimum elevation in each cell. If the cell contains no points, the nearest neighbor interpolation is used to derive the elevation. Subsequently, the morphological operation of opening (erosion followed by dilation) is used to filter the grid surface. This operation is repeated iteratively (each time with a different window size and a different height threshold). Detection of non-ground points is based on the elevation difference threshold which grows with each iteration and is calculated based on the difference in window size between the current and last iteration, slope (Slope) based on the average slope in study area, cell size and initial elevation difference threshold (Initial distance). If the difference in elevations between original grid and result of opening exceeds the elevation difference threshold, it is treated as non-ground. Window size and elevation difference threshold calculation are increased iteratively until window size is greater than user defined maximum window size (Max window size). We kept increasing the window size exponentially and as there are no buildings in the study area, we used a default maximum elevation difference threshold (Zhang et al. 2003).

The other morphological filter available in PDAL is the Simple Morphological Filter (SMRF; Pingel et al. 2013). It differs from PMF by using "painting technique" to interpolate empty cells in initial elevation grid, it only allows a linearly increasing window size up to a specified maximum (Window size), and the change of the elevation difference threshold for classifying the points as non-ground is controlled by a

single parameter (Slope) which simplifies exploratory analysis (Pingel et al. 2013). When the iteration process is finished, a binary grid where each cell is determined as ground or non-ground is produced. This grid is used as a mask for identification of non-ground cells in the initial elevation grid– these are interpolated using the "painting technique" and the resulting grid is used in the final step to identify ground points. Ground points are identified by applying a user defined threshold (Threshold) to vertical distances between each point and the grid. An additional parameter (Scalar) can be used to increase the threshold on the steep slopes (Pingel et al. 2013).

4.2.4 Quantitative and Qualitative Validation

The classified point clouds were compared with manually classified reference data to quantify the performance of individual classification methods. We calculated the Type I error (omission error), representing the percentage of ground points that are incorrectly classified as non-ground as:

$$Type\,I\,error = \frac{b}{a+b} \tag{4.1}$$

where a is the number of correctly classified ground points and b is the number of ground points misclassified as non-ground points.

Type II error representing non-ground points incorrectly classified as ground points was calculated as:

$$Type\,II\,error = \frac{c}{c+d} \tag{4.2}$$

where c represents the number of non-ground points misclassified as ground points and d stands for the number of correctly classified non-ground points.

In addition, we calculated the success rate, i.e., the ratio between the number of correctly classified points and the total number of points.

$$Succes\,rate = \frac{a + d}{e} \tag{4.3}$$

where e stands for total number of all points.

In addition, points classified as ground were used to generate DTMs with a cell size of 0.5 m. We used a bin-average method calculating the elevation for each cell by assigning the average value of all points within that cell. Areas containing no ground points were triangulated across and linearly interpolated to determine their cell values. We used several accuracy measures to assess the vertical accuracy of DTMs. The GNSS survey, representing the most accurate data, was used as the reference dataset (true elevation) for DTMs evaluation. We first calculated vertical differences among the 1439 surveyed point elevations and the corresponding DTMs. Those differences were subsequently used to calculate the mean error (ME) and root mean square error (RMSE). We also calculated the normalized absolute deviation (NMAD), which is a robust metric less sensitive to the presence of outliers (Höhle and Höhle 2009).

A common approach in existing studies is to compare algorithms based on results obtained using parameters that resulted in the highest filtering accuracy (Korzeniowska et al. 2014, Montealegre et al. 2015). Parameter tuning, however, is greatly dependent on the user's experience and the parameters are not always optimally tuned (but see Wan et al. 2018 for automated tuning of ground filtering algorithms). Therefore, we calculated above mentioned quantitative metrics for all evaluated parametrizations to assess whether the algorithms tend to cause Type I or Type II error regardless of a parameters set. In other words, the "within algorithm variability" based on different parametrizations was evaluated. In addition to the above, we selected the best ground filtering setting for each algorithm and performed both qualitative

and quantitative "between algorithms" comparison. The qualitative assessment consisted of a visual examination and comparison of a shaded relief of the generated DTMs. Note that a more complex qualitative validation (e.g., through the number of properly preserved terrain features) would require a larger study area (Sithole and Vosselman 2004, Montealegre et al. 2015). This would however be incompatible with our efforts to cover the whole area with GNSS measurements.

To study the effect of the character of the environment (i.e., the combined effect of vegetation and terrain), the assessment was performed separately for each area (I–V, Figure 4.1). These areas differ mainly in vegetation character (i.e., grass, shrub, forest); however, they also differ in terrain complexity (Table 4.1). Therefore, the effect of terrain on the results of filtering algorithms was also evaluated using the terrain slope calculated from the national DTM of the Czech Republic (see Moudrý et al. 2019d for more details about this dataset) and divided into four categories (0°–5°, 5°–10°, 10°–15° and >15°). We investigated differences in the Type I error, Type II error, and Success rate between areas (I–V) and between classification algorithms using linear mixed models, with an identifier of 50 randomly distributed buffers as a random effect. We thus fitted three different models (one for each error measure as a response variable) with algorithm and area as predictors, including their interaction. Similarly, we tested whether the elevation difference measured in the 1439 checkpoints differed between areas and algorithms, again using a linear mixed model with interactions. Statistical analysis was performed using the R statistical software (R Core Team 2018), the models were fitted using *lme4* package for R (Bates et al. 2015a), and statistical significance of fixed effects of the model was evaluated using Wald chi-square tests (function Anova in the package *car* for R; Fox and Weisberg 2011).

4.3 Results and Discussion

4.3.1 Algorithms' Tendency to Cause Type I or Type II Error

In total, 120 classifications were performed (Table 4.2). Different settings produce different Type I and Type II errors even within individual algorithms (Figure 4.2), a general tendency of the algorithms to Type I or Type II errors can however be observed. SMRF, CSF and RW successfully identified most of the ground points. However, they often classified non-ground points as ground (i.e., they have lower Type I error than Type II error). In contrast, ARC, PTIN, and PMF showed a lower tendency to classify non-ground points as ground, but failed more frequently in successful identification of ground points (i.e., they have lower Type II error than Type I error). Note however that we only used a few parameters and their settings, which in general performed well in the study area (see Figure 4.2 for variability in RMSE) and more extensive evaluation of settings is needed to comprehensively evaluate the algorithms' tendency to cause Type I or Type II error. For example, Sithole and Vosselman (2004) found that most algorithms produced Type I errors rather than Type II errors.

In every analysis, researchers must accept some level of tradeoff between resulting Type I and Type II errors, all the more due to the fact that usually, one of those two types of error is considered (depending on the application) more serious than the other. For most applications, Type I error is less costly and not a serious handicap as the point clouds are processed further. It can be assumed that gaps caused by misclassified ground points are filled by interpolation and hence do not create an issue (but this might not be true in case of complete failure at the ridges or depressions). Therefore, it makes sense to generally fine-tune algorithms towards the reduction of Type II error. This may be the
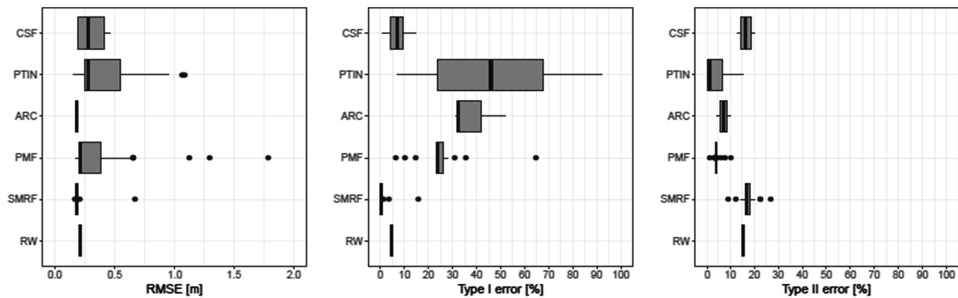
Figure 4.2: Comparison of individual ground filtering algorithms' performance (RMSE) and their tendency to cause Type I and Type II error. The boxplots show the extent of variability in RMSE, Type I error and Type II errors with respect to different settings of individual algorithms. The central vertical line in the box marks the median. The boxes show interquartile range (25th to 75th percentile) and the whiskers show 1.5 times the interquartile range. Note that CSF, SMRF and RW tends to cause Type II error while PTIN, ARC and PMF tend to Type I error.

case for example for applications in forestry at plot and larger scales that do not require DTMs with sub-meter resolution (Frazer et al. 2011, Hawryło et al. 2017). However, Sithole and Vosselman (2004) proposed that from the practical point of view, fine-tuning towards the reduction of Type I errors might be beneficial even if this is at the expense of an increase in Type II error, as Type II errors are considered conspicuous and therefore easy to remove by manual editing. This is however true for small areas only. For large areas such as states, manual editing would be extremely time demanding.

4.3.2   Quantitative Assessment of the Best Results

In the following sections, point clouds acquired with parameters achieving the best results for the individual algorithms will be compared. The optimal set of parameters in this respect was a set that resulted in a terrain model with the minimum number of visually apparent errors (evaluated using shaded relief) and the lowest RMSE in combination with the highest success rate for each algorithm. Where similar RMSEs

and success rates were obtained, parameters resulting in a lower Type II error were selected. The summary of optimal combinations of parameters for our study area and their validation metrics are presented in the Table 4.3 and Figure 4.3, respectively. The RMSE ranged from 0.15 m to 0.21 m. PTIN yielded the best result with the RMSE of 0.15 m. The success rate of point clouds filtered using the optimal parameters for each algorithm ranged from 79.2% to 90.8%. Success rates of all software solutions (with the exception of ARC) were higher than 85%. CSF yielded the highest success rate (90.8%) closely followed by RW (90.6%), both however have a notably high Type II error (>15%). On the other hand, ARC yielded the lowest success rate (79.2%), particularly due to the highest Type I error of all algorithms (32.4%). The Type II error ranged from 0.5% to 19.2%. The lowest Type II error was observed for PTIN (<1%) while the highest for CSF (19.2%) and RW (15.3%). The lowest Type I error, on the other hand, was obtained by the CSF (<1%).

Table 4.3: Optimal settings of individual algorithms in our study area.

Algorithm	Optimal parameters
CSF	General settings: *Flat*; Slope processing: *enabled*; Cloth resolution: *0.2*
PTIN	Predefined parameters for *Nature* setting
ARC	Ground detection method: *Standard*
PMF	Exponential: *true*; Initial distance: *0.15*; Maximum difference elevation threshold: *2.5*; Max window size: *10*; Slope: *1*
SMRF	Scalar: *1.25*; Slope: *0.15*; Threshold: *0.05*; Window size: *18*
RW	–

4.3.3 Qualitative Assessment of the Best Results

In our study area, we identified three problematic circumstances under which classification algorithms were likely to fail: (i) sharp ridge/steep slope; (ii) very dense vegetation and (iii) vegetation on slopes or in ditches. The most notable deterioration of the classification results
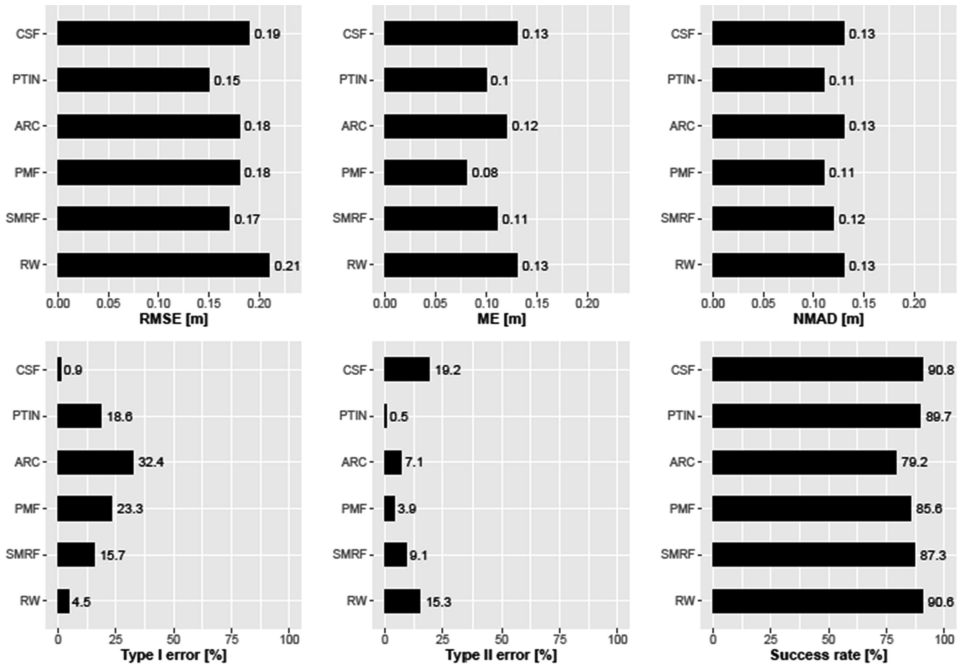
Figure 4.3: Best results achieved by evaluated algorithms.

caused by dense vegetation and vegetation on steep slopes was observed for PMF and CSF algorithms (Figure 4.4 b, e). The terrain derived from both PMF and CSF filters showed obvious erroneous peaks throughout the study area that were caused by the vegetation and present even in the area with prevailing grass vegetation (some shrubs and dense vegetation in ditches were misclassified as ground; Figure 4.4 b, e). RW filter tended to eliminate ground points excessively and result in omission of many terrain features such as ditches and steep slopes in densely vegetated areas (Figure 4.4 g). PTIN, ARC and SMRF preserved the terrain relatively well; they however excessively eliminated ground points, partly omitted some of the steep slopes and they failed where dense vegetation was present. (Figure 4.4 c, d, f). It should be however noted that in places, the dense vegetation formed an impenetrable surface and only very few LiDAR pulses penetrated it; in other words, in such places, almost no ground points were present in the raw data. Where this was the case, any failures were more due to

the problematic character of the data itself than due to a problem with the algorithm. For some algorithms, we were able to filter out even the dense vegetation during a manual fine-tuning of the algorithms, it was however only at the cost of failure at the ridges, the convex shape of which was then not preserved (results not presented here).
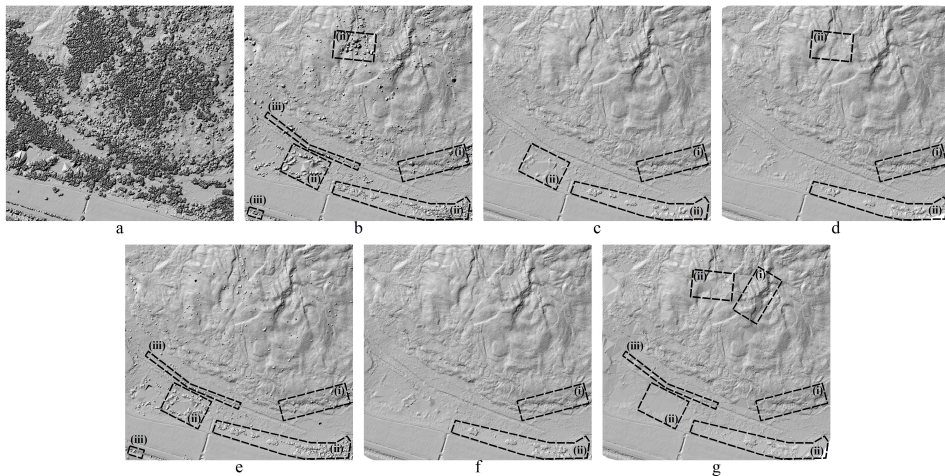
Figure 4.4: Hillshaded surface models generated from unfiltered point cloud (a) and ground points filtered using CSF (b), PTIN (c), ARC (d), PMF (e), SMRF (f), RW (g) algorithm. Highlighted areas represent problematic circumstances as follows: (i) sharp ridge/steep slope; (ii) very dense vegetation and (iii) vegetation on slopes or in ditches. Note the problematic area (right bottom corner) with very dense vegetation that formed an impenetrable surface and only very few LiDAR pulses penetrated it.

4.3.4   Effect of Vegetation Cover and Terrain Slope

The results show obvious differences between the performances of ground filtering algorithms in five areas with different vegetation cover (i.e., grass, shrub, forest) and terrain complexity (i.e., slope). The effects of the area, algorithm and their interaction on elevation difference, Success rate, Type I and Type II error were statistically significant (Table 4.4). This corroborates findings of previous studies that also highlighted that vegetation and terrain character have a serious effect on

the success of filtering algorithms (Tinkham et al. 2011, Korzeniowska et al. 2014, Montealegre et al. 2015).

For CSF, PTIN, ARC, and PMF algorithms, the tendency to cause Type I or Type II error was consistent across all areas (Figure 4.5). SMRF tended to cause Type I error in areas with relatively low slope, and Type II error in areas of high slope. RW tend to cause Type II error in all areas except for the forest area with low slope. This can be attributed to the fact that RealWorks is primarily designed for Terrestrial laser scanning (TLS), and although it has also been successfully used for photogrammetric point clouds (Kršák et al. 2016), its behaviour with ALS data might be erratic.

Table 4.4: Significance of the effect of the algorithm, area, and their interactions on Type I and Type II errors, Success rate, and elevation difference.

Fixed effect	Type I error			Type II error		
	χ^2 stat.	DF	P	χ^2 stat.	DF	P
Algorithm	197.757	5	$< 10^{-16}$	126.184	5	$< 10^{-16}$
Area	32.324	4	$1.6 \cdot 10^{-6}$	15.361	4	0.0040
Interaction	62.182	20	$3.3 \cdot 10^{-6}$	81.233	20	$2.4 \cdot 10^{-9}$
	Success rate			Elevation difference		
	χ^2 stat.	DF	P	χ^2 stat.	DF	P
Algorithm	67.897	5	$2.8 \cdot 10^{-13}$	463.049	5	$< 10^{-16}$
Area	35.892	4	$3.0 \cdot 10^{-7}$	317.745	4	$< 10^{-16}$
Interaction	37.038	20	0.0116	80.946	20	$2.7 \cdot 10^{-9}$

4.3.4.1   Grass Vegetation

In general, all filters performed relatively well in the area of low complexity characterized by grass vegetation and flat terrain. PTIN algorithm yielded the best classification accuracy in the areas dominated by grass with (see range of success rate in Figure 4.5) as well as the best ability to remove vegetation in ditches (Figure 4.4 e). However, with increasing terrain complexity and low vegetation density, error rates caused by the filters increased (Figures 4.5 and 4.6).
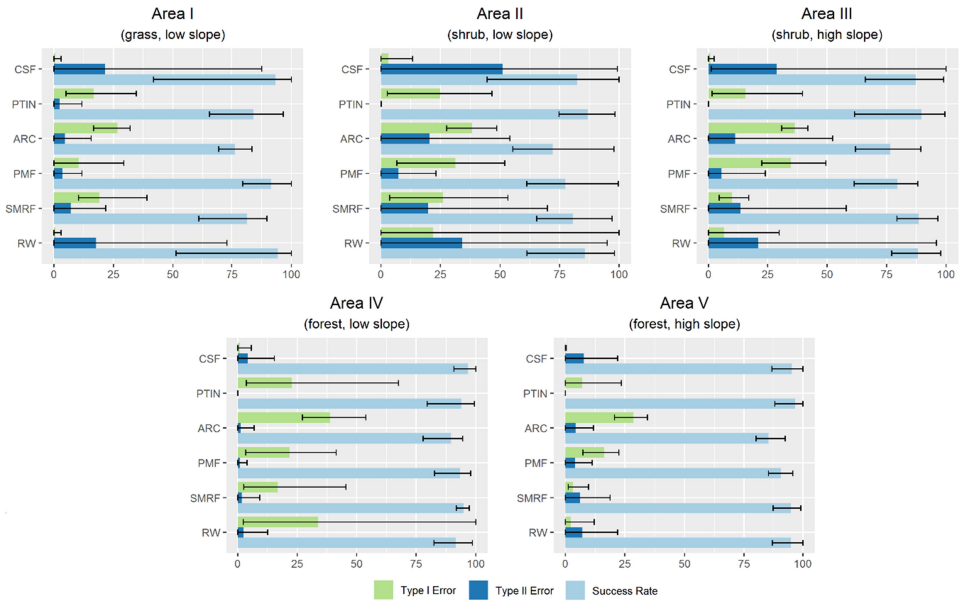
Figure 4.5: Comparison of six algorithms in five areas of different vegetation structure and terrain slope (classification error). Columns denote the mean error (Type I, Type II and Success rate) while the error bars show error range (maximum and minimum). The maximum, minimum and mean error are calculated from 10 buffers in each of the Areas IV. Note the relatively stable performance (low error bars) of all algorithms in forested areas in contrast to shrub and grass areas.

4.3.4.2   Shrub Vegetation

In areas dominated by shrub vegetation (Areas II and III), the RMSE ranged from 0.17 m to 0.23 m (Area II) and from 0.16 m to 0.21 m (Area III). PTIN, PMF and SMRF yielded the best results with RMSE ≤ 0.20 min both areas (Figure 4.6). The average success rate ranged from 72.1% to 86.9% and from 76.4% to 89.7% for Area II and Area III, respectively (Figure 4.5). Sites with low vegetation and shrubs were problematic for all algorithms and the Type II error in such areas was higher than in forested areas. Some of the vegetation was incorrectly classified as ground points due to similarities in the distribution of points (i.e., their slope and elevation differences). In particular, CSF, ARC, SMRF and RW tended to misclassify non-ground
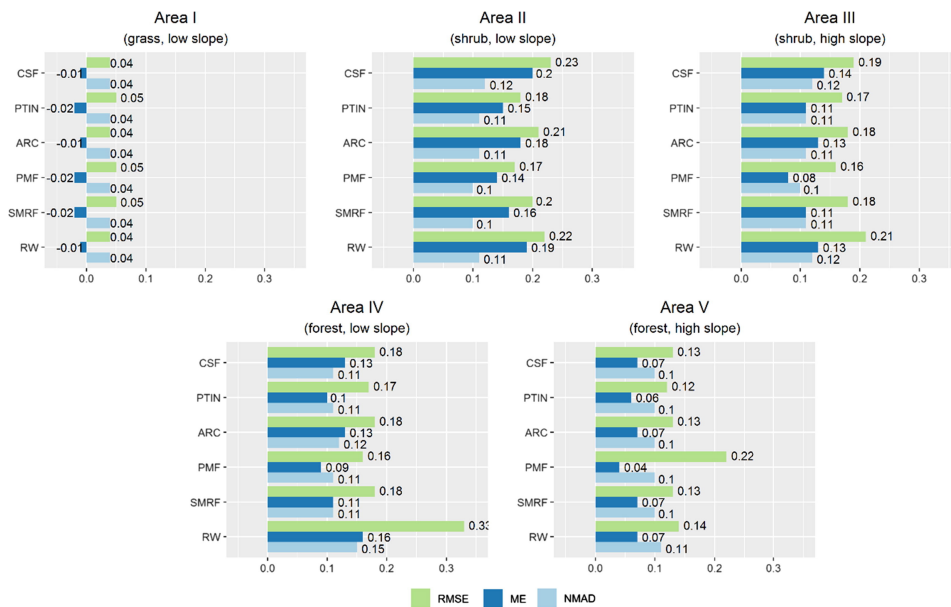
Figure 4.6: Comparison of six algorithms in five areas of different vegetation structure and terrain slope. Root mean square error (RMSE), mean error (ME) and normalized absolute deviation (NMAD) of differences between DTMs and GNSS measurements.

objects (e.g., low shrubs) as ground, thus having a high Type II error. On the other hand, the performance of PTIN and PMF was relatively good even in the shrub vegetation with relatively low Type II error; PMF however showed obvious erroneous peaks or bumps on the shaded relief map.

4.3.4.3 Forests

All algorithms performed better in the forested areas than in the shrub vegetation, which is likely caused by the fact that in forests, there is a relatively lower representation of low vegetation (see Table 4.1) bearing a profound effect on misclassification, especially in combination with steep slopes. In forests, RMSE ranged from 0.16 m to 0.33 m and from 0.12 m to 0.22 m for Area IV and Area V, respectively (Figure 4.6). All algorithms yielded average success rates >90% except for

ARC (Figure 4.5). The best results in forested areas were yielded by PTIN and SMRF.

4.3.4.4 Slope

The increasing terrain slope negatively affected the algorithms' performance and resulted in deterioration of the terrain accuracy. Most of the evaluated algorithms showed relatively good results for slopes up to 15°; with slopes over 15°, however, the performance of all algorithms decreased rapidly (Table 4.5). The most accurate and consistent results with respect to the terrain slope were obtained when using PTIN and SMRF. This corroborates with results of Montealegre et al. (2015) who also demonstrated the low vulnerability of PTIN to slope. PMF also provided very good results but a significant drop in accuracy was detected at intermediate slopes (10°–15°).

Table 4.5: The effect of the terrain slope on the filter accuracy. Evaluated by RMSE calculated for four slope categories.

Algorithm	Slope			
	0° - 5°	5° - 10°	10° - 15°	> 15°
CSF	0.17	0.18	0.19	0.24
PTIN	0.14	0.15	0.17	0.22
ARC	0.16	0.17	0.19	0.24
PMF	0.13	0.14	0.27	0.22
SMRF	0.15	0.16	0.18	0.23
RW	0.19	0.21	0.23	0.27
Num. of checkpoints	557	506	245	131

4.4 Conclusions

In this study, we evaluated the performance of six ground filtering algorithms. In principle, two error types can occur while filtering ground points of LiDAR data. The first error type is the failure to identify true

ground points, classifying them as non-ground objects (Type I error, omission error), the other type is incorrect classification of non-ground points as bare earth (Type II error, commission error). Our results show that PTIN, ARC and PMF tended to cause Type I error while CSF, SMRF and RW tended more to producing Type II error. In addition, this tendency was consistent across areas with different vegetation and terrain character, except for SMRF and RW, the tendencies of which to Type I and Type II error were affected by vegetation and terrain character. All tested ground filtering algorithms achieved relatively good results but their performance is notably affected by the terrain slope and vegetation cover. In our study area, PTIN implemented in LAStools provided the best overall results, although some other algorithms performed better in specific environments. In general, algorithms performed better in forests than in steppes with a high density of low vegetation. For example, the recently proposed SMRF algorithm has shown promising results in the forests. The algorithm implemented in the commercial ArcGIS software also performed quite well, particularly in forested areas, despite the fact that it allows the use of only a few predefined options. However, its high initial cost is a serious drawback. With increasing slope, the performance of all algorithms tended to deteriorate with a noticeable drop at terrain slope over 15°.

It is evident from our results and from prior studies that to achieve the optimal filtering performance, the selection of the algorithms and parameter settings should be guided by a specific landscape type. Such principle is for example implemented in LAStools, which allows users to select a set of parameters for a particular landscape (e.g., nature or town). It is worth mentioning that results of the PTIN algorithm with such predefined settings implemented in LAStools provided the best results of all tested software solution, which only confirmed the value of such approach. Until more automated approaches for parameters estimation will be developed, we can suggest this approach to be used also by other software developers.

Chapter 5

Sensitivity Analysis of Parameters and Contrasting Performance of Ground Filtering Algorithms with UAV Photogrammetry-Based and LiDAR Point Clouds

Petr Klápště, Michal Fogl, Vojtěch Barták, Kateřina Gdulová, Rudolf Urban, Vítězslav Moudrý

Author's contribution: 50%

Abstract

Most ground filtering algorithms are primarily designed for airborne LiDAR point cloud processing and their successful use in identifying ground points from photogrammetric point clouds remains questionable. We compared six ground filtering algorithms implemented in Metashape, ArcGIS, CloudCompare, LAStools, and PDAL. We used UAV photogrammetry-based (acquired under leaf-off conditions) and airborne LiDAR (leaf-on) point clouds of the same area to: (i) compare accuracy of generated DTMs; (ii) evaluate the effect of vegetation density and terrain slope on filtering accuracy; and (iii) assess which algorithm parameters have the greatest effect on the filtering accuracy. Our results show that the performance of filtering algorithms was affected by the point cloud type, terrain slope and vegetation cover. The results were generally better for LiDAR (RMSE 0.13–0.19 m) than for photogrammetric (RMSE 0.19–0.23 m) point clouds. The behavior in varying vegetation and terrain conditions was consistent for LiDAR point clouds. However, when applied on photogrammetric point clouds, the algorithms' behavior was inconsistent, especially in areas of steep slope (except for the Progressive Triangulated Irregular Network in LAStools). Parameters related to the selection of the initial minimum elevation ground points were the most influential in all algorithms and point clouds.

5.1 Introduction

Point clouds derived from light detection and ranging (LiDAR) and airborne photogrammetry have become commonplace data sources for digital terrain models (DTMs) production. DTMs are generated through point cloud filtering (i.e., the process of identification of points representing bare ground and dividing the point cloud into the ground and non-ground parts) followed by interpolation. Both airborne laser scanning (ALS; i.e., LiDAR sensor is mounted on-board an aircraft or helicopter) and UAV photogrammetry-derived DTMs have been equally used in many disciplines such as forestry (Balenović et al. 2018, Tomaštík et al. 2017), hydrology (Rahman et al. 2017), restoration ecology (Koska et al. 2017, Szostak et al. 2019), or precision agriculture (Kumhálová and Moudrý 2014, Méndez-Vázquez et al. 2019).

The point cloud filtering (i.e., correct bare ground detection) poses the greatest challenge for generating DTMs (Sithole and Vosselman 2004). Many ground filtering algorithms (e.g., cloth simulation, progressive morphological filter) have been implemented in various GIS software solutions (e.g., ArcGIS, LAStools, PDAL) and are now readily available for filtering of both LiDAR and photogrammetric point clouds (e.g., Petras et al. 2016). The use of such algorithms for filtering of photogrammetric point clouds is constantly increasing. For example, Kachamba et al. (2016) used the ground filtering algorithm implemented in Agisoft PhotoScan (now known as Agisoft Metashape) as a basis for estimation of biomass in a tropical woodland. Similarly, ground filtering algorithms implemented in LAStools (Wallace et al. 2012, 2016), CloudCompare (Yan et al. 2020) and PDAL (Graham et al. 2019) were successfully used for forestry applications. However, most of the algorithms were designed for ALS data filtering (Meng et al. 2009, Susaki 2012, Rashidi and Rastiveis 2017) and their performance with photogrammetric point clouds (usually denser than ALS point clouds, containing a lot of noise) is unknown (Zhang et al. 2018). In addition,

ALS records the order of multiple laser pulse returns (first, intermediate and last). Some ground filtering algorithms use this attribute as it is assumed that the last return most likely represents the ground (Chen et al. 2007, Pingel et al. 2013).

Ground filtering is affected by the presence of above-ground objects (e.g., buildings and vegetation) and terrain morphology. The higher the complexity of above-ground objects, the more errors are likely to arise (Meng et al. 2010). Therefore, specialized algorithms are developed and tested for different types of environment (e.g., build-up area, forests, steppes, river banks) and their use in other types of environment requires additional testing (e.g., Tinkham et al. 2011, Chen et al. 2017b, Tan et al. 2018).

Successful ground filtering of photogrammetric point clouds is particularly problematic under dense canopies due to large discontinuities without or with only sparse ground points (Wallace et al. 2016). While laser pulses can penetrate through gaps in the canopy to the bare earth surface, photogrammetry requires "seeing" the same patch of ground from multiple views to be able to acquire the 3D information. It is, therefore, challenging to obtain detailed information of the terrain under the canopy obscuring it and reducing the likelihood of multiple views (White et al. 2013). A possible solution for increasing the density of ground points is to use images acquired under leaf-off conditions (Aguilar et al. 2019, Moudrý et al. 2019b,d). Such conditions can, however, result in point clouds with lots of noise closer to the ground. This is in contrast with leaf-on conditions under which the high canopies (resembling ground or even a complete absence of ground points) represent the biggest problem (Jensen and Mathews 2016, Wallace et al. 2019) – and therefore make filtering more challenging.

Prior studies that evaluated ground filtering algorithms concentrated mostly on ALS data (e.g., Sithole and Vosselman 2004, Podobnikar and Vrečko 2012, Montealegre et al. 2015, Polat and Uysal 2015). Few recent studies evaluated the performance of ground filtering algorithms on

dense photogrammetrically acquired point clouds. Serifoglu Yilmaz and Gungor (2018) tested five filtering algorithms implemented in Airborne LiDAR Data Processing and Analysis Tools (ALDPAT) in a small part of a university campus (7.3 ha). In the same university campus, Serifoglu Yilmaz et al. (2018) distinguished two testing sites with areas of 2.5 and 6.2 ha, respectively, and with different conditions (i.e., terrain slope, presence of vegetation and buildings of varying size) and tested seven filtering algorithms implemented in various software solutions. The altitude in both studies ranged approximately from 10 to 100 m AMSL. Zeybek and Şanlıoğlu (2019) compared four filtering algorithms at a study site located in a mountain area of 50 ha and an altitude of approximately 1400 m AMSL. However, they proposed different filtering algorithms to be optimal for photogrammetrically acquired point clouds; Serifoglu Yilmaz and Gungor (2018) recommended the Adaptive Triangulated Irregular Network algorithm, while Serifoglu Yilmaz et al. (2018), as well as Zeybek and Şanlıoğlu (2019), recommended the Cloth Simulation Filter. In addition, unexpected behavior was encountered in some of the studies. For example, Serifoglu Yilmaz et al. (2018) found accuracy increasing with increasing slope. Such results indicate that the selection of an optimal algorithm is likely dependent on the character of the study area (e.g., terrain slope and vegetation density) and that the behaviour known from ALS point clouds (i.e., filtering accuracy decrease with increasing slope and presence of low vegetation) does not necessarily apply to dense photogrammetric point clouds. However, none of the previous studies compared both ALS and photogrammetric data in the same area. Hence, it is difficult to conclude whether or not can the same behavior of an algorithm be expected for both types of point clouds.

Our goal is to show the behavior of filtering algorithms with respect to the increasing slope and vegetation density. While this is well known for ALS point clouds and all algorithms behave in the very same way, we hypothesize that this is not true for dense photogrammetric point

clouds. We used ALS and photogrammetric point clouds of the same area: (i) to compare the accuracy of DTMs generated by six different ground filtering algorithms implemented in widely used software; three available in commercial software and three in open source software; (ii) to evaluate the effect of vegetation density and terrain slope on filtering accuracy; and (iii) to assess the sensitivity of parameters and differences in performance between algorithms applied on both types of point clouds (i.e., derived from both ALS and UAV photogrammetry).

5.2 Material and Methods

5.2.1 Study Area

Our study area is located in north-west Bohemia, Czech Republic, 50°34'N, 13°34'E (Figure 5.1). Until 1964, when local brown coal mining was terminated, the spoil heap was used to deposit overburden. The spoil heap has never been technically reclaimed and the terrain morphology, therefore, remained rugged as a result of heaping that formed a typical undulated terrain and consequently allowed the development of dense heterogeneous vegetation (e.g., Frouz et al. 2018), which represents a challenge for ground filtering (e.g., Meng et al. 2010, Pingel et al. 2013, Chen et al. 2017b). The vegetation consists of aquatic vegetation in terrain depressions (e.g., *Phragmites australis* and *Typha latifolia*), steppes (low vegetation, especially *Calamagrostis epigejos* and *Arrhenatherum elatius* with scattered shrubs and trees, such as *Sambucus*, *Rosa*, *Betula*, *Crataegus*), and forests (mostly deciduous trees such as *Betula spp.*, *Salix spp.* and *Alnus spp.*). A rectangular area of 30 hectares (550×550 m) that represents typical conditions (Figure 5.1) was selected for testing the ground filtering algorithms.
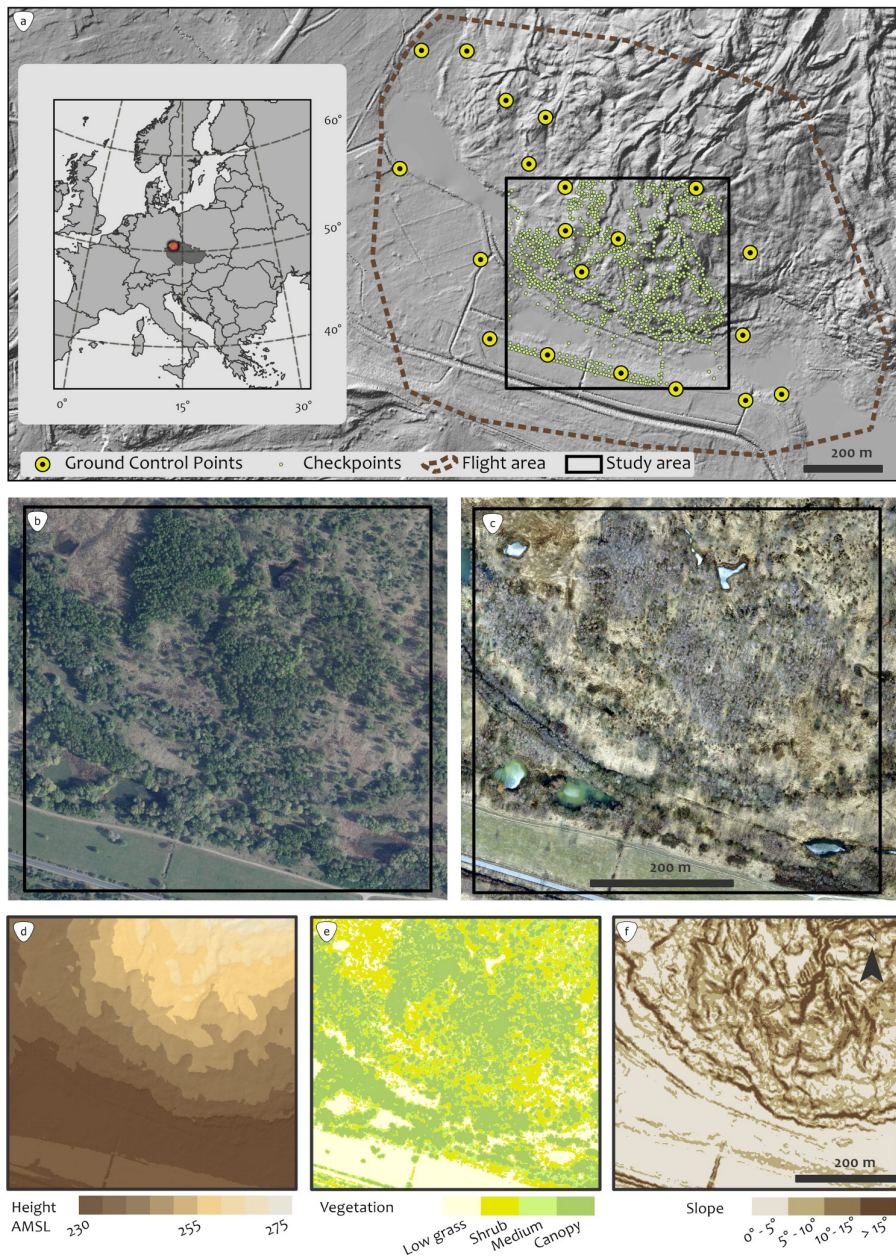
Figure 5.1: Details of the study area. (a) Site position within Europe and hillshaded relief including the location of ground control points and validation checkpoints; (b) Orthophoto under leaf-on period; (c) Orthophoto under leaf-off period; (d) Altitude above mean sea level (m); (e) Character of vegetation based on density (Low grass, Shrub, Medium and Canopy vegetation); (f) Terrain slope.

5.2.2 LiDAR Data Acquisition

The ALS data were acquired by the Flying Laboratory of Imaging Spectroscopy (FLIS) in May 2017 (Hanuš et al. 2016). Although the FLIS is equipped with a Riegl LMS-Q780 fullwaveform laser scanner, we used only discrete return data. The scanner has a rotating polygon mirror and scans in parallel lines. The wavelength is 1064 nm and the scan field of view is 60°. Flights for data collection were conducted at 1030 m above ground at a velocity of 56.5 m·s^{-1} (ground speed) and with 55% flight line side overlap. The LiDAR point cloud was processed by the Global Change Research Institute using their proprietary algorithm. The data were provided in LAZ format with an average point density of 8 points per square meter (Table 5.1), referenced to the European Terrestrial Reference System, Universal Transverse Mercator projection (ETRS UTM33N), and provided with elevations as ellipsoidal heights.

Table 5.1: Summary of point cloud characteristics for the LiDAR and photogrammetric datasets.

Dataset	Total points	Point density (points/sq.m)	Point spacing (m)	Returns $(1^{st}/2^{nd}/3^{rd}/4^{th})$
LiDAR	2,420,802	7.92	0.36	2,173,124/243,784/3882/12
Photogrammetric	91,041,929	299.66	0.06	91,041,929/0/0/0

5.2.3 UAV Data Acquisition

A senseFly eBee Classic UAV equipped with Sony DSC-WX220 RGB camera (18.2 MP, sensor 1/2.3, 4.45 focal length equivalent to 25 mm) was used for image acquisition. The camera has been set to automatic mode; senseFly eBee is a ready-to-fly proprietary solution and flight planning software does not allow the user to set camera parameters such as ISO, aperture or shutter speed (ISO ranged 100–200, aperture F/3.3, shutter speed ranged 1/250–1/800). Flight lines were programmed in the senseFly eMotion 3 software and the UAV was flying autonomously.

The lateral overlap of the images was 75% and the longitudinal overlap 85%. The average flight altitude was 95 m above the ground level and almost 1,300 images were acquired during three flights, covering an area of 130 ha with the ground sampling distance (GSD) of 3.16 cm/pix. The UAV survey was performed in early spring (3rd of March 2017) under leaf-off conditions, the maximum wind speed was 5 m·s^{-1} and the cloud cover was minimal (0–1/8). Changes in the shadow length resulting from solar positioning during the UAV survey or variable image contrast across a scanned area can negatively affect point matching (Carrivick et al. 2016). Therefore, to minimize these effects, all flights were performed during midday hours with constant solar conditions.

5.2.4 Ground Control Points and Checkpoints Survey

The point cloud location was georeferenced using 20 ground control points (GCPs) distributed across the study area. GCPs were made from white fiberboard squares (40×40 cm) with a black round target in the middle. The coordinates of each GCP were measured using a Trimble GeoXR 6000 GNSS in combination with the Zephyr 2 external antenna supporting RTK. The antenna received signal from GPS and GLONASS satellites and was connected to the CZEPOS permanent RTK network, which improved the horizontal positional accuracy to 2–4 cm and vertical to 4–6 cm.

To evaluate DTMs generated by ground filtering algorithms, another set of points (hereafter referred to as "checkpoints") was spread throughout the study area. To locate these checkpoints, an RTK GNSS survey was conducted in March 2017 (leaf-off period) using Leica GPS1200 system that was connected to the CZEPOS permanent RTK network and provided the same horizontal and vertical accuracy as described above. Locations of checkpoints were chosen in a way ensuring sufficient representation of all vegetation categories and slope types. In total, 1,414

checkpoints were collected for this study. All GCPs and checkpoints were measured in the European Reference Terrestrial System (ETRS 89) and projected to the Universal Transverse Mercator (UTM 33N).

5.2.5 UAV Data Processing

Agisoft Metashape Professional (Agisoft LLC, Russia) was used to generate a 3D point cloud from the acquired UAV geotagged images. Metashape uses Structure from Motion (SfM) in combination with Multi-View Stereo (MVS) photogrammetric methods to generate point clouds representing a 3D model of the study area. The processing was executed in several steps. In the first step (*Align photo*), external and internal camera orientations and camera locations were iteratively refined using the least squares method and a *Tie point cloud* was generated. The alignment was computed with the *Accuracy* parameter set to *High* and the *Generic preselection* and *Reference preselection* parameters were enabled. The *Accuracy* setting ensured that the original image resolution was used while the other two parameters speeded up the alignment process. The limit for *Key points* was set to zero (indicating as many points as possible sampled within each image), the *Tie point* limit (the number of points used for image matching) was set to 10,000 and the *Adaptive camera fitting* parameter was enabled. The final *Tie point cloud* consisted of 1 million key points. The next step was to *Build dense point cloud* with *High* reconstruction quality and *Aggressive Depth filtering* (the setting recommended for aerial imagery). The dense point cloud was georeferenced using 20 GCPs with the total RMSE of 0.03 m and total reprojection error of 0.2 pix. Final *Dense point cloud* consisting of 91 million points and with a density of 300 points per square meter (Table 5.11; Figure 5.2) was cropped to our study area and exported into the LAS format.
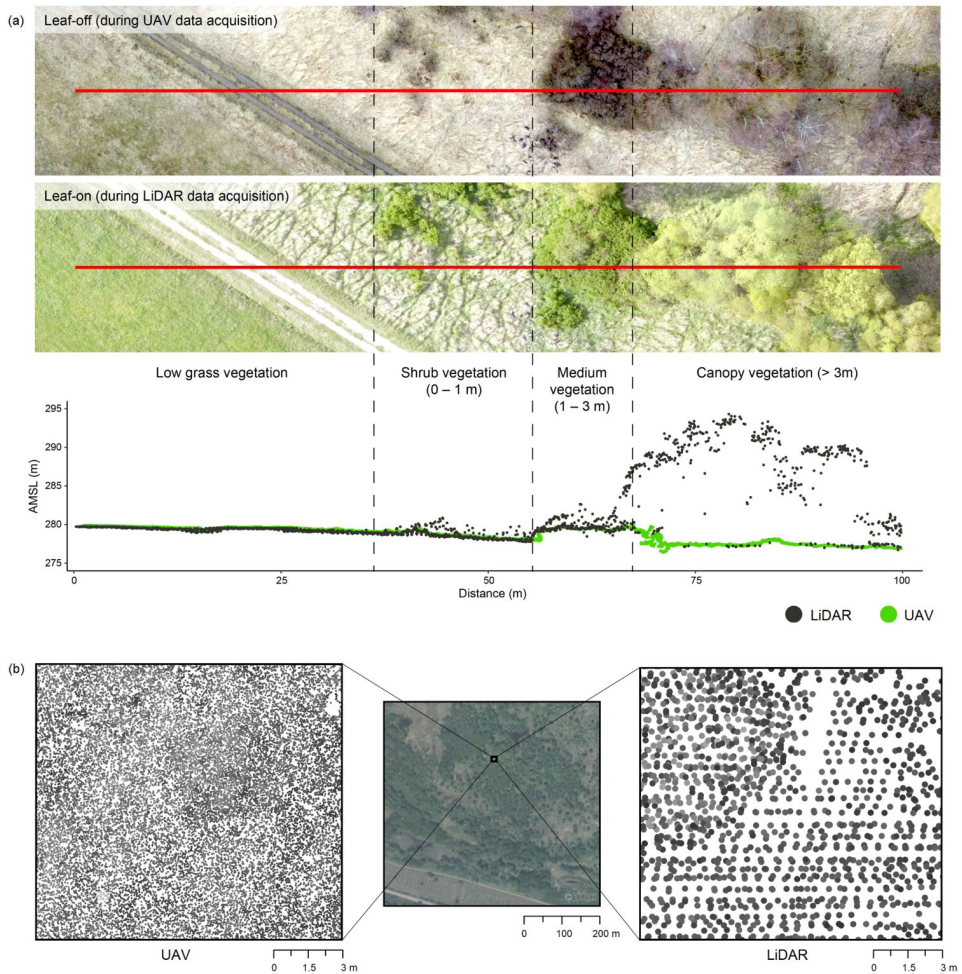
Figure 5.2: Comparison of photogrammetric and LiDAR point clouds (a) on different types of the vegetation (low grass, shrub, medium, canopy) and (b) based on point cloud density.

5.2.6 Ground Point Filtering Algorithms and DTM Generation

We evaluated six algorithms implemented in five commonly used software solutions that have been increasingly used for ground point filtering (Table 5.2). We selected algorithms that are able to work with LAS file format and are ready to use (i.e., implemented in existing software). One of the most popular commercial software solutions used to generate and

filter point clouds from UAV imagery is Agisoft Metashape Professional (version 1.6.2; agisoft.com). Rapidlasso LAStools is however almost as popular (rapidlasso.com). We also tested the algorithm implemented in the probably most widespread commercial GIS software – Esri ArcGIS (version 10.6; esri.com) and algorithms available in popular open-source software CloudCompare (danielgm.net/cc) and PDAL (pdal.io). Short descriptions of the basic principles underlying the algorithms are given below; parameters used for each algorithm are detailed in Table 5.2.

Table 5.2: List of evaluated software solutions, algorithms and their parameters fine-tuned in this study.

Software	Algorithm	Author	Filter description	Number of evaluated settings for UAV/LiDAR	Parameters
Metashape	ATIN	Agisoft LLC, Russia	Surface-based	45/48	
				Max angle; Max distance; Cell size	
ArcGIS	ArcGIS	Esri Inc., USA	–	3/3	
			Predefined options: *Aggressive, Standard, Conservative*		
Cloud Compare	CSF	Zhang et al. (2016)	Surface-based	143/162	
			Predefined options: *Steep slope, Relief, Flat;*		
			Slope processing: *enabled/disabled*; Cloth resolution		
LAStools	PTIN	Isenburg (2018)	Surface-based	56/56	
				Step; Spike; Offset	
PDAL	PMF	Zhang et al. (2003)	Morphology-b.	600/600	
			Initial distance; Max distance; Max window size; Slope		
	SMRF	Pingel et al. (2013)	Morphology-b.	900/900	
			Scalar; Slope; Threshold; Window		

ATIN – Adaptive Triangulated Irregular Network; CSF – Cloth Simulation Filter; PTIN – Progressive Triangulated Irregular Network; PMF – Progressive Morphological Filter; SMRF – Simple Morphological Filter. Filter description based on classification by Favorskaya and Jain (2017).

The algorithm implemented in Agisoft Metashape is based on the Adaptive Triangulated Irregular Network algorithm (ATIN) (Axelsson 1999, 2000). The ATIN algorithm uses an iterative process where a coarse triangulated irregular network (TIN) of initial seed points is

densified. First, seed points (the points with the lowest elevation in each grid cell) are selected from a point cloud based on a user defined grid (*Cell size*). From these points, an initial TIN is created as the first approximation of the terrain. Subsequently, for each iteration, one point above each TIN facet is added to the ground TIN if they are within a specified distance to the TIN facets (*Max distance*) and angles to the nodes (*Max angle*). This iteration process stops when no more points are added to the TIN.

The ground filtering algorithm implemented in Esri ArcGIS 10.6 (Classify LAS Ground) comes without description and Esri answered to our query on the algorithm implemented in ArcGIS: *"The classification method used by the Classify LAS Ground tool is a comprehensive proprietary solution that does not fit in the given classes of algorithms, and no information has been published regarding the technique which is used"*. We tested all three options available (*Aggressive, Standard* and *Conservative*) for ground filtering.

The algorithm implemented in CloudCompare is called Cloth Simulation Filter (CSF; Zhang et al. 2016). This algorithm inverts (upside-down) the point cloud and "covers" it with a simulated surface (cloth). Before running the algorithm itself, outliers have to be removed. Then, the resolution of the starting grid (*Cloth resolution*) determines the number of cloth particles that are placed above the highest point of the inverted point cloud. Subsequently, the position of each particle (shape of the cloth) is calculated analyzing the interactions between the cloth particles and corresponding points in the cloud under the influence of gravity, intersections and internal forces. The simulation terminates when it exceeds the *Maximum iteration number* (default 500). Finally, distances between the cloth particles and cloud points are computed and the points with distance lower than the specified threshold (default 0.5 m) are classified as ground (Zhang et al. 2016). We tested all options for various terrain characters (*Steep slope, Relief* and *Flat*) in combination with several values of the initial grid resolution. We also

tested the post-processing method for a sharply changing terrain (Zhang et al. 2016).

Similarly to the algorithm used in Agisoft Metashape, the algorithm implemented in LAStools is based on ATIN proposed by Axelsson (2000). To distinguish the two implementations, we refer to the implementation in LAStools as a Progressive Triangulated Irregular Network (PTIN) densification algorithm hereinafter as this reference is common in the literature (Montealegre et al. 2015). First, the point cloud is overlapped with user defined grid (*Step* parameter), the lowest points in each grid cell are selected and serve as the initial ground points. Subsequently, a triangulated irregular network (TIN) is built with these selected ground points (reference surface) and the remaining points are used iteratively for TIN densification. We used a *LASground new* tool which allows modification of several settings. In addition to the initial step parameter, we also modified *Spike* (the vertical threshold at which spikes are removed) and *Offset* (the maximum offset up to which points above the ground are included). Suitable selected points are used as ground points of TIN in the next iteration and the iterative process continues until all points are classified as ground or non-ground (Axelsson 2000, Isenburg 2018).

Two morphological filters are available in PDAL. The Progressive Morphological Filter (PMF; Zhang et al. 2003) first generates the initial elevation grid from a point cloud by selecting the point with minimum elevation in each cell and the point coordinates are stored in that grid. If there is no point in the cell, a nearest neighborhood interpolation is used to derive the elevation. Subsequently, the morphological operation of opening (erosion followed by dilation) is used to filter the grid surface. This operation is repeated iteratively (each time with a different window size and a different height threshold). Detection of non-ground points is based on the elevation difference threshold, which grows with each iteration and is calculated based on the difference in the window size between the current and last iteration, slope (*Slope*) based on the

average slope in the study area, cell size (default value 1 m) and initial elevation difference threshold (*Initial distance*). If the difference in elevation between the original grid and the result of opening exceeds the elevation difference threshold, it is treated as non-ground. The window size and elevation difference threshold calculation are increased iteratively until the window size is greater than the user defined maximum window size (*Max window size*). Two possibilities of increasing window size are available, linear and exponential. Due to the fact that the SMRF allows only a linear increase of the window size (see the next paragraph), we decided to keep increasing the window sizes exponentially in case of PMF to see whether there is a significant difference and to reduce the number of iterations. We did not use the maximum elevation difference threshold as there are no buildings in the study area (Zhang et al. 2003).

The other morphological filter available in PDAL is the Simple Morphological Filter (SMRF; Pingel et al. 2013). It differs from PMF in using the painting technique for interpolating the empty cells in the initial elevation grid (the default value of the initial elevation grid *Cell size* is 1 m) . Besides, it only allows a linearly increasing window size up to the maximum specified size (*Window size*), and the change of the elevation difference threshold for detecting non-ground points is controlled by a single parameter (*Slope*), which simplifies the exploratory analysis (Pingel et al. 2013). Once the iteration process is completed, a binary grid where each cell is determined as ground or non-ground is produced. This grid is used as mask to identify non-ground cells in the initial elevation – these are interpolated using the painting technique and the resulting grid is used in the final step to identify ground points. Ground points are identified by applying user-defined threshold (*Threshold*) to vertical distances between each point and the grid. An additional parameter (*Scalar*) can be used to increase the threshold on the steep slopes (Pingel et al. 2013).

Points classified as ground were used to generate DTMs. For rigorous

comparison, it is necessary to compare both DTMs at the same resolution. We were limited by the density of LiDAR point cloud (8 points per square meter) and selected the best possible resolution for such density (i.e., the cell size of 0.5 m) . We considered it a reasonable compromise but, obviously, the UAV photogrammetric point cloud provides much more detail and even better resolution can be used. For DTM generation, we used a bin-average method, i.e., calculated the elevation of each cell as the average value of all points within that cell. Areas containing no ground points were triangulated across and linearly interpolated to determine their cell values.

5.2.7 Accuracy Assessment and Comparison of Algorithms

A sensitivity analysis was performed to identify the best parameter setting for each ground filtering algorithm and point cloud. Several parameter values were used for each parameter and the resulting elevation error was subsequently plotted as a function of the parameter values. We decided the ranges of individual parameters based on our experience and on values used in other published studies (Podobnikar and Vrečko 2012, Korzeniowska et al. 2014, Montealegre et al. 2015, Serifoglu Yilmaz et al. 2016). From these plots, the best sets of parameters were identified by visual assessment (see Table 5.2 for a list of evaluated parameters for each algorithm and Table 5.4 for the best settings). These parameter values were used for subsequent analyses.

Several accuracy measures were applied to assess the vertical accuracy of DTMs. The GNSS survey, representing the most accurate data, was used as the reference dataset (true elevation) for evaluation of the DTMs. First, the elevation error between the 1,414 checkpoints and the corresponding DTM was calculated for each checkpoint. Those differences were subsequently used to calculate the mean error (ME), standard deviation (SD) and root mean square error (RMSE).

To evaluate the effect of the vegetation structure and terrain slope on performance of ground filtering algorithms, ALS data available for our study area were utilized. The best results acquired with LAStools using predefined settings for natural environments (a setting providing the best results according to preliminary testing) were set as ground points. The resulting point cloud was visually assessed and the remaining troublesome areas (e.g., impenetrable dense vegetation) manually edited. DTMs were generated at a 2-meter resolution and slope was calculated, which was subsequently used in further analyses as a continuous variable. As there were no manmade structures in our study area, all above-ground points were classified as vegetation (except the removed noise). The vegetation was categorized at a 2-meter resolution according to its density in individual layers into four categories: low grass vegetation, shrub vegetation (0–1 m) , medium vegetation (1–3 m) and canopy vegetation (> 3 meters). LAStools (*lascanopy* tool) was used to calculate the vegetation density. First, the number of all points above the cover cutoff was counted and divided by the number of all points (i.e., density) in three vegetation height levels. Subsequently, each grid cell was classified according to the layer with the highest density. Areas without returns in three vegetation height levels were classified as low grass vegetation. This classification is more appropriate for assessment of the effect of vegetation on the filtering accuracy as it takes into account the vertical distribution of points that were potentially misclassified as ground. The effects of ground filtering algorithms, point cloud type (photogrammetry vs LiDAR), slope (continuous covariate), and vegetation (classified as low grass, shrub, medium, and canopy vegetation; see the previous paragraph) on the difference between the estimated elevation and reference (GNSS-based elevation) were evaluated by means of a linear mixed-effect model. Because repeated measurements on each validation checkpoint were available (one for each algorithm and point cloud), the checkpoint ID was included as a random-intercept term in the model. We first fitted a "full" model,

including all possible interactions. Then the "final" model including only significant (based on type-II Wald χ^2 test) interaction terms was fitted. Only this final model is reported in the paper. For each parameter of this final model (including random-effect and residual standard deviations), 95% confidence intervals were calculated by profiling likelihood. The goodness of fit was assessed by conditional R^2 as defined by Nakagawa and Schielzeth (2013). To investigate differences between individual algorithms together with the effect of vegetation and slope, the fixed effects with Wald 95% confidence bands (conditional on the random-effect variance estimate) were plotted. All data processing and statistical computations were performed in the R software (R Core Team 2018; see Table 5.3 for a list of R packages and functions used).

Table 5.3: Used R packages and functions.

Package	Function	Purpose	Author
lme4	lmer	linear mixed-effect modeling	Bates et al. (2015b)
car	Anova	Wald χ^2 test of fixed effects	Fox and Weisberg (2019)
MuMIn	r.squaredGLMM	conditional R^2 computation	Bartoń (2019)
raster	–	GIS computations	Hijmans (2019)
ggplot2	–	statistical graphics	Wickham (2009)

5.3 Results

5.3.1 Sensitivity Analysis

Our results show that some parameters are important for both types of point clouds. For each algorithm, a reasonable range and resolution of each parameter were identified, and ground filtering algorithm was then run for all combinations of these parameter values. The resulting ground elevation was then compared with the "true" (GNSS based) elevation at the 1,414 checkpoints.

Figure 5.3: Sensitivity analysis of the Adaptive Triangulated Irregular Network (ATIN) algorithm implemented in the Agisoft Metashape Professional software.

The Adaptive Triangulated Irregular Network (ATIN) algorithm allows setting of the following parameters: *Maximum angle* (°), *Maximum distance* (m), and *Cell size* (m). As can be seen from Figure 5.3, the higher the value of the Maximum angle parameter applied on photogrammetric point cloud, the lower the effect of remaining parameters. With the Maximum angle of 20°, the elevation bias stabilized at approx. 0.20 m. With this value of Maximum angle, the algorithm was insensitive to the cell size. For LiDAR point cloud, the Cell size parameter elicited the greatest effect. With the value of Maximum distance set to 1 m and

Maximum angle higher than 10°, the Cell size of 25 and 50 m led to the best performances in terms of random-error and bias combination. The RMSE for tested parameters ranged 0.19–0.89 m and 0.23–1.08 m for LiDAR and photogrammetric point cloud, respectively.
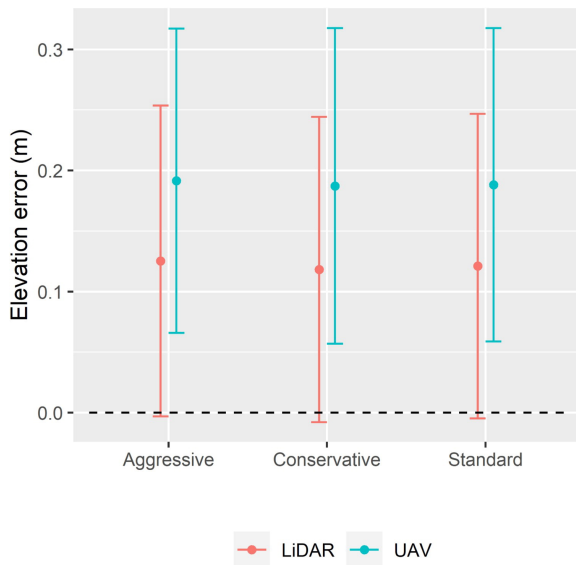
Figure 5.4: Sensitivity analysis of the algorithm implemented in ArcGIS.

The ArcGIS algorithm allows three settings of *Ground detection method*, namely *Aggressive*, *Conservative*, and *Standard*. The type of the point cloud (LiDAR vs photogrammetric) was, however, the principal difference-causing variable (see Figure 5.4), the former point cloud being overestimated by approx. 0.12 m, whereas the latter was overestimated by almost 0.20 m. For all parameter-point cloud combinations, however, a relatively large random error of about 0.13 m was observed. Consequently, it can be concluded that with both point cloud types, the choice of the parameter setting has practically no effect on the algorithm performance. The RMSE for tested parameters were 0.17–0.18 m for LiDAR point clouds and 0.23 m for photogrammetric point cloud.

The Cloth Simulation Filter (CSF) algorithm implemented in Cloud-Compare uses four main parameters: *Slope processing* (True/False),
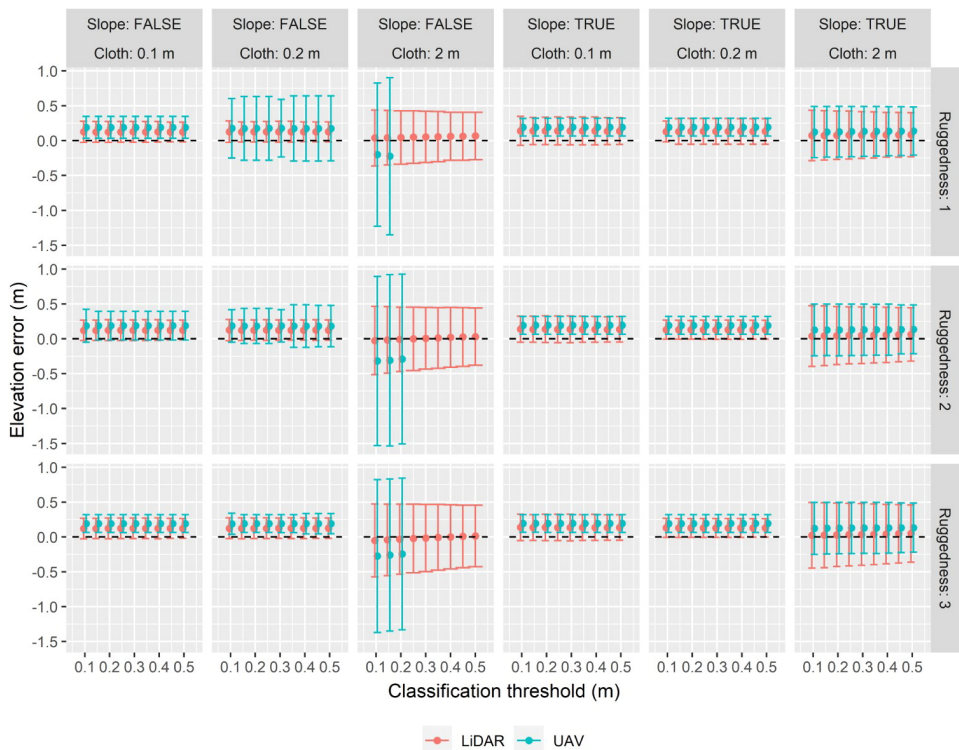
Figure 5.5: Sensitivity analysis of the Cloth Simulation Filter (CSF) algorithm implemented in the CloudCompare software.

Cloth resolution (m), *Ruggedness* (1 – "Mountain", 2 – "Complex", or 3 – "Flat"), and *Classification threshold* (m). The greatest effect was observed for the Cloth resolution parameter (see Figure 5.5), with the value of 0.1 m leading to the best performances in terms of random-error and bias combination. It should be noted, however, that for LiDAR point cloud, the parameter Cloth resolution 2 m in combination with either Slope processing False, or Slope processing True and Ruggedness 2 or 3, lead to almost zero bias, although the random error was relatively high. The algorithm generally performed slightly better for the LiDAR data than for the UAV data. The parameter Classification threshold was practically irrelevant. The RMSE for all tested parameters ranged between 0.18–0.53 m for LiDAR point cloud and 0.23–1.26 m for photogrammetric point cloud.
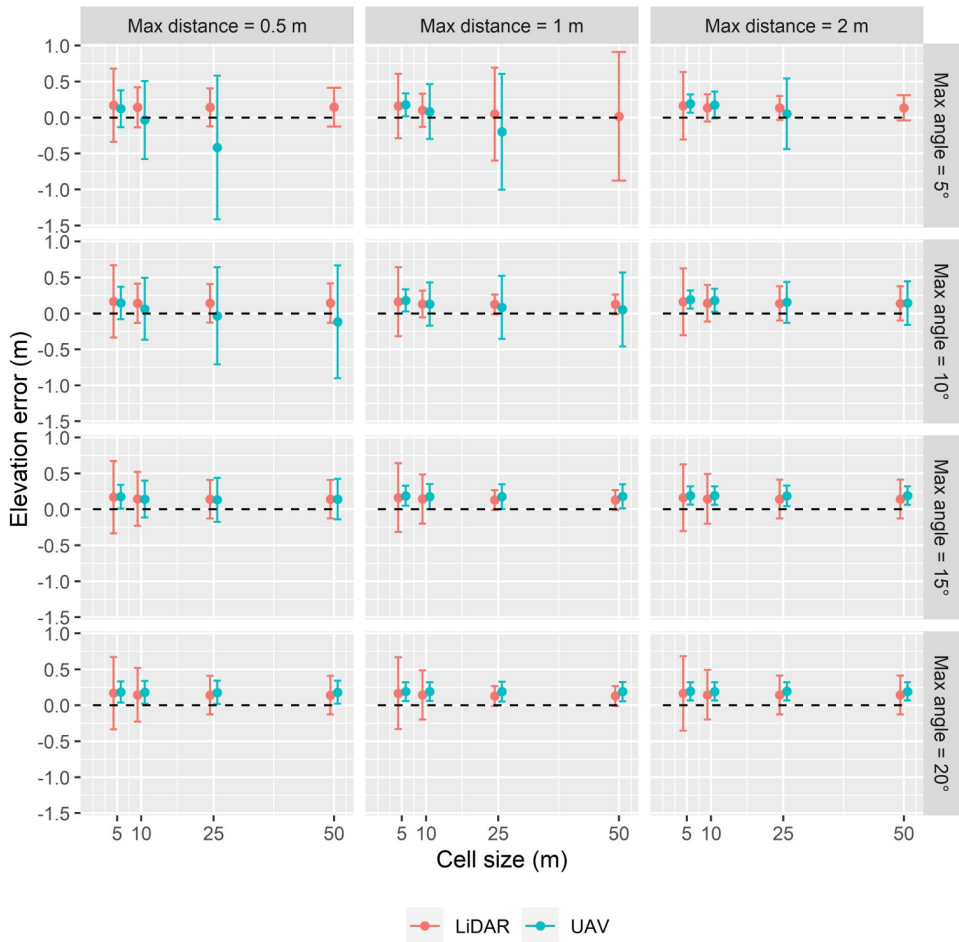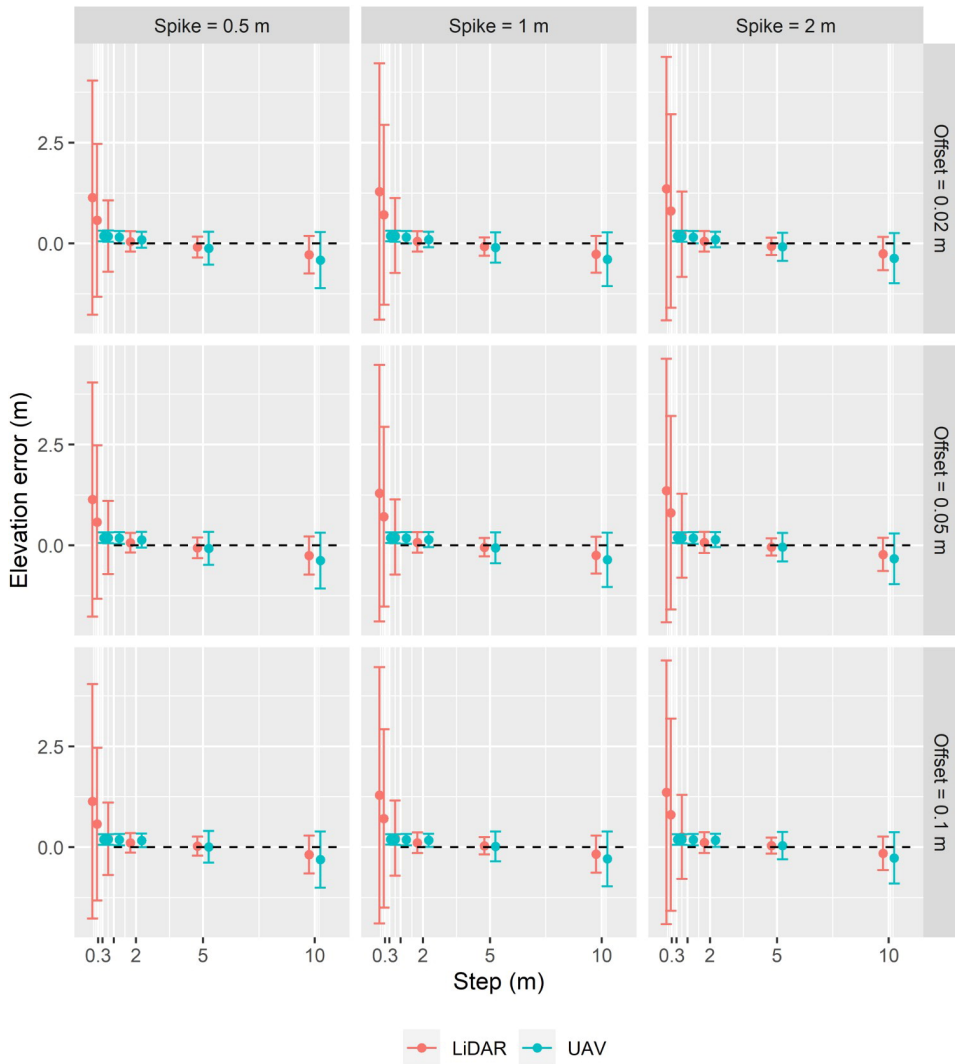
Figure 5.6: Sensitivity analysis of the Progressive Triangulated Irregular Network (PTIN) algorithm implemented in the LAStools software.

The Progressive Triangulated Irregular Network (PTIN) algorithm as implemented in LAStools is controlled by three principal parameters: *Spike* (m), *Offset* (m), and *Step* (m). Figure 5.6 shows a major difference between LiDAR and photogrammetric point clouds for small values of the Step parameter (up to approx. 1 m). For larger Step values (> 2 m), however, this difference diminishes. The best results, both in terms of random error and bias, were obtained for Step values between 2 and 5

m (although for the photogrammetric point cloud, even smaller values led to a slightly lower error variance but slightly higher overestimation). The effect of the other two parameter was negligible. The RMSE for all tested parameters ranged 0.15–3.54 m for LiDAR point cloud, and 0.21–0.80 m for photogrammetric point cloud.
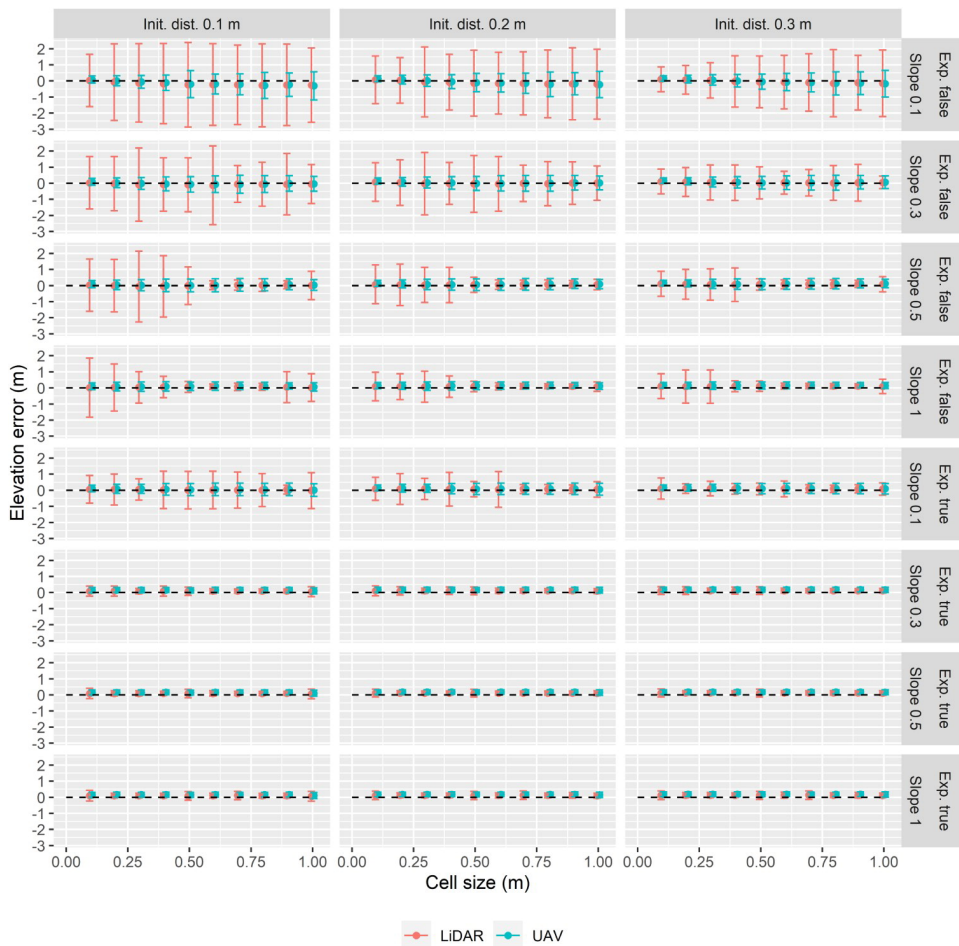
Figure 5.7: Sensitivity analysis of the PMF algorithm implemented in the PDAL software.

The Progressive Morphological Filter (PMF) algorithm implemented in the PDAL software allows four settings: *Initial distance* (m), *Slope* (−), *Cell size* (m) and *Exponential* (true/false). As Figure 5.7 shows, the algorithm performed generally better with the photogrammetric than

with LiDAR point cloud. The Exponential parameter turned out to be the most important setting in our experiment. Setting it as True and combining with Slope values greater than 0.1 led to considerably lower error variances as well as much smaller differences between point clouds. With these settings, both the Cell size and Initial distance parameters were without effect. The RMSE ranged between 0.15–3.04 m for LiDAR and 0.20–1.43 m for photogrammetric point cloud.
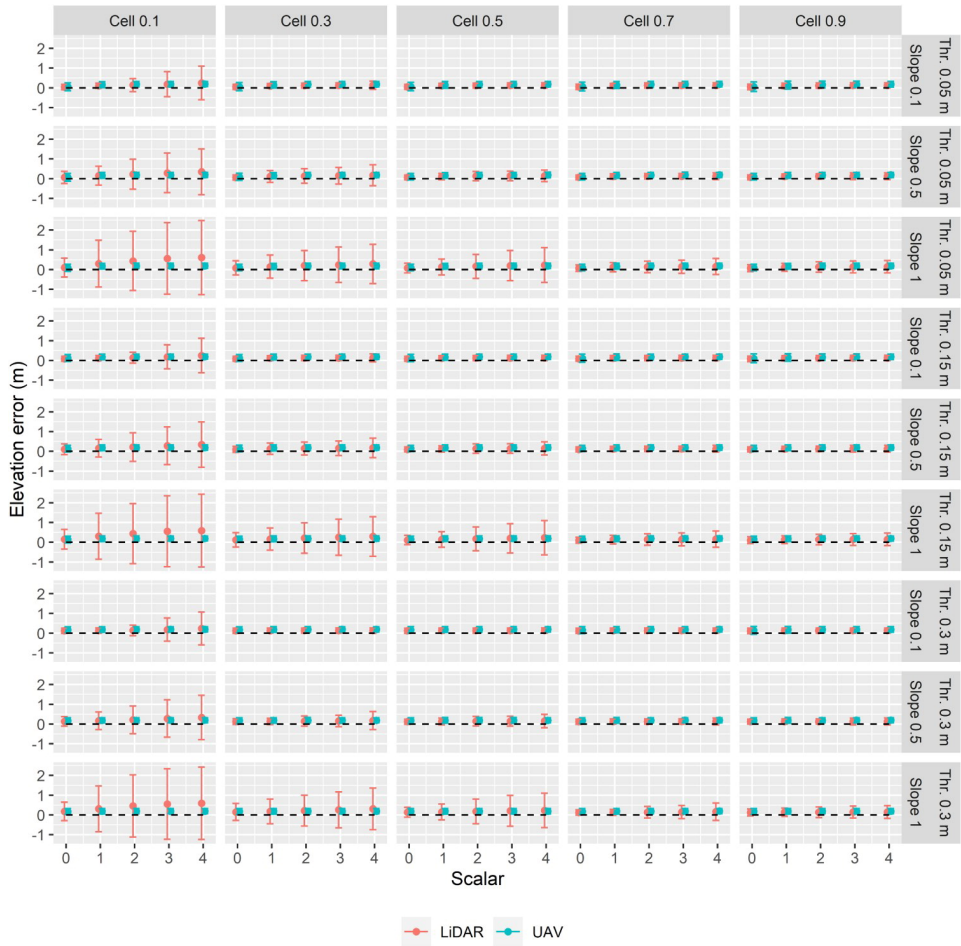
Figure 5.8: Sensitivity analysis of the SMRF algorithm implemented in the PDAL software.

The Simple Morphological Filter (SMRF) algorithm implemented in the PDAL software also offers four parameters: *Cell* (m), *Scalar* (–),

Threshold (m), and *Slope* (−). Similarly to the PMF algorithm, the algorithm produced much better results with photogrammetric point cloud, especially for lower values of the Cell parameter (see Figure 5.8). Increasing the value of this parameter improved the performance with LiDAR point cloud, even to the level of being comparable to results obtained with the photogrammetric point cloud. Less importantly, the higher the value of the Scalar parameter, the higher both the overestimation and error variance. The slope and threshold parameters didn't affect the elevation error substantially. The RMSE for tested parameters ranged between 0.13–1.97 m for the ALS point cloud and between 0.19–0.26 m for the photogrammetric one, respectively.

5.3.2   Quantitative Comparison of Algorithms

Based on the sensitivity plots, the summary of optimal combinations of parameters selected for our study area can be found in Table 5.4. In terms of RMSE, all algorithms yielded very good results, with RMSE ranging from 0.13 m (SMRF algorithm with LiDAR point cloud) to 0.23 m (ATIN algorithm with UAV data). LiDAR – on average – performed 0.05 m better than the photogrammetric point cloud. At the same time, regardless of the point cloud, PTIN, PMF and SMRF performed 0.03– 0.05 m better than ATIN, ArcGIS or CSF. All algorithms overestimated the terrain, and the differences in ME ± SD among algorithms and point clouds followed the same pattern as in RMSE. Overestimation was – on average – 0.05 m lower for LiDAR than for photogrammetric point cloud. With LiDAR data, the best performing algorithm was SMRF with 0.04 ± 0.13 m overestimation, followed by PMF and PTIN with overestimation of 0.08 ± 0.12 and 0.10 ± 0.12 m, respectively. ATIN, ArcGIS and CSF all overestimated the terrain by approx. 0.12–0.13 (± 0.13–0.14) m. With photogrammetric point cloud data, PTIN, PMF and SMRF algorithms overestimated the terrain by approx. 0.10–0.12 (± 0.16–0.19) m, whereas ATIN, ArcGIS

and CSF all showed relatively highest overestimation of 0.19 ± 0.13 m (Table 5.4).

Table 5.4: Best results achieved by evaluated algorithms.

Platform	Algorithm	RMSE [m]	ME [m]	SD [m]	Parameters
LiDAR	ATIN	0.187	0.126	0.139	Max angle: *10*; Max distance: *1*; Cell size: *50*
	ArcGIS	0.175	0.121	0.126	Ground detection method: *Standard*
	CSF	0.186	0.129	0.134	General settings: *Flat*; Slope processing: *enabled*; Cloth resolution: *0.2*; Classification threshold: *0.25*
	PTIN	0.154	0.098	0.119	Predefined: *Nature*
	PMF	0.147	0.079	0.123	Exponential: *true*; Cell size: *0.9*; Initial distance: *0.05*; Max distance: *63.0*; Max window size: *33*; Slope: *0.3*
	SMRF	0.132	0.040	0.126	Cell size: *0.4*; Threshold: *0.05*; Slope: *0.1*; Scalar: *0.0*; Window: *18*
UAV	ATIN	0.231	0.193	0.127	Max angle: *10*; Max distance: *2*; Cell size: *5*
	ArcGIS	0.228	0.187	0.130	Ground detection method: *Conservative*
	CSF	0.230	0.192	0.127	General settings: *Flat*; Slope processing: *enabled*; Cloth resolution: *0.1*; Classification threshold: *0.1*
	PTIN	0.214	0.096	0.191	Step: *2*; Spike: *2*; Offset: *0.02*
	PMF	0.200	0.117	0.162	Exponential: *true*; Cell size: *0.5*; Initial distance: *0.05*; Max distance: *63.0*; Max window size: *33*; Slope: *0.5*
	SMRF	0.194	0.104	0.163	Cell size: *0.8*; Threshold: *0.05*; Slope: *0.5*; Scalar: *0.0*; Window: *18*

All predictors (algorithm, slope, vegetation type, and point cloud) proved to have an effect on the ground filtering accuracy, with a complex interaction structure (see Table 5.5). The model explained 67% of the elevation error variability (Nakagawa and Schielzeth conditional R^2). The elevation error variability between the checkpoints (i.e., the random-effect standard deviation) was 0.106 m (the profiled confidence interval: 0.101; 0.110); the residual standard deviation was 0.087 m (the profiled

confidence interval: 0.086; 0.088).

The interaction structure of the model can be described as follows (see Table 5.5): (1) there were significant pair-wise interactions between the algorithm, slope, and vegetation type; (2) all these pair-wise interactions as well as all the main effects differed significantly between photogrammetric and LiDAR point clouds. Further insight into the

Table 5.5: Analysis of deviance table (Type II) for linear mixed-effect models of elevation difference on algorithm, slope, vegetation type, and point cloud.

Predictor	χ^2	DF	p value
Algorithm	2938.663	5	< 0.001
Slope	1.675	1	0.196
Vegetation type	99.139	3	< 0.001
Cloud	1412.076	1	< 0.001
Algorithm: Slope	83.116	5	< 0.001
Algorithm: Vegetation type	166.756	15	< 0.001
Slope: Vegetation type	16.587	3	0.001
Cloud: Algorithm	363.605	5	< 0.001
Cloud: Slope	386.507	1	< 0.001
Cloud: Vegetation type	371.418	3	< 0.001
Cloud: Algorithm: Slope	30.106	5	< 0.001
Cloud: Algorithm: Vegetation type	226.515	15	< 0.001
Cloud: Slope: Vegetation type	93.933	3	< 0.001

DF – Degrees of freedom.

effects of predictors can be gained from the effect plots (Figure 5.9). Clearly, the differences between algorithms follow a similar pattern across the values of the other predictors. Namely, the ATIN, ArcGIS, and CSF algorithms were almost indistinguishable in their effect on ground filtering accuracy and performed generally poorer than the remaining three algorithms (PTIN, PMF, SMRF). Among remaining algorithms, SMRF performed in most cases best when using LiDAR point cloud. For the photogrammetric point cloud, the performance of those three algorithms (i.e., PTIN, PMF, and SMRF) differed with slope. In higher slopes, the SMRF algorithm again performed best but in lower slopes, the performance of PTIN was similar or better. The

LiDAR point cloud elevation error increased with the slope. For the photogrammetric point cloud, however, this relationship was sometimes reversed, especially in the case of SMRF algorithm.
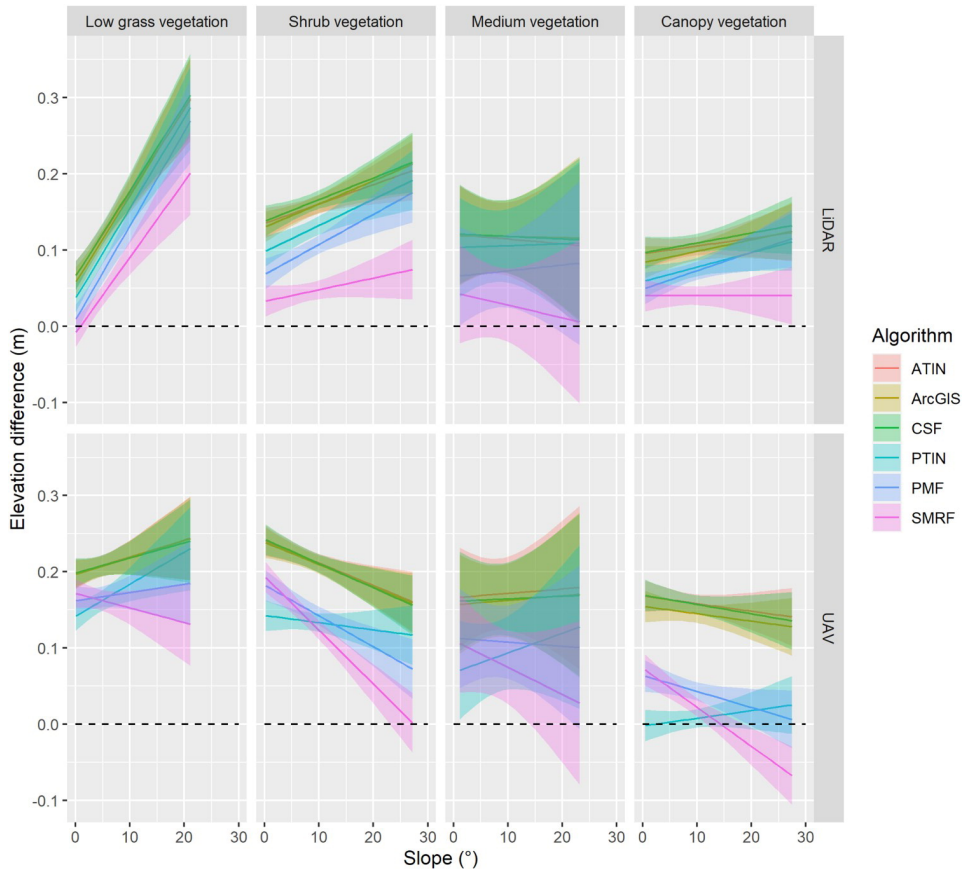
Figure 5.9: Effect plots for fixed effects of the linear mixed-effect model of elevation difference on algorithm, slope, vegetation type, and point cloud (UAV photogrammetry vs LiDAR). The confidence bands are based on the point-wise Wald confidence intervals conditional on the estimates of the random-effect variance.

5.4   Discussion

We compared six ground filtering algorithms implemented in five software solutions (ArcGIS, CloudCompare, LAStools, Metashape, PDAL)

to extract ground from LiDAR and photogrammetric (UAV-based, acquired under leaf-off conditions) point clouds. All algorithms achieved promising results. However, their performance differed with respect to the type of the point cloud (photogrammetry, LiDAR) and environmental conditions (i.e., vegetation density and terrain slope).

The results were generally better for LiDAR point clouds than for photogrammetric ones, which corresponds to the fact that the algorithms were originally developed for LiDAR data and assume the ability of LiDAR pulses to penetrate through gaps in vegetation canopies. The RMSEs of the DTM derived from LiDAR point cloud ranged from 0.13 to 0.19 m. The terrain accuracy (in terms of both random-error and bias) decreased with increasing slope (Figure 5.9). The mean bias tended to increase with slope, especially in the low grass vegetation class. The same pattern was observed for example by Hollaus et al. (2006). However, they found a mean bias of 0.15 to 0.25 m for slopes steeper than approximately 30°, while we observed the same bias for slopes steeper than approximately 10°. We assume that to be due to the presence of vegetation close to the ground, which is more problematic to filter out on the relatively steep slopes. Such vegetation is not present under canopy vegetation (i.e., in forests), which is also evident from our photogrammetric UAV-based point cloud acquired under leaf-off conditions that has lower bias under canopy vegetation than in low vegetation class due to the same effect of persisting dry vegetation. The higher random-error (i.e., the width of confidence intervals) observed on steep slopes can be attributed to relatively low number of validation points especially in case of medium vegetation class at higher slopes. To lower degree it might be also affected by relative horizontal displacements of the DTM and validation checkpoints (e.g., Hodgson and Bresnahan 2004). Similarly, Estornell et al. (2011) observed gradual deterioration of LiDAR derived DTM and increase in random error with increasing slope. In addition, Hyyppä et al. (2005) showed that increase in random error with increasing slope is often more dramatical

under tree canopy then in open areas. We also observed the increase in random-error as the slope increased in all vegetation classes, however, the difference between low grass vegetation and canopy vegetation classes was minimal.

With RMSE ranging from 0.19 to 0.23 m, we achieved similar accuracy for photogrammetric point clouds as for LiDAR point clouds. Our results show that in areas of low grass vegetation and low terrain slope (Figure 5.9), the acquired DTMs accuracy is similar for all algorithms. However, the overestimation of terrain was slightly higher for photogrammetric than for LiDAR point clouds, especially in flat or moderate-slope terrain (Figure 5.9). As already mentioned, this can be attributed to presence of low dry vegetation that persists in the study area even in winter and reduce the visibility of ground, but can be penetrated by LiDAR (e.g., Spaete et al. 2011). All algorithms yielded the worst results in areas of shrub vegetation, consistently with LiDAR point clouds. In contrast to the LiDAR point clouds where the performance of all algorithms clearly decreased with increasing slope, results were different with photogrammetric point clouds; the same can be said about the effect of vegetation. With the increase of the terrain slope and with the increasing representation of dense high vegetation, two groups of algorithms with different behavior could be distinguished. The first group consists of ATIN, ArcGIS, and CSF algorithms while the second group includes PTIN, PMF, SMRF algorithms. The algorithms within the first group behave relatively consistently and their performance slightly increases with increasing slope. The second group of algorithms performs better than the first group under the vegetation canopy but SMRF underestimate terrain in areas of high slope.

Our results show an improvement in DTMs accuracy with increasing slope (except for the PTIN algorithm implemented in LAStools) for photogrammetric point clouds. However, areas of high slope are typically problematic for ground filtering of both LiDAR and photogrammetric point clouds (e.g., Meng et al. 2010). On the other hand,

Serifoglu Yilmaz et al. (2018), for example, also found better results for the area with higher slopes. High slopes are typically problematic in combination with vegetation (e.g., branches) close to the ground (Serifoglu Yilmaz et al. 2016). The improvement with slope can be related to the presence of grass vegetation in flat non-forested areas, which cause slight overestimation (Tan et al. 2018), while (at least in our study area), the steep slopes are predominantly overgrown by forest and the shrub vegetation is not present. However, we did not find any interaction between vegetation density and slope. This may be explained by the fact that LiDAR data used for vegetation density estimation were acquired in May during leaf-on period and it is likely that different vegetation prevailed at this time (Moudrý et al. 2019b). Besides, SMRF underestimated the terrain in areas of high slope which is likely due to the fact that ground points were not identified in areas of steep slope and the terrain was interpolated.

Moreover, our results corroborate with other studies and show that shrub vegetation has a profound negative effect on filtering algorithms (with both types of point clouds). Recently, for example, Graham et al. (2019) showed that in case of photogrammetric point clouds, the canopy cover is three times more influential than terrain slope. In our study area, however, the effect of vegetation on filtering of photogrammetric point clouds was relatively lower than in other studies. The most notable problems were observed in areas with dense vegetation close to the water bodies; only ArcGIS and partly PTIN were able to filter it. Moreover, the effect of vegetation density and terrain slope on the resulting terrain accuracy was significantly lower than that of filtering algorithms, which indicates that important differences exist in performance of ground filtering algorithms with photogrammetric point clouds in our study area.

The algorithms evaluated by prior studies vary significantly and most algorithms tested in this study were already included in some comparative study (Sithole and Vosselman 2004, Montealegre et al. 2015, Polat

and Uysal 2015). However, this is the first study that included the algorithm implemented in ArcGIS into the comparison. It achieved very good results with both types of point clouds (RMSE 0.18 m for LiDAR and 0.23 m for photogrammetric point cloud, respectively), but in particular, it outperformed other methods when used for the photogrammetric point cloud; unfortunately, it is considered proprietary solution. The PTIN algorithm implemented in LAStools also achieved very good results with both types of point clouds (RMSE 0.15 m for LiDAR and 0.21 m for photogrammetric point cloud, respectively) and it was the only algorithm with consistent behavior across various terrain slopes and vegetation density regardless of the point cloud type. Wallace et al. (2019) showed that in dense forested areas where ground points are missing, PTIN often misclassifies high dense vegetation as ground. In our study, however, this problem was not observed, probably due to the fact that we used photogrammetric point clouds acquired under leaf-off conditions. In contrast to Wallace et al., Zeybek and Şanlıoğlu (2019) compared four ground filtering algorithms (Multiscale Curvature Classification, Surface-based filtering, PTIN, and CSF) and recommended PTIN implemented in LAStools as suitable for UAV-based point clouds of forested areas. In addition, Zhang et al. (2018) showed that PTIN is relatively robust to random noise inherent in photogrammetric point clouds. Similarly, Graham et al. (2019) found that PTIN was able to model terrain more accurately than SMRF over larger areas. Our results also suggest it as a good option due to its robustness and (therefore) consistent behavior with both types of point clouds.

Algorithms implemented in non-commercial software also achieved good results; both PMF and SMRF filters resulted in accurate DTMs. While SMRF (RMSE 0.13 m for LiDAR point cloud and 0.19 m for photogrammetric point cloud, respectively) performed better than PMF with LiDAR point cloud, PMF (RMSE 0.15 m for LiDAR point cloud and 0.20 m for photogrammetric point cloud, respectively) was a little

bit more successful than SMRF in canopy vegetation class with the photogrammetric point cloud. The worst results in our study area were achieved by CSF (RMSE 0.19 m for LiDAR point cloud and 0.23 m for photogrammetric point cloud, respectively) for both types of point clouds, which is likely due to the terrain complexity as other studies show good performance in flat terrains (Tan et al. 2018) or areas dominated by buildings (Serifoglu Yilmaz et al. 2018).

5.5   Conclusions

In this study, we compared the performance of six algorithms for ground filtering of LiDAR and photogrammetric point clouds of the same study area. The accuracy of the filtered point clouds was investigated by comparing generated DTMs with data acquired using traditional surveying methods. All tested ground filtering algorithms achieved relatively good results but their performance was affected by the terrain slope and vegetation cover. In addition, we found that while the behavior of all algorithms was consistent for LiDAR point clouds (i.e., decreasing accuracy with terrain slope and presence of low vegetation), it was disparate in case of photogrammetric point clouds. The only robust exception behaving consistently with both LiDAR and photogrammetric point clouds was the PTIN algorithm implemented in LAStools.

The most influential parameters did not differ between LiDAR and photogrammetry point clouds. For all algorithms, the most influential were those related to selection of the initial minimum elevation ground points (i.e., Cell size for ATIN, PMF, SMRF, Step size for PTIN and Cloth resolution for CSF). Other parameters had only minor effect and were important rather for fine tuning of ground filtering. For point cloud datasets that are of similar vegetation structure and slope as our study area, we recommend the following settings: for ATIN algorithm a Cell size ≥ 25 m for LiDAR and ≤ 10 m for photogrammetric point cloud,

respectively. In case of PMF and LiDAR, a Cell size ≥ 0.5 m is the most suitable while ≤ 0.3 m is preferable in case of photogrammetric point cloud. This is almost the same for SMRF, where for LiDAR point cloud, we recommend a value ≥ 0.5 m and in case of photogrammetric point cloud, ≤ 0.4 m. In case of PTIN, the difference in parameters is more noticeable; the Step size recommended for LiDAR should be between 2 and 5 m while in case of photogrammetric point cloud, the optimal value is ≤ 1 m. In case of LAStools, the use of predefined options is also worth considering. In case of CSF, which is based on different principles than previous algorithms, the most suitable parameters are similar for both types of point clouds (photogrammetric and LiDAR) and we can recommend Cloth resolution value from 0.1–0.2 m. Note however, that these are recommendations for initial testing only and that fine tuning of parameters is always necessary.

It is obvious that there is no universal ground filtering algorithm that would outperform the others and the visibility of ground from multiple views is the primary and necessary prerequisite for the ground detection and classification of photogrammetric point clouds (and hence for successful generation of accurate DTMs). In this study, we successfully avoided problems with uneven distribution of ground points and presence of high vegetation resembling ground using leaf-off imagery. Our results provide necessary guidelines for practitioners working with ALS and photogrammetric point clouds.

Chapter 6

Comparison of Leaf-off and Leaf-on Combined UAV Imagery and Airborne LiDAR for Assessment of a Post-Mining Site Terrain and Vegetation Structure: Prospects for Monitoring Hazards and Restoration Success

Vítězslav Moudrý, Kateřina Gdulová, Michal Fogl, **Petr Klápště**, Rudolf Urban, Jan Komárek, Lucie Moudrá, Martin Štroner, Vojtěch Barták, Milič Solský

Author's contribution: 20%

Abstract

Mining is an important human activity that significantly affects the landscape character, particularly through excavation of spoil material and its deposition on spoil banks. The information on terrain or vegetation cover of spoil banks is often required for two different reasons: (i) to monitor and prevent adverse effect of hazards associated with unstable terrain; and (ii) to assess restoration success. Traditionally used in situ methods for monitoring surface displacement or restoration success are restricted in terms of spatial and temporal coverage. Therefore, in this study, we assessed the value of photogrammetrically and Light Detection and Ranging (LiDAR) derived point clouds for characterizing a post-mining site. We acquired images under leaf-off and leaf-on conditions and showed that point densities of point clouds acquired photogrammetrically under leaf-off conditions exceeded densities of those acquired under leaf-on conditions and uniformly covered ground of the entire study area (an average density of 288 points per m^2). In addition, the accuracy of the digital terrain model (DTM; 1 m resolution) derived from images acquired under leaf-off conditions was comparable to the LiDAR-derived DTM (RMSE of 0.19 m and 0.12 m, respectively). While LiDAR-derived DTM accuracies were consistent across vegetation categories (RMSE 0.12–0.14 m), accuracy of image-based DTMs declined in the following order: forest (RMSE 0.15 m), steppes (RMSE 0.21 m), and aquatic vegetation (RMSE 0.36 m). We suggest the leaf-off UAV imagery as a viable alternative for building DTMs that can be utilized for assessment of risks associated with instability of spoil banks terrain. In addition, we also suggest that a combination of acquisitions under leaf-off and leaf-on conditions have a potential to replace expensive airborne LiDAR surveys for applications requiring information on vegetation cover or vegetation height.

Keywords: Forest, Leaf-off, Leaf-on, Mining, Structure from motion, Vegetation

6.1 Introduction

Mining is an important human activity with strong social, environmental, and economic impacts (Lechner et al. 2017). It significantly affects landscape character, including ecological stability (Hendrychová and Kabrna 2016, Popelková and Mulková 2018), aesthetic value (Svobodova et al. 2012), and morphology (Tarolli and Sofia 2016, Brown et al. 2017). Open-pit mining and associated extensive disturbances, especially within the coal mining industry, significantly influence large areas. This involves formation of large pits as well as deposition of the excavated spoil material on spoil banks.

Mining is in general associated with geomorphic processes such as erosion, subsidence, landslides and runoff (Tarolli and Sofia 2016). This is particularly true for spoil banks that are for various reasons (e.g. slope inclination, composition of waste material, subterranean combustion), especially prone to erosion (Haigh and Gentcheva-Kostadinova 2002, Hancock et al. 2008, Nyssen and Vermeersch 2010), terrain subsidence (Bell and Donnelly 2006, Dulias 2016, Sedlák et al. 2018), and landslides (Steiakakis et al. 2009, Cho and Song 2014, Bednarczyk 2017, Wasowski et al. 2018). To be able to study these processes or even to identify instability problems and to prevent potential adverse effects of such events (or at least minimize their impact), the knowledge of spoil banks terrain and vegetation cover is essential. Besides, spoil banks have been shown, curiously enough, to become important biodiversity refuges (e.g. Harabiš et al. 2013, Harabiš 2016). Hence, information on the terrain and vegetation cover of spoil banks is not only needed for studying geomorphic processes but is also useful for assessment of their conservation value (Doležalová et al. 2012) and for understanding factors affecting the successional trajectory (Frouz et al. 2018) or restoration success (Vymazal and Sklenicka 2012, Wortley et al. 2013).

To efficiently manage spoil banks, namely for detection and quantification of terrain changes (e.g. Xiang et al. 2018) or terrain stability

analyses (e.g. Close et al. 2016, Stephenne et al. 2014, Zalesky and Capova 2017), repeated topographic surveys and information on vegetation cover are required. The traditional techniques used to monitor spoil banks terrain such as total station and GNSS surveys are expensive and restricted in terms of spatial and temporal coverage (e.g. Zalesky et al. 2008, Hogarth et al. 2017). Similarly, terrain topography and vegetation cover used by restoration ecologists are usually determined by spatially limited and simple categorical variables due to the labour intensive field collection of data (e.g. Šálek 2012, Harabiš et al. 2013, Vojar et al. 2016). A great benefit of remote sensing over more traditional techniques lies in its ability to provide continuous information over a large area. However, references to the use of remotely sensed data for monitoring or restoration success assessment of post-mining sites are scarce (Wężyk et al. 2015, Cordell et al. 2017, Koska et al. 2017, Cmielewski et al. 2018).

Remote sensing methods commonly used to collect data for generation of digital terrain models (DTMs) and derivation of vegetation cover variables include terrestrial and airborne light detection and ranging (LiDAR; Wehr and Lohr 1999) and, more recently, Structure from Motion (SfM) and Multi-View Stereo (MVS) photogrammetry workflows (Fonstad et al. 2013, Smith et al. 2016). Although airborne laser scanning (ALS) data are increasingly available, sometimes even free of charge (in some European countries, for example, they are available through government agencies; e.g. Fogl and Moudrý 2016, Langhammer et al. 2018), the coverage is still lacking in many countries (e.g. Hofierka et al. 2018) and high acquisition costs limit a wider use of the data when repeated measurements are needed. In contrast, photogrammetric methods offer low-cost alternatives for repeated measurements, especially so in combination with unmanned aerial vehicles (UAVs), which makes such a combination a potentially valuable and practically applicable tool for monitoring of terrain and vegetation cover changes (e.g. van Iersel et al. 2018, Xiang et al. 2018).

The DTM generation is however affected by vegetation cover and the prospects to acquire accurate DTMs under dense vegetation canopies are limited. Spoil banks are usually covered by heterogeneous vegetation, which further complicates the use of photogrammetric methods. Negative effects of vegetation on building of DTMs have been reported for various types of environment and vegetation cover. Forested areas are among the most challenging environments and failure to record a single ground point in such areas is not uncommon. For this reason, recent studies on the use of photogrammetric methods in forests mostly focus on partially open canopies. For example, Kachamba et al. (2016) derived a DTM from UAV imagery in order to estimate biomass at miombo woodlands. Jensen and Mathews (2016) showed that in a woodland ecosystem in Texas, SfM DTM provided a suitable representation of the bare ground under a vegetation cover (compared to LiDAR-derived DTM). More recently, Tomaštík et al. (2017) assessed the quality of a DTM under temperate broadleaf and mixed forests derived from UAV imagery with different level of canopy openness.

The obvious advantage of LiDAR is the ability of the pulses to penetrate through gaps in vegetation canopies and registering multiple returns representing both canopy and terrain. Many studies concentrated on the accuracy of LiDAR-derived DTMs in dense forest environments that might be difficult to penetrate even for LiDAR pulses, such as tropical forests (e.g. Clark et al. 2004) or temperate coniferous forest (e.g. Reutebuch et al. 2003). Only few studies, however, concentrated recently on temperate deciduous forests, which are among the principal canopies in our study. For example, Aryal et al. (2017) evaluated a DTM accuracy in temperate forests of Bavarian forests national park, Balenović et al. (2018) in an oak forest in Central Croatia, and Simpson et al. (2017) in mixed deciduous woodland in northeast England.

In the case of deciduous forest stands, a promising strategy to generate accurate DTM is to use images acquired under leaf-off conditions – an approach that has been only scarcely tested for photogrammetric

methods (Dandois and Ellis 2013, Ni et al. 2015, DeWitt et al. 2017) but commonly used for ALS data acquisition (e.g. Hodgson et al. 2005). Bare ground is clearly visible on the leaf-off imagery and the DTM accuracy similar to that derived over non-vegetated surfaces can be therefore expected; however, leaf-off imagery may include complex shadowing and branch patterns and the quality (and extent) of the terrain visibility strongly depends on the density of forest stands.

The general aim of this study was to assess the value of photogrammetrically and LiDAR-derived data for characterizing a post-mining site. We acquired ALS data during summer (leaf-on period) and UAVborne imagery during different seasons (summer, spring, winter) and we (1) assessed the character of the generated point clouds with emphasis on the ability to capture bare earth and compared results yielded by both methods; (2) assessed whether the accuracy of SfM-derived DTMs can be improved by acquisition of images under leaf-off conditions and hence potentially used in combination with leaf-on conditions to estimate vegetation cover characteristics; and (3) evaluated the influence of vegetation cover (aquatic vegetation, steppes, and forests) on the DTM quality.

6.2 Materials and Methods

6.2.1 Study Area

The present study was conducted on an area of 61 ha located in the southern part of the Hornojiřetínská spoil heap in the Most basin (northwest Bohemia, Czech Republic, 50°34'N, 13°34'E, Figure 6.1). The spoil heap's elevation ranges from 220 m to 280 m above sea level. Due to plans to mine the underlying coal seam in the future, this part of the Hornojiřetínská spoil heap has never been technically reclaimed. The terrain morphology has remained rugged as a result of heaping that

has formed a typical undulated terrain and consequently heterogeneous vegetation (e.g. Doležalová et al. 2012, Frouz et al. 2018). The vegetation is in a late succession stage 35–50 years after heaping and consists of aquatic vegetation in terrain depressions (e.g. *Phragmites australis* and *Typha latifolia*), steppes (low vegetation, especially *Calamagrostis epigejos* and *Arrhenatherum elatius* with scattered shrubs and trees, for example *Sambucus*, *Rosa*, *Betula*, *Crataegus*), and forests. Three forest types are present in our study area; homogenous plantations of even-aged growth of European ash (*Fraxinus excelsior*; eastern part of the study area), spontaneously grown forest dominated by Birch (*Betula pendula*; central part of the study area), and mature forests of Willow (*Salix spp.*) and Alder (*Alnus spp.*) (western part of the study area; Table 6.1, Figure 6.1).

6.2.2   ALS and UAV Image Data Collection

Airborne LiDAR data was collected over the study area in May 2017 using a remote sensing platform FLIS (The Flying Laboratory of Imaging Spectroscopy) (Hanuš et al. 2016). Although the system is equipped with a Riegl LMS-Q780 full-waveform laser scanner, we used only discrete return data. The scanner has a rotating polygon mirror and scans in parallel lines. The scan field of view is 60° and the wavelength is 1064 nm. Flights for data collection were conducted at 1030 m above ground with a velocity of 110 knots (ground speed) and with 55% flight line side overlap, which provided the average density of 7.7 points per square meter.

A home-assembled UAV consisting of an Easy Star II airframe by Multiplex and 3DR Pixhawk autopilot equipped with a Nikon Coolpix A camera (28 mm prime lens with f/2.8) was used for the series of flights (in different phenological conditions) over the study area. Hereafter, we refer to these three flights as Winter (11 March 2017 – leaf-off), Spring
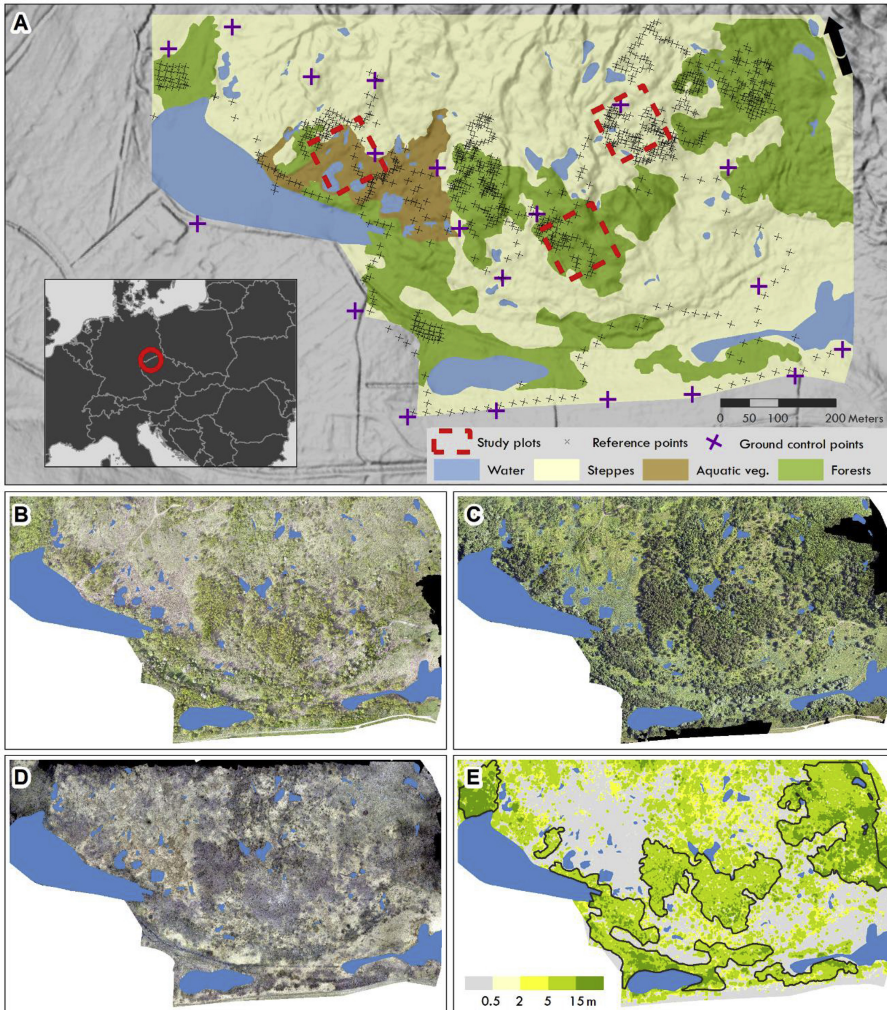
Figure 6.1: Study Area. (A) Hill-shaded terrain and location of the study area in the southern part of the Hornojiřetínská spoil heap in the Most basin (northwest Bohemia, Czech Republic, 50°34'N, 13°34'E); (B) Spring orthophotomap; (C) Summer orthophotomap; (D) Winter orthophotomap; (E) Canopy height model. The study plots were used for visual comparison of DTMs, see Figure 6.4

(29 April 2016 – partly leaf-on), and Summer (1 July 2016 – leaf-on) flights. Parallel flight lines were set to acquire an image overlap of 85% and sidelap of 65%. Approximately 1000 images were taken during each survey from an average flight altitude of 100 m above ground level, resulting in a 3 cm ground sampling distance. The camera settings

were manually set to ISO 400 and shutter speed priority 1/1250 s.

Table 6.1: General characteristics of the study area. Maximum, mean and standard deviation of height are calculated from a LiDAR derived pit free Canopy Height Model (LiDAR data were collected in May). Other characteristics are calculated directly form LiDAR classified point cloud. Canopy cover is calculated as the number of first returns above breast height (1.37 m) divided by the number of all first returns. Density of ground, shrubs and trees are number of returns in each height interval divided by total number of returns.

Vegetation type	Area	Canopy	Height [m]		
	[ha]	cover [%]	Max.	Mean	Std. dev.
Aquatic	3.4	4	16.5	0.5	94.4
Steppe	38.5	25	27.1	3.6	69.4
Forest	19.0	63	29.4	11.5	37.5
Vegetation type	Density [%]				
	Ground and low vegetation		Shrubs	Low trees	High trees
	(< 0.3 m)		(0.3–3 m)	(3–15 m)	(> 15 m)
Aquatic	94.4		2.5	3.0	0.0
Steppe	69.4		7.7	22.1	0.8
Forest	37.5		4.4	47.2	10.9

6.2.3 Ground Control Points and Verification Data Survey

Prior to UAV flights, 20 ground control points in the form of white square fiberboard targets (40×40 cm) with black round centre (15 cm in diameter) were distributed over the study area. The coordinates of the ground control points were surveyed using a Trimble GeoXR 6000 handheld differential GPS with a pole-mounted Zephyr 2 external antenna in the dual-frequency differential real-time kinematic (RTK) mode. It was connected to the CZEPOS permanent GNSS network and provided 2–4 cm horizontal and vertical relative accuracies.

The RTK GNSS survey was conducted in the study area on 28 March 2017 (leaf-off period) to locate reference points for DTMs evaluation

using a Leica GPS1200 system. In order to quantitatively assess the effect of different vegetation canopies on DTMs' accuracy, the information about vegetation canopy (i.e., aquatic vegetation, steppes, and forest) was recorded for each surveyed point. Because collection of GNSS data under tall canopies was challenging even during the leaf-off period, a conventional, total-station survey was used in forested areas. All reference points were transformed into the Datum of Uniform Trigonometric Cadastral Network (S-JTSK; EPSG: 5514) and Baltic Vertical Datum - After Adjustment (Bpv; EPSG: 5705) coordinate systems. In total, 796 reference points were collected for this study (55 in aquatic vegetation, 311 in steppes, and 430 points in forests).

6.2.4   Point Clouds Processing and DTM Generation

The LiDAR point cloud was processed using a proprietary software by Global Change Research Institute CAS, referenced to the local Datum of Uniform Trigonometric Cadastral Network and Baltic Vertical Datum – After Adjustment. The LiDAR point cloud was further processed using Rapidlasso LAStools (rapidlasso.com/lastools). LASnoise and LASground tools of the LAStools software were used to determine ground points. We tested several settings for LASground and visually assessed the resulting DTMs using hill-shaded terrain and the success of ground points identification in the most troublesome areas. Our final setting was as follows: step 4, bulge 1, spike 2.3, offset 0.1, and stddev 10.

The UAV-acquired images, along with positional data measured by the onboard GPS during the flight, were loaded into Agisoft Photoscan Professional version 1.2.4 (Agisoft LLC, Russia) and used to generate a 3D point cloud. Agisoft Photoscan follows a common SfM–MVS workflow (Smith et al. 2016). First, the alignment algorithm iteratively refined external and internal camera orientations and camera locations

through a least squares method and generated a sparse point cloud. The alignment process was completed with the accuracy parameter set to "high" and the pair pre-selection parameter to "disabled". The accuracy setting ensured the use of the original image resolution while the "disabled" setting of the pair pre-selection ensured the best image matching. The limit was set to 20,000 for key points (indicating the maximum number of points sampled within each image) and to 5,000 for tie points (the number of points used for image matching). Dense point clouds were built using a dense Multi-View 3D reconstruction algorithm with a high reconstruction quality and mild depth filtering. Point clouds were georeferenced using ground control points in the same horizontal and vertical datum as LiDAR and exported into the LAS format (hereafter we refer to these point clouds as SfM$_{SPRING}$, SfM$_{SUMMER}$, and SfM$_{WINTER}$). Points representing the ground surface were identified using Classify LAS Ground tool of the ArcGIS 10.4.1 software (Esri Inc., USA).

The identified ground points were used to create DTMs with a cell size of 1 m (hereafter, we refer to these point clouds as DTM$_{SPRING}$, DTM$_{SUMMER}$, DTM$_{WINTER}$, and DTM$_{LIDAR}$). We used a bin-average method, which calculates the elevation for each cell by assigning the average value of all points within that cell. Areas containing no ground points (voids, see below) were triangulated and linearly interpolated to determine their cell values. Water areas were manually vectorized over a winter orthophoto and removed from the analysis.

6.2.5   Comparison of LiDAR and SfM Point Clouds

Both LiDAR and SfM point clouds were compared by quantifying the overall point density, density of identified ground points, and percentage of ground points in relation to all points. Subsequently, point clouds were overlaid with a 1×1 m grid and the number of grid cells containing no ground points was calculated (termed the "void fraction"). The void

fraction represents areas that had to be interpolated in order to create a DTM. We also visually compared the point clouds with orthophoto maps for the three seasons (spring, summer, and winter) and through all assessed types of canopy (i.e. aquatic vegetation, steppes, and forest).
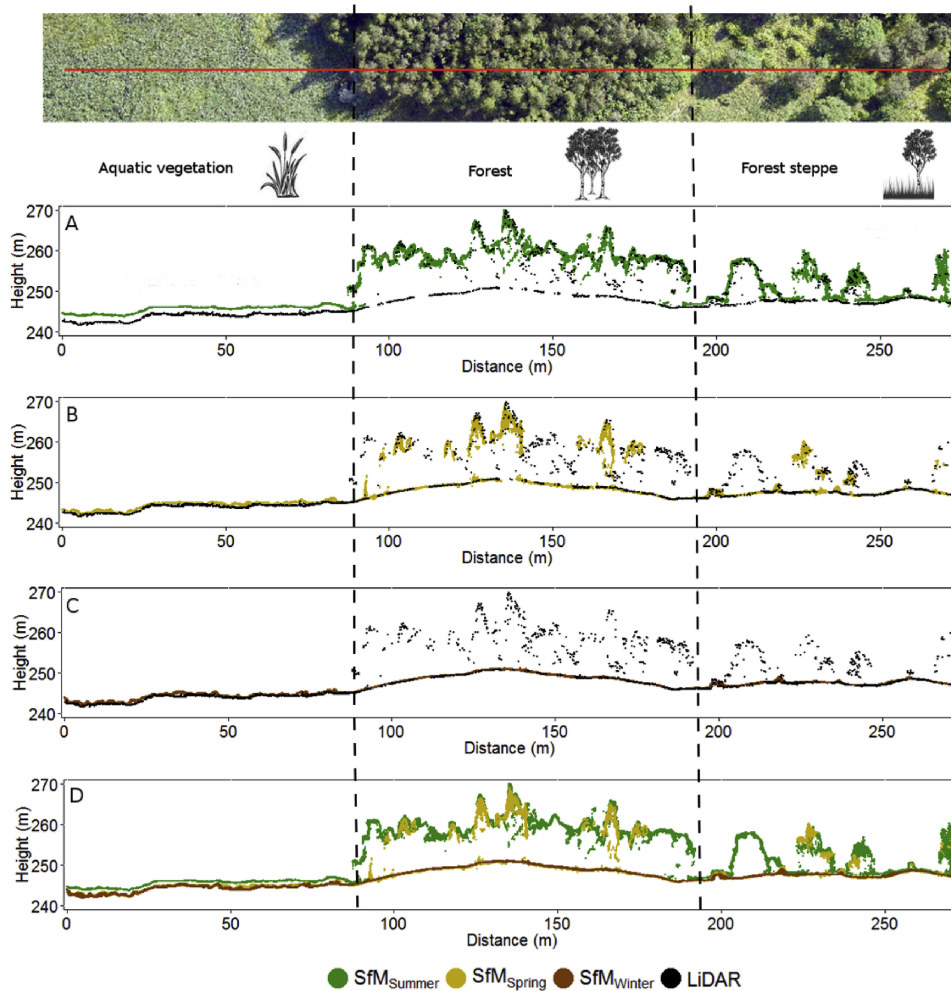
Figure 6.2: *Structure of four point clouds (winter, spring, summer, and LiDAR) over three different environments (aquatic vegetation, forest, and forest steppe). Comparison of LiDAR and summer point cloud (A) demonstrates the known fact that dense vegetation prevents SfM ground detection. However, spring (B) and especially winter (C) point clouds show a good potential for detecting ground even under forest stands. The combination of all three SfM point clouds (D) allows the identification of both ground and vegetation canopy. The profile is 1 m wide.*

6.2.6 DTM Accuracy Assessment

We used six accuracy measures to assess the vertical accuracy of DTMs generated from data collected using the SfM and LiDAR surveying techniques (i.e., maximum, minimum, mean, skewness, RMSE, NMAD). The GNSS survey, representing the most accurate data, was used as the reference dataset (true elevation) to evaluate the DTMs. We first calculated vertical differences among the 796 surveyed point elevations and the corresponding DTM_{SPRING}, DTM_{SUMMER}, DTM_{WINTER}, and DTM_{LIDAR} grid cell elevations. Descriptive statistics (i.e., maximum, minimum, and mean) were calculated for vertical differences. To evaluate the success of ground identification and vegetation removal, we calculated the Bowley's coefficient of skewness. We also used the differences to calculate root mean square error (RMSE). We assessed the deviation from the normal distribution using histograms and Q-Q-plots. As we detected a highly non-normal distribution (fat-tailed), we also calculated normalized absolute deviation (NMAD), a robust metric that is less sensitive to the presence of outliers (see Höhle and Höhle 2009).

6.2.7 Analysis of Vegetation Cover Effect on DTM Accuracy

Inaccuracy in the generated DTMs results partially from an interpolation of cells containing no ground points. Therefore, to compare solely the accuracy of the two methods (and not of the interpolation algorithm), we identified cells containing ground points from both SfM and LiDAR surveys and performed a pairwise combination between DTM_{WINTER} and DTM_{LIDAR} using cell-by-cell subtraction. Being the best of all available SfM point clouds, only the winter point cloud was used for this evaluation as a representative of SfM models (Table 6.2; Figure 6.2). Furthermore, we visually compared the results with respect

115

to prevailing vegetation type (aquatic vegetation, forest steppe, and forests) over the study area. To quantitatively evaluate the impact of vegetation on DTM accuracy for each vegetation type, we calculated the same descriptive statistics as mentioned above for individual vegetation categories (which had been recorded for all reference points during the field surveys).

Table 6.2: Summary of point cloud characteristics for the SfM and LiDAR datasets. Point density is shown as Mean $\pm$ Standard deviation. Voids fraction is the percentage of cells (1$\times$1 m resolution) not containing any ground point.

Dataset	Total points	Point density (points/sq. m)	Ground points
SfM$_{WINTER}$	196,103,451	333 $\pm$ 57	167,631,147
SfM$_{SPRING}$	83,358,151	139 $\pm$ 74	31,383,865
SfM$_{SUMMER}$	78,098,227	135 $\pm$ 77	18,241,318
LiDAR	4,667,778	7.7 $\pm$ 3.3	2,696,995

Dataset	Ground point density (points/sq. m)	Percent ground (%)	Void fraction (%)
SfM$_{WINTER}$	288 $\pm$ 83	85.5	0.6
SfM$_{SPRING}$	61 $\pm$ 30	37.6	15.8
SfM$_{SUMMER}$	56 $\pm$ 27	23.4	45.1
LiDAR	5.3 $\pm$ 3.0	57.8	15.6

6.3 Results

6.3.1 Comparison of Point Clouds

Point cloud characteristics varied substantially for the acquired datasets (Table 6.2; Figure 6.2). Point densities acquired with SfM significantly exceeded densities of the LiDAR point cloud. Of the 196,103,451 SfM$_{WINTER}$ points (i.e., under optimal conditions for terrain measurements), 85.5% were classified as ground points. In contrast, both SfM$_{SPRING}$ and SfM$_{SUMMER}$ (i.e., suboptimal conditions) resulted in

just 83,358,151 and 78,098,227 points, respectively, of which 37.6% and 23.4% were classified as ground points. Accordingly, when overlaid with a 1×1 m resolution grid, the number of cells containing no ground points was the highest for leaf-on conditions. For both total points and ground points, the identified point densities for individual flights differed significantly. The most evident difference was observed for the forest environment, for which no ground points were identified through the summer flight (Table 6.2; Figure 6.3).
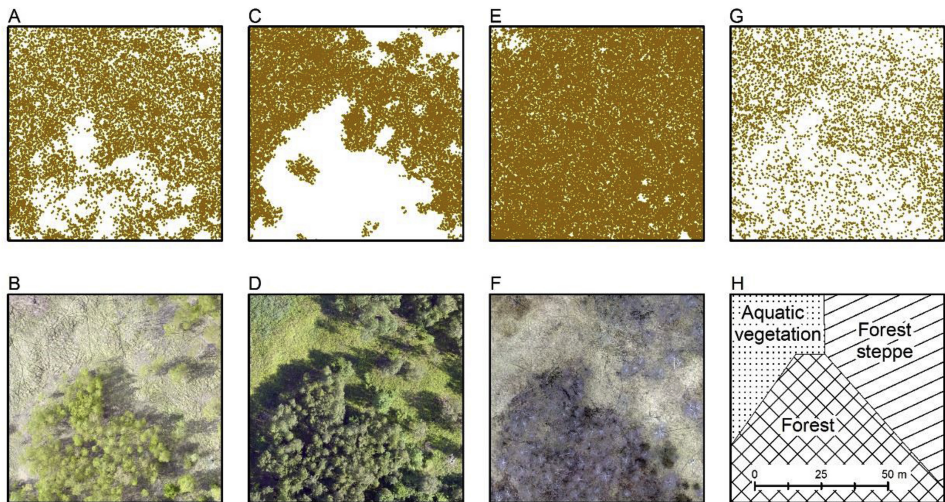
Figure 6.3: Visual comparison of ground point densities. All figures are from the same location. (A) Spring SfM point cloud and (B) orthophoto; (C) summer SfM point cloud and (D) orthophoto; (E) winter SfM point cloud and (F) orthophoto; (G) LiDAR point cloud; (H) approximate distribution of the three types of vegetation under study in the displayed area. No ground points were identified in the summer (leaf-on period) under the forest vegetation (C) while the ground is perfectly identified in the winter survey (E). Although ground points are identified in aquatic vegetation and forest steppes in summer (C), these may capture low vegetation (e.g., reed, grass) and do not accurately represent bare ground. See also Figure 6.2.

The density of photogrammetrically derived point clouds is much greater than that of the LiDAR point clouds but that greater point density does not necessarily indicate a greater accuracy. The reason is that only LiDAR can penetrate through the gaps in vegetation canopies

and capture underlying canopy layers or ground elevation. It is evident that with the point density used in our study, there are many gaps in LiDAR ground coverage (Figure 6.3 G). By comparison, the density of ground points in the SfM$_{WINTER}$ point cloud (Figure 6.3 E) is much higher. This is quantitatively shown in the percentage of void cells ("void fraction") (Table 6.2). On the other hand, although the percentages of void cells are similar for LiDAR and SfM$_{SPRING}$ point clouds, LiDAR ground points are more evenly distributed. Furthermore, the point density of SfM$_{WINTER}$ was considerably greater (333 points per square meter) than those of SfM$_{SPRING}$ and SfM$_{SUMMER}$ (with fewer than 140 points per square meter).

6.3.2   Combination of Point Clouds Acquired Under Leaf-on and Leaf-off Conditions

SfM$_{SUMMER}$ (leaf-on conditions) recorded elevation for the top surface, which in this case means vegetation canopy (Figure 6.2 A). By comparison, SfM$_{SPRING}$ (partly leaf-off conditions) and SfM$_{WINTER}$ (leaf-off conditions) point clouds were able to capture ground elevation, albeit with varying degrees of success in various studied environments (i.e., aquatic vegetation, forest steppe, and forest; Figure 6.2 B and C). Given the differences in the point clouds acquired in the different phenological phases, a combination of SfM$_{SPRING}$, SfM$_{SUMMER}$, and SfM$_{WINTER}$ point clouds allowed us to record both vegetation canopy and ground elevation and resembled the structure of the LiDAR point cloud (Figure 6.2 D).

6.3.3   Comparison of DTMs

With RMSE of 0.19 m and of 0.12 m, respectively, DTM$_{WINTER}$ and DTM$_{LIDAR}$ achieved very similar results (Table 6.3). DTM$_{WINTER}$ had a higher maximum and minimum error than DTM$_{LIDAR}$ and exhibited

a slight positive skew. This higher frequency of positive errors suggests a persistent presence of above-ground features even in winter (see vegetation category comparison). In contrast, DTM_{SPRING} and in particular DTM_{SUMMER} achieved poorer results. DTM_{SUMMER} had the highest mean error of 0.83 m and RMSE of 1.71 m. DTM_{SPRING} had a mean error of 0.07 m and RMSE of 0.46 m (see Table 6.3).

Table 6.3: Results of DTMs error analysis. Comparison of each DTM with 796 GNSS-gathered validation points. Bowley coefficient of skewness is used. NMAD is a normalized absolute deviation – a robust metric less sensitive to the presence of outliers than RMSE.

DTM	Maximum (m)	Minimum (m)	Mean (m)
DTM_{SPRING}	1.43	-6.23	0.07
DTM_{SUMMER}	12.88	-4.26	0.83
DTM_{WINTER}	1.39	-1.25	0.09
DTM_{LiDAR}	0.56	-0.48	0.05
DTM	Skewness (m)	RMSE (m)	NMAD (m)
DTM_{SPRING}	-0.002	0.46	0.15
DTM_{SUMMER}	0.21	1.71	0.58
DTM_{WINTER}	0.12	0.19	0.13
DTM_{LiDAR}	0.002	0.12	0.10

6.3.4 The Effect of the Vegetation on DTMs Accuracy

A high maximum positive error in DTM_{SUMMER} indicates an existence of artefacts resulting from an unsuccessful filtering of the tree foliage. These have been successfully avoided in DTM_{SPRING} and DTM_{WINTER} due to the smaller amount of tree foliage (or absent foliage in case of DTM_{WINTER}) during data acquisition (Figure 6.3 B and F). A low minimum negative error is however present in DTM_{SPRING} and DTM_{SUMMER} indicating that some areas are below the ground. This is due to the inability to capture the undulated terrain over void areas without ground points that had to be interpolated. In addition to

these void areas, low vegetation is often identified as terrain in summer and the DTM_{SUMMER} therefore showed a positive error skew. Both DTM_{WINTER} and DTM_{LIDAR} tend to overestimate the terrain elevation in all vegetation categories (Table 6.4). While the quality of DTM_{LIDAR} is relatively consistent across vegetation categories, DTM_{WINTER} shows variable accuracy. Both methods achieved the best accuracy in forests (Figure 6.4).

Table 6.4: Results of DTMs error analysis for SfM winter and LiDAR in three environments. Comparison of each DTM with 796 GNSS gathered validation points.

DTM	Mean (m)	Skewness (m)	RMSE (m)	NMAD (m)
Aquatic vegetation				
DTM_{WINTER}	0.32	0.21	0.36	0.12
DTM_{LiDAR}	0.07	0.03	0.14	0.11
Steppes				
DTM_{WINTER}	0.08	0.25	0.21	0.12
DTM_{LiDAR}	0.07	−0.06	0.12	0.09
Forests				
DTM_{WINTER}	0.06	−0.02	0.15	0.11
DTM_{LiDAR}	0.04	−0.003	0.12	0.11

6.4   Discussion

The negative effect of the vegetation on DTM quality and overestimation of bare earth due to the inconsistent ability of passive methods to penetrate vegetation canopies is a common observation (Dandois and Ellis 2013, Tonkin et al. 2014, Lovitt et al. 2017). Both methods achieved best accuracy in forests, which is not surprising if we consider the vertical vegetation structure. The density of the most problematic, i.e., shrub, vegetation in forests is low (Figure 6.4 H, Table 6.1) while it is considerably higher in forest steppes (Figure 6.4 E). Although an effective use of UAVs in combination with photogrammetry in
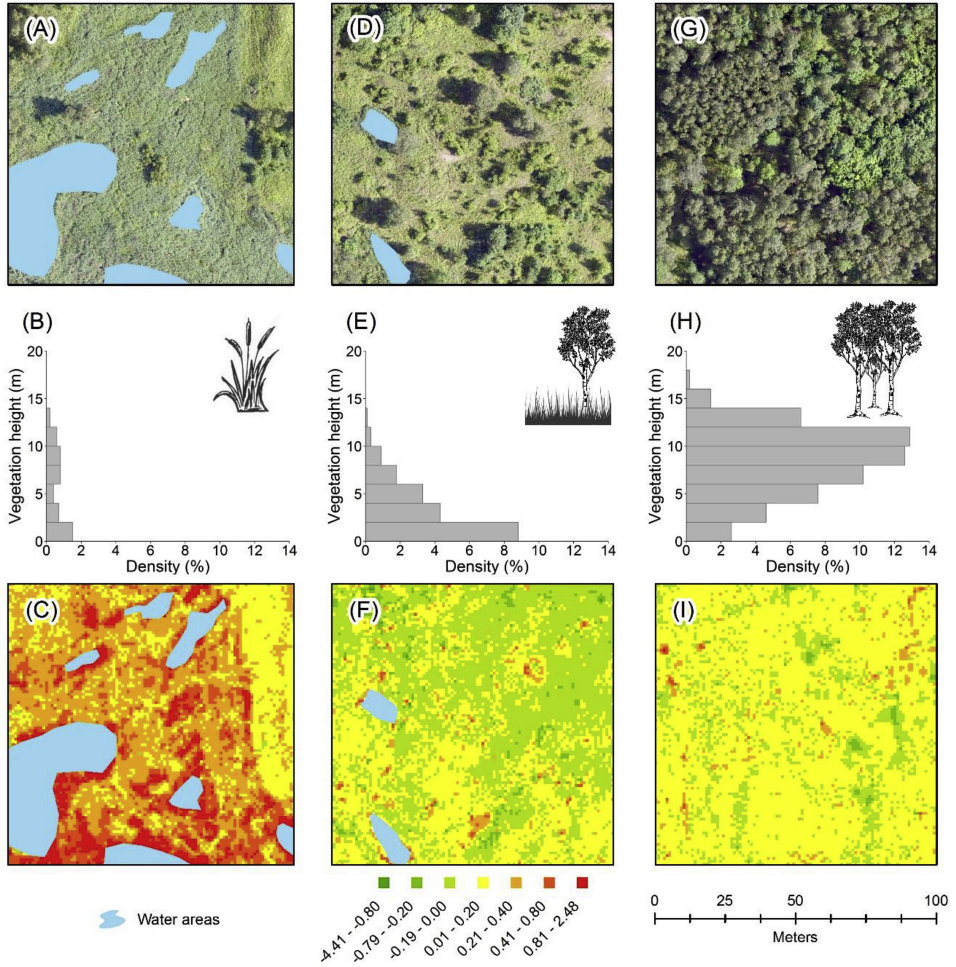
Figure 6.4: Orthophoto images of 1 ha plots inside study area at three different environments. (A) aquatic vegetation; (D) forest steppe; (G) forest. The above-ground height distribution of LiDAR returns (B, E, H), and a raster surface of vertical difference ($DTM_{WINTER} - DTM_{LIDAR}$) at 1 m resolution (C, F, I). The colour scale indicates the differences between DTM_{WINTER} and DTM_{LIDAR}, see legend. Red colour shows areas of overestimation and green colour areas of underestimation of DTM_{WINTER} compared to DTM_{LIDAR}. Note that overestimation occurs mainly in areas of aquatic vegetation around water areas. Density is calculated as number of returns in each bin (here 2 m) divided by the total number of returns. See Figure 6.1 for location of the plots.

ecosystems dominated by shrub vegetation has been demonstrated by Cunliffe et al. (2016), the quality of acquired DTMs depends on the

character of the vegetation and terrain. In our study area, the accuracy of DTMs in steppes was better for DTM_{LIDAR} (with RMSE of 0.12 m) but DTM_{WINTER} also achieved a very good result (with RMSE of 0.21 m). DTM_{WINTER} error was skewed slightly positively. Positive elevation errors can be attributed to the effect of short vegetation, which is often misclassified as ground by the filtering algorithms due to the small height difference between the vegetation and terrain (Meng et al. 2010). Another reason for such errors may lie in the presence of very dense shrubs that form an impenetrable flat area and resemble terrain (e.g., *Symphoricarpos albus*). Besides, for photogrammetrically derived point clouds, we performed no manual processing of the data acquired under leaf-off conditions while both datasets acquired under leaf-on conditions required further manual processing as the tops of the dense canopies had been identified as ground. Distinguishing ground points from dense vegetation is particularly complicated for photogrammetric point clouds due to the very high densities, but its influence is only local and should be evident and easy to remove by manual evaluation.

LiDAR ground height estimation is particularly problematic for aquatic vegetation due to the weak laser backscatter caused by water absorption. As most LiDAR systems operate in the infrared region (like the one adopted in this study), free water surfaces and saturated soils dampen the returning signal (Hopkinson et al. 2005). As photogrammetry methods are based on images from passive sensors, acquired point clouds do not suffer from this issue and they may be better suited for DTMs acquisition (Kalacska et al. 2017). Aquatic vegetation stands however often persist during the winter, and our results show a large difference of RMSE 0.36 m versus 0.14 m between DTM_{WINTER} and DTM_{LIDAR}, respectively, for aquatic vegetation. DTM_{WINTER} error shows a positive skew due to stands of dry aquatic vegetation (e.g. *Typha latifolia* and *Phragmites australis*). These create dense vegetation stands completely obscuring the bare earth and making its detection impossible. On the other hand, the soil in the area of aquatic vegetation

is not constantly saturated (and was not at the time of LiDAR acquisition) and LiDAR was therefore able to detect the bare earth. This is also evident from the cell-by-cell comparison of DTM_{WINTER} and DTM_{LIDAR} (Figure 6.4). DTM_{WINTER} overestimated the bare earth in areas of aquatic vegetation compared to DTM_{LIDAR}. Recently, Lovitt et al. (2017) compared the performance of photogrammetric and LiDAR point clouds for characterizing terrain under peatland vegetation. In contrast to our study, they found photogrammetric point clouds to perform better than LiDAR point clouds in characterizing terrain under peatland vegetation. This difference is likely caused by differences in the vegetation type within the study areas as the authors also reported significant decline in accuracy for the most densely vegetated areas (RMSE of 0.42 m, which is similar to our results). Luo et al. (2015) reported RMSE of 0.15 m for a LiDAR-derived DTM under short wetland vegetation, which is consistent with our result (RMSE of 0.14 m).

Besides the evaluation of the digital terrain models, we also investigated the possibility of replacing costly LiDAR data with a combination of SfM data acquired from leaf-off and leaf-on imagery. Our results suggest that at least for some applications (e.g., calculation of vegetation structure characteristics often used to measure restoration success; Wortley et al. 2013, Shackelford et al. 2018), such a substitution may be possible. This is a significant improvement as studies usually relied on DTMs acquired from external sources, such as ALS (Lisein et al. 2013, Hawryło et al. 2017) or close-range terrestrial photogrammetry (Mikita et al. 2016). However, it is important to note that photogrammetric point clouds are inherently different from LiDAR point clouds, lacking detail in the lower canopy. In addition, the point density can be affected, for example, by flight parameters, camera settings, and environmental conditions such as foliage movement in the wind (Jensen and Mathews 2016, Moudrý et al. 2019d). Consequently, the densities of point clouds combined from different acquisition periods could be unpredictably biased and their use likely limited to deriving simple variables (e.g., canopy height

and canopy cover). It is however fair to point out that many of the above mentioned problems can also affect LiDAR data (e.g., Coops et al. 2007, Roussel et al. 2017).

Our results have shown that DTMs derived from UAV-borne images acquired during leaf-off period are comparable with a LiDAR-derived point cloud in a forest and only slightly poorer in forest steppes and in aquatic vegetation. This is consistent with recent findings by DeWitt et al. (2017) that satellite images acquired under leaf-off conditions can be used successfully to mitigate the effect of above-ground vegetation and to acquire DTMs of similar accuracy to that of LiDAR-derived DTMs. Similarly, Dandois and Ellis (2013) showed an improvement in a DTM generated under leaf-off conditions of a temperate deciduous forest; the benefit in their study was however not as significant as our results (they reported RMSEs from 0.73 m to 2.72 m). This is likely due to the differences in structure of the forests and thus of acquired point clouds. The species composition on the three deciduous forest plots (250×250 m) in their study was different (mainly American beech *Fagus grandifolia*, oak *Quercus spp.*, hickory *Carya spp.*, and tulip-poplar *Liriodendron tulipifera*) and the canopy was higher (mean canopy height between 20 m and 37 m; maximum height up to 42 m). In contrast with Dandois and Ellis (2013; see Figures 2 and 7 in their paper) high vegetation was only residually present in our point clouds (Figure 6.2). Besides, they used a hexacopter and flew only 40 m above the peak canopy height (our flying altitude was almost double that above the canopy). Given the differences in accuracy between our results and those acquired by Dandois and Ellis (2013), additional investigations covering a range of various forest stands are needed to investigate the accuracy, precision, and resolution of photogrammetrically derived DTMs under deciduous forests. In addition, although our results indicate that natural conditions in winter appear promising, it must be noted that the operation of UAVs is restricted to specific conditions that must be met to acquire accurate terrain information. Meeting

such conditions in winter may be problematic because of snow, wind, and relatively short duration of proper light conditions.

6.5   Conclusions

This work evaluated the quality of LiDAR and UAV-borne digital terrain models of a spoil bank that could be possibly used for various safety, remediation or ecological research purposes. We generated DTMs from images acquired under leaf-on and leaf-off conditions in three different environments (aquatic vegetation, steppe, and forest). Bare ground was identified using ground classification methods and then binned or interpolated over void areas to create DTMs at 1 m resolution. The point cloud derived from images acquired under leaf-off conditions was of the highest density. Vegetation artefacts were more successfully removed by the filtering procedure for leaf-off point clouds than for leaf-on point clouds and the identified ground points covered almost the entire study area. The accuracy of DTMs generated from leaf-off point cloud differed among the three environments. Overall accuracy was close to that of LiDAR-derived DTMs, with the best agreement in forests and the worst in the environment with aquatic vegetation. We suggest that accuracy of both methods is sufficient to monitor spoil banks terrain and provide information complementary to that acquired by more traditional methods. However, careful consideration must be given to site conditions at the time of image acquisition because the accuracy of methods is highly dependent on the vertical vegetation structure. While airborne LiDAR is suitable for monitoring ground instability problems and mitigation measures for all seasons and vegetation structures, UAV image-based photogrammetry can be used successfully in steppes and deciduous forest stands only under leaf-off conditions. The greatest advantage of the methodology described in this paper is that leaf-off images allow accurate detection of ground surface and, therefore, DTMs that can easily be compared to any subsequent

DTMs derived from photos taken at a later date; such a comparison could detect any potential terrain changes. In addition, the combination of UAV imagery from leaf-off and leaf-on periods can be potentially used to calculate vegetation structure characteristics for studying a susceptibility of slope failure or restoration success assessment. Further research should quantitatively assess the sensitivity of images acquired under leaf-off conditions to the various structures seen in deciduous forest stands.

Chapter 7

Discussion and Summary

The presented dissertation thesis consists of three published studies focusing on the topic of point cloud filtering in a complex artificial terrain. All three published studies presented in the previous chapters investigate the field of LiDAR and UAV photogrammetry-based point cloud filtering including the comparison of various methods, parameters of sensitivity analyses, and the use of point clouds in the field of ecological restoration.

The individual studies will be referred to in the text as follows:

Study I: Assessment of LiDAR ground filtering algorithms for determining ground surface of non-natural terrain overgrown with forest and steppe vegetation.

Study II: Sensitivity analysis of parameters and contrasting performance of ground filtering algorithms with UAV photogrammetry-based and LiDAR point clouds.

Study III: Comparison of leaf-off and leaf-on combined UAV imagery and airborne LiDAR for assessment of a post-mining site terrain and vegetation structure: Prospects for monitoring hazards and restoration success.

All presented studies were performed on the Hornojiřetínská spoil heap. This study area was not selected by chance but because of a research project, the aim of which was a fusion of LiDAR and multispectral data

for the assessment of the physiographic diversity of post-mining sites. Accurate derivation of the DTM was a necessary initial step for all subsequent analyses performed within the project. Although most spoil heaps are technically restored, which includes major alterations of the terrain and leads to a uniform terrain, a significant proportion of spoil heaps included within the project (including the Hornojiřetínská spoil heap) has never been technically reclaimed. Therefore, the terrain has remained rugged as a result of heaping that has formed an undulated terrain and consequently led to the development of heterogeneous vegetation consisting of various types of meadows, steppes with scattered shrubs and trees, and spontaneously grown mixed forests. The following part of the dissertation thesis includes comments on the individual research topics, conclusions, and summary of the thesis as well as suggestions for further research in the field of point cloud filtering. As the full discussion and conclusions of the performed studies are included in the published papers detailed in Chapters 4 – 6, this chapter will only summarize the findings and provide the author's comments on the individual research topic and the discussion on how the aims of the dissertation were met.

7.1   Ground Filtering of ALS Data

The first study comparing the performance of filtering algorithms was presented by Sithole and Vosselman (2004), who provided a single ALS dataset to several researchers who developed filtering algorithms, and summarized the results (e.g., Axelsson 2000, Elmqvist et al. 2001, Pfeifer et al. 2001, Roggero 2001, Briese et al. 2002, Brovelli et al. 2002, Sohn and Dowman 2002, Wack and Wimmer 2002). This study was the first of its kind and unique in a way. It inspired several other groups, including ours, to perform similar comparisons for various environments. The algorithms used in studies that followed Sithole and Vosselman (2004) are listed in Table 7.1 at the end of this chapter. Note that even

a few years ago, the implementation of filtering algorithms in common software was limited and comparison studies concentrated mostly on validation of algorithms implemented in ALDPAT, the development of which, however, has been abandoned. On the other hand, currently available software solutions usually implement only one or two filtering methods. It would be of great value if several options of filtering algorithms were available in a single software. Besides, it would also allow to combine them into ensemble models (see the following chapter Further research).

Algorithms for ground filtering of ALS data are usually designed with some specific environment in mind (e.g., forests, steppes, or urban areas) and their efficiency varies across environments as each environment poses specific challenges (Meng et al. 2009, Rashidi and Rastiveis 2017, Buján et al. 2020). It is not entirely possible to apply a universal filtering method to achieve satisfactory results for all environmental conditions. The terrain and vegetation character of spoil heaps left to natural succession is often very complex and differs from what we can typically observe in the surrounding landscape. During our initial testing, we realized that the proper filtration of point clouds and the generation of accurate terrain will not be easy.

A combination of complex terrain and low vegetation, representing a well-known filtering problem, was common in our study area. Consequently, it was common to observe the following errors during our initial testing: (i) heaps/piles wrongly classified as vegetation or (ii) returns from dense vegetation incorrectly classified as terrain. Obviously, there is a trade-off between these two errors. Testing using multiple settings in a common software was not satisfactory and we were forced to test also other available software/algorithms and to evaluate the ability of the algorithms to produce an accurate DTM in such a complex terrain, which actually triggered the first part of our research (**Study I**). Our results were not much different from what others have shown and basically confirmed that the performance of tested ground filtering algorithms

was affected by the terrain slope and vegetation (Korzeniowska et al. 2014, Montealegre et al. 2015). Most importantly, however, this search allowed us to find the optimal solution for our study area, which was to split the study area into several tiles with relatively similar terrain and vegetation characteristics and classify each tile separately with minor adjustment of parameters.

7.2 Ground Filtering of UAV Photogrammetry-Based Data

Most filtering algorithms were originally designed for ALS point clouds and the knowledge of their performance with UAV photogrammetry-based point clouds is limited (but see Serifoglu Yilmaz et al. 2016, Zhang et al. 2018). Point clouds derived from UAV photogrammetry have a different character than point clouds from ALS; in particular, they are usually denser and contain only the uppermost layer of vegetation.

The comparison of the performance of available ground filtering algorithms when applied on both LiDAR and UAV photogrammetry-based point clouds arose as our next research question. We have shown that all filters achieved relatively good performance; however, the combination of dense vegetation and steep terrain slope complicated the point cloud filtration. This time, however, we analyzed the behavior of the algorithms and their sensitivity to changes in individual parameters in different environmental conditions in more depth. Most of the algorithms were identical to those used in the previous study (**Study I**) but algorithms with poor results were replaced by others (i.e., Trimble Real-Works was removed and Agisoft Metashape was added to the analyses). In addition, the number of combinations of parameter settings was dramatically increased to allow a deeper examination of the sensitivity of the individual parameters. Prior studies typically compared the performance of several algorithms (with both types of point cloud) on

various study sites representing different conditions (Serifoglu Yilmaz et al. 2018, Zhang et al. 2018). Our study area was large enough to contain several types of natural environment, which facilitated a more comprehensive evaluation of the performance (**Study II**). The results were generally better for LiDAR point clouds than for photogrammetric ones, which corresponds to the facts that (i) the algorithms were originally developed for LiDAR data and (ii) that LiDAR pulses penetrate through gaps in vegetation canopies, thus producing relatively more ground points. Despite being tested in exactly the same study area, the behavior of filtering algorithms was inconsistent when applied on photogrammetric point clouds and differed from the behavior observed when they were applied on LiDAR point clouds. Hence, when using photogrammetry-derived point clouds, users can not always rely on their experience with LiDAR point clouds filtering; rather, attention should be paid to the development of new algorithms or adaptation of the existing algorithms to dense photogrammetric point clouds.

7.3 Acquisition of DTMs Under a Forest Canopy During Leaf-off Conditions

In most cases, when results of aerial laser scanning (e.g., by the government in some EU countries) are not publicly available, private acquisition of ALS data is very expensive; for this reason, the use of photogrammetric techniques using UAV imagery seems to be a good alternative. Dense forest areas are the most challenging environment for ground filtering or even ground detection using UAV imagery. In order to at least partially eliminate the problem of difficult capture of the ground using UAV imagery (as it predominantly contains only the uppermost layer of vegetation), UAV imaging can be conducted in the leaf-off period (see for example DeWitt et al. 2017 who used a similar approach with satellite imagery). Existing studies on the use of UAV

imagery in forests focused on partially open canopies (Kachamba et al. 2016) where ground filtering is more likely to be successful. The forest stands in our study area comprised predominantly temperate deciduous forests. Obtaining images during the leaf-off period, therefore, appeared to be promising. I would like to say that this approach was inspired by studies that obtained ALS data in the leaf-off period (e.g., White et al. 2013). To be honest, however, the data were obtained by chance due to the impossibility to meet the original intended flight date. We just did not expect such a difference between the leaf-on and leaf-off flights and such a significant improvement. Several studies have already followed up on our findings (**Study III**) and used them in their research, for example, for supporting teak plantations inventories in Ecuador or for modeling coastal ecosystems in the southeastern United States, where a leaf-off derived DTM served as the ground reference (Aguilar et al. 2019, DiGiacomo et al. 2020). Another study confirmed the validity of this method, testing the influence of seasonal variation in vegetation for mapping hard-to-access and hazardous parts of forests (Tomaštík et al. 2019). We suggest that in deciduous forests, a combination of two UAV image acquisitions at different time points could provide a potential substitution for ALS scanning when vegetation cover or height is of concern.

7.4 Evaluation of Filtering Algorithms

There are several ways to evaluate the performance and accuracy of filtering algorithms. The most important aspect of every evaluation is the quality of the used reference data. The best reference dataset is a manually classified point cloud. Manual classification of a point cloud is possible for ALS data but it would be extremely time-consuming for a (several times denser) UAV photogrammetry-based point cloud. Another option is to validate the accuracy of the generated DTM using a more accurate source of elevation data, such as the differential

GNSS (**Study II** and **III**). This, however, provides significantly less information about the actual accuracy of the filtering itself and may result in misleading conclusions as the validation points are seldom located in areas problematic from the perspective of filtering methods – field operators who collect the validation data are likely to subconsciously or for safety reasons avoid such areas (e.g., steep slopes, dense vegetation). In any case, the validation data are usually limited to small areas. Despite the time-demanding manual classification of point clouds, some recent studies used manually classified samples of UAV photogrammetry-based point clouds to determine the error trends of the algorithms (e.g., Zeybek and Şanlıoğlu 2019). However, only a few square meters of validation data out of tens of hectares of the study area were classified. A slightly different approach to the assessment of Type I and II errors was proposed by Zhang et al. (2003) and Zhang and Whitman (2005) who examined a sample of 648 randomly selected test points (x and y coordinates) across their testing site.

It is important to note that most of the existing studies only reported the algorithm that worked best for their study area but did not mention specific values of the tested parameters. Only a few studies reported also the range of tested parameters and none of them reported the performance of all tested settings. This, however, limits the usability of their results as the sensitivity of algorithms to parameter settings is equally important for users as the best performance. For example, Montealegre et al. (2015) presented results of filtering LiDAR point clouds in forests in Spain acquired using the best settings. Results from several test sites in Poland were presented by Korzeniowska et al. (2014) who tried to find the best settings for various types of land cover and terrain slope. Serifoglu Yilmaz et al. (2016) used a part of a university campus in Turkey to determine the most suitable settings for built-up areas. Reporting the best results gives important insights into the potentially best performance of filtering algorithms (i.e., information about the accuracy that can be theoretically expected

from the classification using the particular method in a particular environment) and provide a combination of parameters that will likely perform relatively well in a similar environment. However, this approach lacks information on how sensitive the algorithm is to the change of parameters and whether it generally tends to cause the Type I error (percentage of ground points that are incorrectly classified as non-ground), Type II error (non-ground points incorrectly classified as ground points) or whether the susceptibility to the type of error depends on parameter settings. This information is also important for users as it can help them to make an informed selection of algorithms and fine-tune the parameters. Therefore, we also studied the overall tendency of algorithms to cause the Type I and/or Type II error and showed that the tendency may differ between algorithms (**Study I**). I believe that this topic deserves further research to determine whether the main role in causing Type I and Type II error is played by the algorithm or by the character of the environment.

The typical best success rate reported in individual studies ranges between 76 – 96% (Axelsson 2000, Elmqvist et al. 2001, Brovelli et al. 2002). It is, therefore, clear that all classifications require additional manual processing and, therefore, the question arises, which error (Type I or Type II error) poses a greater problem. Generally, this depends on the cost of the error for the intended data application (Sithole and Vosselman 2004). However, as noted by Sithole and Vosselman (2004) it is far easier to manually fix Type II errors than Type I errors. Results of **Study I** showed that for all algorithms but SMRF, fine-tuning caused considerably larger variation in Type I error than in Type II error. In addition, PTIN, ARC, and PMF algorithms tended on average to a higher Type I than Type II error while in CSF, SMRF, and RW, we observed the opposite. However, our study area contained only one specific type of landscape (e.g., a forested steppe with overgrown vegetation). Testing the same in other landscapes (e.g., a built-up area), more sites, and using a wider range of parameters would be beneficial.

To evaluate filtering algorithms in more depth, we also performed a sensitivity analysis for identifying the best parameter settings for each ground filtering algorithm and both types of the point cloud (**Study II**). Only a few studies evaluated the differences between these two types of point clouds together with the effect of heterogeneous vegetation and slope changes on algorithm performance (Montealegre et al. 2015, Serifoglu Yilmaz et al. 2018). In our case, the "grain" turned out to be the most important parameter. This is not surprising as we validated the accuracy with respect to the height of the terrain (i.e., DTM). Indeed, our study was particularly limited by the used validation dataset (GNSS survey) as mentioned above. Further studies should, therefore, focus on the sensitivity analysis considering individual parameters with respect to their effects on the Type I and Type II error. This would be a truly unique step that would benefit all users. Knowing the sensitivity of parameters can provide valuable advice when most of the predefined settings of algorithms fail and fine-tuning using custom parameters is necessary.

Another approach to the assessment lies in a visual examination and comparison of a shaded relief of the generated DTMs. This approach is rarely used (Korzeniowska et al. 2014, Montealegre et al. 2015), but it facilitates the identification of differences between the best results among several algorithms. The main benefit of this approach lies in the opportunity to observe small differences in the parameter tuning, as such differences may not be obvious from numerical values but are visually apparent at the first glance. It is also possible to quickly detect errors caused by misclassification of ground points (filled by interpolation), which can sometimes inaccurately smoothen the terrain.

7.5 Conclusions

Point clouds from ALS or UAV imagery constitute an important data source for terrain mapping. The introduction of this thesis briefly summarized various aspects of these methods and their role in obtaining a detailed structure of the Earth's surface. Dozens of algorithms have been developed to automatically detect the bare earth from point clouds. In this thesis, I presented the results of the in-depth evaluation of filtering algorithms' performance in complex terrain. The detailed findings can be found in the conclusions of the individual presented studies. Although all algorithms performed relatively well, it is a matter of perspective and a result considered good by one person (or from the perspective of a certain application) might be seen as poor by another. Hence, I describe the main points that should be in my opinion considered when filtering point clouds below:

- Algorithms behave consistently when filtering LiDAR point clouds, with problems typically more common when filtering low vegetation and/or with increasing slope; however, when filtering photogrammetric point clouds, this may not be true and caution is needed.

- LAStools, in my opinion, present a good option for inexperienced users due to the useful interface and several predefined options for parameter settings. In addition, the PTIN algorithm implemented in LAStools yielded the best results for both types of point clouds. I propose that software developers should provide users with predefined sets of optimal parameters for individual environments under study.

- Some algorithms tended to cause Type I error while others tended rather to the Type II error; future research should evaluate whether these tendencies are universal and how they relate to the vegetation and terrain character.

- Fine-tuning of parameters is necessary. Parameters affecting the selection of initial ground points turned out to be the most important for the accuracy of the resulting DTMs.

- The combination of UAV imagery from leaf-off and leaf-on periods can be potentially used to calculate vegetation structure characteristics such as vegetation cover and height.

7.6   Further Research

Many filtering algorithms have been shown to be able to distinguish ground and non-ground points from point clouds. However, it is often difficult to derive satisfactory filtering results with the existing methods and accurate filtering still requires a lot of manual work. A new ground filter, which would, for example, adapt itself to the surrounding environment, may be created in the relatively near future. Some attempts have already been reported, for example, with a slope estimate (Wang et al. 2020). However, a multitude of issues need to be tested and solved on the way to such an algorithm. Besides, there are many interesting applications in which ground filters are increasingly tested (e.g., ground filtering of raster satellite data) and I would like to use the experience gained in this thesis to further explore this field.

Currently, UAV LiDAR (mounting of a LiDAR sensor with the UAV platform) is becoming increasingly available and represents one of the possible directions of further research. Compared to ALS, it provides denser point clouds and, thus, brings new challenges for ground filtering due to a lot of noise and difficult maintaining of symmetric flight lines. On the other hand, such data offer a great opportunity for very accurate estimation of ground elevation and vegetation characteristics (Liu et al. 2020, Pinton et al. 2020).

Attempts for the use of ground filtering algorithms in satellite data processing, e.g., filtering of DSMs, have been reported. Most satellite

DEMs (including TanDEM-X DEM) include canopy and buildings because radar waves cannot fully penetrate through vegetation and buildings to reach the ground (the same applies to photogrammetry). Therefore, filtering methods are needed if DEMs from satellites are to be used as DTMs. So far, few filtering algorithms have been tested (e.g., the morphological filter; Archer et al. 2018, Zhang et al. 2019) and it would be worth trying other filters or completely new methods.

A promising approach in the current research is represented by combining filtering algorithms into so-called hybrid methods (Maguya et al. 2013, Buján et al. 2020). I myself refer to this approach (i.e., the combination of several algorithms) as ensemble filtering, which is common in many other disciplines such as economy or ecology (Effrosynidis and Arampatzis 2021, Mallick et al. 2021). Ensemble filtering uses the strengths of all adopted methods. In the case of ground filtering, it can be used to identify problematic areas (i.e., points, the classification of which into ground and non-ground differs among algorithms). Besides, ensemble filtering does not necessarily use several algorithms; it might be also implemented by the use of various parameter settings within one algorithm. I believe this is a hot topic as several studies have already tested the combination of two algorithms and ensemble filtering is likely to become a common approach quite soon (Zhao et al. 2016, Wang et al. 2020). Therefore, I consider this a priority in my further research.

Various data fusions may represent another promising direction of further research. One way, for example, is the integration of RGB imagery with UAV photogrammetry-based point clouds or with LiDAR point clouds. The additional RGB information could help to better detect ground points. Filtering point clouds using the information about the land cover type (e.g., Corine Land Cover) is another principle that should be investigated further. The detail (both spatial and thematic) in which the land cover data should be provided, however, remains questionable.

7.7 Afterword

According to the present trends, it is clear that remote sensing technologies will play an ever more important role and will evolve ever faster, driven by the need to obtain more detailed data representing the 3D structure of the Earth's surface in the shortest possible time. I believe this dissertation thesis has addressed these needs and may provide some basic elements filling a gap in knowledge of ground filtering and laying the base for further research. The objectives of this thesis were successfully reached, and the presented studies appropriately demonstrate the principal issues of ground filtering of point clouds. The process of creating DTMs using ground filtering algorithms is just a small piece of knowledge that will help us better understand the environmental processes on Earth.

Table 7.1: List of existing comparative studies evaluating filtering algorithms and their accuracy along with used software.

Algorithm	Sulaiman et al. 2010	Gonçalves and Pereira 2010	Tinkham et al. 2011	Julge et al. 2014	Korzeniowska et al. 2014	Polat and Uysal 2015	Montealegre et al. 2015	Silva et al. 2018
Weighted Linear Least Squares (WLS)				FUSION			FUSION	FUSION
Multi-scale Curvature Classification (MCC)			MCC-LiDAR	MCC-LiDAR			MCC-LiDAR	MCC-LiDAR
Maximum Local Slope (MLS)	ALDPAT	ALDPAT		ALDPAT		ALDPAT	ALDPAT	
Iterative Polynomial Fitting (IPF)	ALDPAT	ALDPAT				ALDPAT		
Elevation Threshold with Expand Window (ETEW)	ALDPAT	ALDPAT		ALDPAT		ALDPAT	ALDPAT	
Adaptive TIN (ATIN)	ALDPAT	ALDPAT		ALDPAT		ALDPAT	ALDPAT	
Progressive TIN densification (PTIN)	TerraScan	TerraScan			LAStools	LAStools	LAStools	LAStools
Progressive Morphological Filter (PMF)	ALDPAT	ALDPAT		ALDPAT	LIS	ALDPAT	ALDPAT	ALDPAT
S (Segmentation) filter					LIS			
Boise Center Aerospace Lab. (BCAL)			BCAL LiDAR				BCAL LiDAR	
Parameter-free (PF)					gLiDAR			
Surface interpolation filters					SCOP++			
Number of used algorithms	6	6	2	6	5	5	7	4

Chapter 8

References

Aguilar, F. J., Rivas, J. R., Nemmaoui, A., Peñalver, A., and Aguilar, M. A. (2019). UAV-Based Digital Terrain Model Generation under Leaf-Off Conditions to Support Teak Plantations Inventories in Tropical Dry Forests. A Case of the Coastal Region of Ecuador. *Sensors*, 19(8):1934.

Archer, L., Neal, J. C., Bates, P. D., and House, J. I. (2018). Comparing TanDEM-X Data With Frequently Used DEMs for Flood Inundation Modeling. *Water Resources Research*, 54(12).

Aryal, R. R., Latifi, H., Heurich, M., and Hahn, M. (2017). Impact of Slope, Aspect, and Habitat-Type on LiDAR-Derived Digital Terrain Models in a Near Natural, Heterogeneous Temperate Forest. *PFG – Journal of Photogrammetry, Remote Sensing and Geoinformation Science*, 85(4):243–255.

Axelsson, P. (1999). Processing of laser scanner data—algorithms and applications. *ISPRS Journal of Photogrammetry and Remote Sensing*, 54(2-3):138–147.

Axelsson, P. (2000). DEM Generation from Laser Scanner Data Using adaptive TIN Models. *International Archives of Photogrammetry and Remote Sensing*, 23(B4):110–117.

Bakx, T. R. M., Koma, Z., Seijmonsbergen, A. C., and Kissling, W. D. (2019). Use and categorization of Light Detection and Ranging

vegetation metrics in avian diversity and species distribution research. *Diversity and Distributions*, 25(7):1045–1059.

Balenović, I., Gašparović, M., Milas, A. S., Berta, A., and Seletković, A. (2018). Accuracy assessment of digital terrain models of lowland pedunculate oak forests derived from airborne laser scanning and photogrammetry. *Croatian Journal of Forest Engineering*, 39(1):117–128.

Baltensweiler, A., Walthert, L., Ginzler, C., Sutter, F., Purves, R. S., and Hanewinkel, M. (2017). Terrestrial laser scanning improves digital elevation models and topsoil pH modelling in regions with complex topography and dense vegetation. *Environmental Modelling & Software*, 95:13–21.

Bao, S. Y. and Savarese, S. (2011). Semantic structure from motion. In *CVPR 2011*, pages 2025–2032. IEEE.

Bartoń, K. (2019). MuMIn: Multi-Model Inference.

Bates, D., Kliegl, R., Vasishth, S., and Baayen, H. (2015a). Parsimonious Mixed Models.

Bates, D., Mächler, M., Bolker, B., and Walker, S. (2015b). Fitting Linear Mixed-Effects Models Using lme4. *Journal of Statistical Software*, 67(1).

Bazzichetto, M., Malavasi, M., Barták, V., Acosta, A. T. R., Moudrý, V., and Carranza, M. L. (2018). Modeling plant invasion on Mediterranean coastal landscapes: An integrative approach using remotely sensed data. *Landscape and Urban Planning*, 171:98–106.

Bednarczyk, Z. (2017). Landslide Monitoring and Counteraction Technologies in Polish Lignite Opencast Mines. In *Advancing Culture of Living with Landslides*, pages 33–43. Springer International Publishing, Cham.

Bell, F. G. and Donnelly, L. J. (2006). *Mining and its Impact on the Environment.* CRC press.

Briese, C., Pfeifer, N., and Dorninger, P. (2002). Applications of the robust interpolation for DTM determination. *International Archives of Photogrammetry Remote Sensing and Spatial Information Sciences*, 34 (3/A):55–61.

Brovelli, M. A., Cannata, M., and Longoni, U. (2002). Managing and processing LIDAR data within GRASS. *Proceedings of the Open source GIS - GRASS users conference*, (September):11–13.

Brown, A. G., Tooth, S., Bullard, J. E., Thomas, D. S. G., Chiverrell, R. C., Plater, A. J., Murton, J., Thorndycraft, V. R., Tarolli, P., Rose, J., Wainwright, J., Downs, P., and Aalto, R. (2017). The geomorphology of the Anthropocene: emergence, status and implications. *Earth Surface Processes and Landforms*, 42(1):71–90.

Buján, S., Cordero, M., and Miranda, D. (2020). Hybrid Overlap Filter for LiDAR Point Clouds Using Free Software. *Remote Sensing*, 12(7):1051.

CAA (2017). Letecký předpis pravidla létání L2 - Doplněk X.

Cai, S., Zhang, W., Liang, X., Wan, P., Qi, J., Yu, S., Yan, G., and Shao, J. (2019). Filtering Airborne LiDAR Data Through Complementary Cloth Simulation and Progressive TIN Densification Filters. *Remote Sensing*, 11(9):1037.

Carrivick, J. L., Smith, M. W., and Quincey, D. J. (2016). *Structure from Motion in the Geosciences.* John Wiley & Sons, Ltd, Chichester, UK.

Chalupa, V., Pánek, T., Tábořík, P., Klimeš, J., Hartvich, F., and Grygar, R. (2018). Deep-seated gravitational slope deformations controlled by the structure of flysch nappe outliers: Insights from

large-scale electrical resistivity tomography survey and LiDAR mapping. *Geomorphology*, 321:174–187.

Chen, Q., Gong, P., Baldocchi, D., and Xie, G. (2007). Filtering Airborne Laser Scanning Data with Morphological Methods. *Photogrammetric Engineering & Remote Sensing*, 73(2):175–185.

Chen, Y., Zhu, X., Yebra, M., Harris, S., and Tapper, N. (2017a). Development of a predictive model for estimating forest surface fuel load in Australian eucalypt forests with LiDAR data. *Environmental Modelling & Software*, 97:61–71.

Chen, Z., Gao, B., and Devereux, B. (2017b). State-of-the-Art: DTM Generation Using Airborne LIDAR Data. *Sensors*, 17(12):150.

Cho, Y.-C. and Song, Y.-S. (2014). Deformation measurements and a stability analysis of the slope at a coal mine waste dump. *Ecological Engineering*, 68:189–199.

Civera, J., Davison, A. J., Magallón, J. A., and Montiel, J. M. M. (2009). Drift-Free Real-Time Sequential Mosaicing. *International Journal of Computer Vision*, 81(2):128–137.

Clark, M. L., Clark, D. B., and Roberts, D. A. (2004). Small-footprint lidar estimation of sub-canopy elevation and tree height in a tropical rain forest landscape. *Remote Sensing of Environment*, 91(1):68–89.

Close, O., Stéphenne, N., and Frippiat, C. (2016). Impact of DEM Processing on the Geotechnical Instability Analysis of Waste Heaps in Wallonia Impact of DEM Processing on the Geotechnical Instability Analysis of Waste Heaps in Wallonia. In *GEOProcessing 2016: The Eighth International Conference on Advanced Geographic Information Systems, Applications, and Services*, number July, pages 7–13.

Cmielewski, B., Dabek, P. B., Patrzalek, C., and Wilczynska, I. (2018). Potential of using unmanned aircraft systems for landslide monitoring:

the case of janowiec landslide in Poland. *Journal of Environmental Science and Management*, 21(1):8–25.

Coops, N. C., Hilker, T., Wulder, M. A., St-Onge, B., Newnham, G., Siggins, A., and Trofymow, J. A. T. (2007). Estimating canopy structure of Douglas-fir forest stands from discrete-return LiDAR. *Trees*, 21(3):295–310.

Cordell, S., Questad, E. J., Asner, G. P., Kinney, K. M., Thaxton, J. M., Uowolo, A., Brooks, S., and Chynoweth, M. W. (2017). Remote sensing for restoration planning: how the big picture can inform stakeholders. *Restoration Ecology*, 25:S147–S154.

Cunliffe, A. M., Brazier, R. E., and Anderson, K. (2016). Ultra-fine grain landscape-scale quantification of dryland vegetation structure with drone-acquired structure-from-motion photogrammetry. *Remote Sensing of Environment*, 183:129–143.

Dandois, J. P. and Ellis, E. C. (2013). High spatial resolution three-dimensional mapping of vegetation spectral dynamics using computer vision. *Remote Sensing of Environment*, 136:259–276.

DeWitt, J. D., Warner, T. A., Chirico, P. G., and Bergstresser, S. E. (2017). Creating high-resolution bare-earth digital elevation models (DEMs) from stereo imagery in an area of densely vegetated deciduous forest using combinations of procedures designed for lidar point cloud filtering. *GIScience & Remote Sensing*, 54(4):552–572.

DiGiacomo, A. E., Bird, C. N., Pan, V. G., Dobroski, K., Atkins-Davis, C., Johnston, D. W., and Ridge, J. T. (2020). Modeling Salt Marsh Vegetation Height Using Unoccupied Aircraft Systems and Structure from Motion. *Remote Sensing*, 12(14):2333.

Doležalová, J., Vojar, J., Smolová, D., Solský, M., and Kopecký, O. (2012). Technical reclamation and spontaneous succession produce

different water habitats: A case study from Czech post-mining sites. *Ecological Engineering*, 43:5–12.

Dulias, R. (2016). Changes in Morphometric Parameters of Terrain Caused by Mining. In *The Impact of Mining on the Landscape*, pages 83–93. Springer.

Effrosynidis, D. and Arampatzis, A. (2021). An evaluation of feature selection methods for environmental data. *Ecological Informatics*, 61:101224.

Elmqvist, M., Jungert, E., Lantz, F., Persson, A., and Söderman, U. (2001). Terrain modelling and analysis using laser scanner data. *International Archives of Photogrammetry Remote Sensing and Spatial Information Sciences*, 34 (3/W4):22–24.

Estornell, J., Ruiz, L., Velázquez-Martí, B., and Hermosilla, T. (2011). Analysis of the factors affecting LiDAR DTM accuracy in a steep shrub area. *International Journal of Digital Earth*, 4(6):521–538.

Favorskaya, M. N. and Jain, L. C. (2017). *Handbook on Advances in Remote Sensing and Geographic Information Systems*, volume 122 of *Intelligent Systems Reference Library*. Springer International Publishing, Cham.

Fischer, W., Hemphill, W., and Kover, A. (1976). Progress in remote sensing (1972–1976). *Photogrammetria*, 32(2):33–72.

Fogl, M. and Moudrý, V. (2016). Influence of vegetation canopies on solar potential in urban environments. *Applied Geography*, 66:73–80.

Fonstad, M. A., Dietrich, J. T., Courville, B. C., Jensen, J. L., and Carbonneau, P. E. (2013). Topographic structure from motion: a new development in photogrammetric measurement. *Earth Surface Processes and Landforms*, 38(4):421–430.

Fox, J. and Weisberg, S. (2011). Multivariate Linear Models in R. *An R Companion to Applied Regression*, (July):1–31.

Fox, J. and Weisberg, S. (2019). *An R Companion to Applied Regression*. Sage, third edit edition.

Frazer, G., Magnussen, S., Wulder, M., and Niemann, K. (2011). Simulated impact of sample plot size and co-registration error on the accuracy and uncertainty of LiDAR-derived estimates of forest stand biomass. *Remote Sensing of Environment*, 115(2):636–649.

Frouz, J., Mudrák, O., Reitschmiedová, E., Walmsley, A., Vachová, P., Šimáčková, H., Albrechtová, J., Moradi, J., and Kučera, J. (2018). Rough wave-like heaped overburden promotes establishment of woody vegetation while leveling promotes grasses during unassisted post mining site development. *Journal of Environmental Management*, 205:50–58.

Fuhrmann, S., Langguth, F., and Goesele, M. (2014). MVE - A Multi-View reconstruction environment. *Eurographics Workshop on Graphics and Cultural Heritage*, pages 11–18.

Furukawa, Y. and Ponce, J. (2010). Accurate, Dense, and Robust Multiview Stereopsis. *IEEE Transactions on Pattern Analysis and Machine Intelligence*, 32(8):1362–1376.

Gonçalves, G. and Pereira, L. G. (2010). Assessment of the performance of eight filtering algorithms by using full-waveform LiDAR data of unmanaged eucalypt forest. In *Proceedings Silvilaser 2010: The 10th International Conference on LiDAR Applications for Assessing Forest Ecosystems*, pages 187 – 196, Freiburg, Germany. Albert-Ludwigs-University of Freiburg.

Graham, A., Coops, N., Wilcox, M., and Plowright, A. (2019). Evaluation of Ground Surface Models Derived from Unmanned Aerial

Systems with Digital Aerial Photogrammetry in a Disturbed Conifer Forest. *Remote Sensing*, 11(1):84.

Guo, X., Coops, N. C., Tompalski, P., Nielsen, S. E., Bater, C. W., and John Stadt, J. (2017). Regional mapping of vegetation structure for biodiversity monitoring using airborne lidar data. *Ecological Informatics*, 38:50–61.

Haigh, M. J. and Gentcheva-Kostadinova, S. (2002). Ecological erosion control on coal-spoil banks: an evaluation. *Ecological Engineering*, 18(3):371–377.

Hancock, G. R., Crawter, D., Fityus, S. G., Chandler, J., and Wells, T. (2008). The measurement and modelling of rill erosion at angle of repose slopes in mine spoil. *Earth Surface Processes and Landforms*, 33(7):1006–1020.

Hanuš, J., Fabiánek, T., and Fajmon, L. (2016). Potential of airborne imaging spectroscopy at CzechGlobe. *ISPRS - International Archives of the Photogrammetry, Remote Sensing and Spatial Information Sciences*, XLI-B1:15–17.

Harabiš, F. (2016). High diversity of odonates in post-mining areas: Meta-analysis uncovers potential pitfalls associated with the formation and management of valuable habitats. *Ecological Engineering*, 90:438–446.

Harabiš, F., Tichanek, F., and Tropek, R. (2013). Dragonflies of freshwater pools in lignite spoil heaps: Restoration management, habitat structure and conservation value. *Ecological Engineering*, 55:51–61.

Hawryło, P., Tompalski, P., and Wężyk, P. (2017). Area-based estimation of growing stock volume in Scots pine stands using ALS and airborne image-based point clouds. *Forestry: An International Journal of Forest Research*, 90(5):686–696.

Hendrychová, M. and Kabrna, M. (2016). An analysis of 200-year-long changes in a landscape affected by large-scale surface coal mining: History, present and future. *Applied Geography*, 74:151–159.

Heritage, G. L. and Large, A. R. (2009). *Laser Scanning for the Environmental Sciences*. Wiley-Blackwell, Oxford, UK.

Hijmans, R. (2019). raster: Geographic Data Analysis and Modeling.

Hodgson, M. E. and Bresnahan, P. (2004). Accuracy of Airborne Lidar-Derived Elevation. *Photogrammetric Engineering & Remote Sensing*, 70(3):331–339.

Hodgson, M. E., Jensen, J., Raber, G., Tullis, J., Davis, B. A., Thompson, G., and Schuckman, K. (2005). An Evaluation of Lidar-derived Elevation and Terrain Slope in Leaf-off Conditions. *Photogrammetric Engineering & Remote Sensing*, 71(7):817–823.

Hofierka, J., Gallay, M., Bandura, P., and Šašak, J. (2018). Identification of karst sinkholes in a forested karst landscape using airborne laser scanning data and water flow analysis. *Geomorphology*, 308:265–277.

Hogarth, J., Hawley, M., and Beale, G. (2017). *Instrumentation and monitoring*. CSIRO Publishing.

Höhle, J. and Höhle, M. (2009). Accuracy assessment of digital elevation models by means of robust statistical methods. *ISPRS Journal of Photogrammetry and Remote Sensing*, 64(4):398–406.

Hollaus, M., Wagner, W., Eberhöfer, C., and Karel, W. (2006). Accuracy of large-scale canopy heights derived from LiDAR data under operational constraints in a complex alpine environment. *ISPRS Journal of Photogrammetry and Remote Sensing*, 60(5):323–338.

Hopkinson, C., Chasmer, L. E., Sass, G., Creed, I. F., Sitar, M., Kalbfleisch, W., and Treitz, P. (2005). Vegetation class dependent

errors in lidar ground elevation and canopy height estimates in a boreal wetland environment. *Canadian Journal of Remote Sensing*, 31(2):191–206.

Hui, Z., Hu, Y., Yevenyo, Y., and Yu, X. (2016). An Improved Morphological Algorithm for Filtering Airborne LiDAR Point Cloud Based on Multi-Level Kriging Interpolation. *Remote Sensing*, 8(1):35.

Hyyppä, H., Yu, X., Hyyppä, J., Kaartinen, H., Kaasalainen, S., Honkavaara, E., and Rönnholm, P. (2005). Factors affecting the quality of DTM generation in forested areas. *International Archives of Photogrammetry, Remote Sensing and Spatial Information Sciences*, 36 (3/W19):85–90.

Indirabai, I., Nair, M. H., Jaishanker, R. N., and Nidamanuri, R. R. (2019). Terrestrial laser scanner based 3D reconstruction of trees and retrieval of leaf area index in a forest environment. *Ecological Informatics*, 53:100986.

Isenburg, M. (2018). LAStools - efficient LiDAR processing software.

Jakubowski, M. K., Guo, Q., and Kelly, M. (2013). Tradeoffs between lidar pulse density and forest measurement accuracy. *Remote Sensing of Environment*, 130:245–253.

Javernick, L., Brasington, J., and Caruso, B. (2014). Modeling the topography of shallow braided rivers using Structure-from-Motion photogrammetry. *Geomorphology*, 213:166–182.

Jensen, J. and Mathews, A. (2016). Assessment of Image-Based Point Cloud Products to Generate a Bare Earth Surface and Estimate Canopy Heights in a Woodland Ecosystem. *Remote Sensing*, 8(1):50.

Johansen, K., Phinn, S., and Witte, C. (2010). Mapping of riparian zone attributes using discrete return LiDAR, QuickBird and SPOT-5 imagery: Assessing accuracy and costs. *Remote Sensing of Environment*, 114(11):2679–2691.

Julge, K., Ellmann, A., and Gruno, A. (2014). Performance analysis of freeware filtering algorithms for determining ground surface from airborne laser scanning data. *Journal of Applied Remote Sensing*, 8(1):083573.

Kachamba, D., Ørka, H., Gobakken, T., Eid, T., and Mwase, W. (2016). Biomass Estimation Using 3D Data from Unmanned Aerial Vehicle Imagery in a Tropical Woodland. *Remote Sensing*, 8(11):968.

Kalacska, M., Chmura, G., Lucanus, O., Bérubé, D., and Arroyo-Mora, J. (2017). Structure from motion will revolutionize analyses of tidal wetland landscapes. *Remote Sensing of Environment*, 199:14–24.

Klouček, T., Lagner, O., and Šímová, P. (2015). How does data accuracy influence the reliability of digital viewshed models? A case study with wind turbines. *Applied Geography*, 64:46–54.

Komárek, J., Klouček, T., and Prošek, J. (2018). The potential of Unmanned Aerial Systems: A tool towards precision classification of hard-to-distinguish vegetation types? *International Journal of Applied Earth Observation and Geoinformation*, 71:9–19.

Korzeniowska, K., Pfeifer, N., Mandlburger, G., and Lugmayr, A. (2014). Experimental evaluation of ALS point cloud ground extraction tools over different terrain slope and land-cover types. *International Journal of Remote Sensing*, 35(13):4673–4697.

Koska, B., Jirka, V., Urban, R., Křemen, T., Hesslerová, P., Jon, J., Pospíšil, J., and Fogl, M. (2017). Suitability, characteristics, and comparison of an airship UAV with lidar for middle size area mapping. *International Journal of Remote Sensing*, 38(8-10):2973–2990.

Kraus, K. and Pfeifer, N. (1998). Determination of terrain models in wooded areas with airborne laser scanner data. *ISPRS Journal of Photogrammetry and Remote Sensing*, 53(4):193–203.

Kršák, B., Blišťan, P., Pauliková, A., Puškárová, P., Kovanič, , Palková, J., and Zelizňaková, V. (2016). Use of low-cost UAV photogrammetry to analyze the accuracy of a digital elevation model in a case study. *Measurement*, 91:276–287.

Kumhálová, J. and Moudrý, V. (2014). Topographical characteristics for precision agriculture in conditions of the Czech Republic. *Applied Geography*, 50:90–98.

Lagner, O., Klouček, T., and Šímová, P. (2018). Impact of input data (in)accuracy on overestimation of visible area in digital viewshed models. *PeerJ*, 6(5):e4835.

Langhammer, J., Janský, B., Kocum, J., and Minařík, R. (2018). 3-D reconstruction of an abandoned montane reservoir using UAV photogrammetry, aerial LiDAR and field survey. *Applied Geography*, 98:9–21.

Lechner, A. M., McIntyre, N., Witt, K., Raymond, C. M., Arnold, S., Scott, M., and Rifkin, W. (2017). Challenges of integrated modelling in mining regions to address social, environmental and economic impacts. *Environmental Modelling & Software*, 93:268–281.

Leica Geosystems (2003). *Leica Photogrammetry Suite OrthoBASE & OrthoBASE Pro User's Guide*. Leica Geosystems GIS & Mapping, LLC, Atlanta (GA).

Leitold, V., Keller, M., Morton, D. C., Cook, B. D., and Shimabukuro, Y. E. (2015). Airborne lidar-based estimates of tropical forest structure in complex terrain: opportunities and trade-offs for REDD+. *Carbon Balance and Management*, 10(1):3.

Lisein, J., Pierrot-Deseilligny, M., Bonnet, S., and Lejeune, P. (2013). A Photogrammetric Workflow for the Creation of a Forest Canopy Height Model from Small Unmanned Aerial System Imagery. *Forests*, 4(4):922–944.

Liu, Q., Fu, L., Chen, Q., Wang, G., Luo, P., Sharma, R. P., He, P., Li, M., Wang, M., and Duan, G. (2020). Analysis of the Spatial Differences in Canopy Height Models from UAV LiDAR and Photogrammetry. *Remote Sensing*, 12(18):2884.

Lovitt, J., Rahman, M. M., and McDermid, G. J. (2017). Assessing the Value of UAV Photogrammetry for Characterizing Terrain in Complex Peatlands. *Remote Sensing*, 9(7):715.

Lowe, D. G. (2004). Distinctive Image Features from Scale-Invariant Keypoints. *International Journal of Computer Vision*, 60(2):91–110.

Luo, S., Wang, C., Pan, F., Xi, X., Li, G., Nie, S., and Xia, S. (2015). Estimation of wetland vegetation height and leaf area index using airborne laser scanning data. *Ecological Indicators*, 48:550–559.

Maguya, A., Junttila, V., and Kauranne, T. (2013). Adaptive algorithm for large scale dtm interpolation from lidar data for forestry applications in steep forested terrain. *ISPRS Journal of Photogrammetry and Remote Sensing*, 85:74–83.

Maguya, A., Junttila, V., and Kauranne, T. (2014). Algorithm for Extracting Digital Terrain Models under Forest Canopy from Airborne LiDAR Data. *Remote Sensing*, 6(7):6524–6548.

Mallick, J., Talukdar, S., Alsubih, M., Ahmed, M., Islam, A. R. M. T., Shahfahad, and Thanh, N. V. (2021). Proposing receiver operating characteristic-based sensitivity analysis with introducing swarm optimized ensemble learning algorithms for groundwater potentiality modelling in Asir region, Saudi Arabia. *Geocarto International*, pages 1–28.

Mandlburger, G., Wenzel, K., Spitzer, A., Haala, N., Glira, P., and Pfeifer, N. (2017). Improved topographic models via concurrent

airborne LiDAR and dense image matching. *ISPRS Annals of Photogrammetry, Remote Sensing and Spatial Information Sciences*, IV-2/W4:259–266.

May, N. C. and Toth, C. K. (2007). Point positioning accuracy of airborne LiDAR systems: A rigorius analysis. *International Archives of Photogrammetry, Remote Sensing and Spatial Information Sciences*, 36 (3/W49B:107–111.

Méndez-Vázquez, L. J., Lira-Noriega, A., Lasa-Covarrubias, R., and Cerdeira-Estrada, S. (2019). Delineation of site-specific management zones for pest control purposes: Exploring precision agriculture and species distribution modeling approaches. *Computers and Electronics in Agriculture*, 167:105101.

Meng, X., Currit, N., and Zhao, K. (2010). Ground Filtering Algorithms for Airborne LiDAR Data: A Review of Critical Issues. *Remote Sensing*, 2(3):833–860.

Meng, X., Wang, L., Silván-Cárdenas, J. L., and Currit, N. (2009). A multi-directional ground filtering algorithm for airborne LiDAR. *ISPRS Journal of Photogrammetry and Remote Sensing*, 64(1):117–124.

Mesas-Carrascosa, F.-J., Notario García, M., Meroño de Larriva, J., and García-Ferrer, A. (2016). An Analysis of the Influence of Flight Parameters in the Generation of Unmanned Aerial Vehicle (UAV) Orthomosaicks to Survey Archaeological Areas. *Sensors*, 16(11):1838.

Mikita, T., Janata, P., and Surový, P. (2016). Forest Stand Inventory Based on Combined Aerial and Terrestrial Close-Range Photogrammetry. *Forests*, 7(12):165.

Mongus, D., Lukač, N., and Žalik, B. (2014). Ground and building extraction from LiDAR data based on differential morphological

profiles and locally fitted surfaces. *ISPRS Journal of Photogrammetry and Remote Sensing*, 93:145–156.

Montealegre, A. L., Lamelas, M. T., and de la Riva, J. (2015). A Comparison of Open-Source LiDAR Filtering Algorithms in a Mediterranean Forest Environment. *IEEE Journal of Selected Topics in Applied Earth Observations and Remote Sensing*, 8(8):4072–4085.

Moore, I. D., Grayson, R. B., and Ladson, A. R. (1991). Digital terrain modelling: A review of hydrological, geomorphological, and biological applications. *Hydrological Processes*, 5(1):3–30.

Moudrý, V., Beková, A., and Lagner, O. (2019a). Evaluation of a high resolution UAV imagery model for rooftop solar irradiation estimates. *Remote Sensing Letters*, 10(11):1077–1085.

Moudrý, V., Gdulová, K., Fogl, M., Klápště, P., Urban, R., Komárek, J., Moudrá, L., Štroner, M., Barták, V., and Solský, M. (2019b). Comparison of leaf-off and leaf-on combined UAV imagery and airborne LiDAR for assessment of a post-mining site terrain and vegetation structure: Prospects for monitoring hazards and restoration success. *Applied Geography*, 104:32–41.

Moudrý, V., Lecours, V., Gdulová, K., Gábor, L., Moudrá, L., Kropáček, J., and Wild, J. (2018). On the use of global DEMs in ecological modelling and the accuracy of new bare-earth DEMs. *Ecological Modelling*, 383:3–9.

Moudrý, V., Lecours, V., Malavasi, M., Misiuk, B., Gábor, L., Gdulová, K., Šímová, P., and Wild, J. (2019c). Potential pitfalls in rescaling digital terrain model-derived attributes for ecological studies. *Ecological Informatics*, 54:100987.

Moudrý, V., Urban, R., Štroner, M., Komárek, J., Brouček, J., and Prošek, J. (2019d). Comparison of a commercial and home-assembled

fixed-wing UAV for terrain mapping of a post-mining site under leaf-off conditions. *International Journal of Remote Sensing*, 40(2):555–572.

Nakagawa, S. and Schielzeth, H. (2013). A general and simple method for obtaining R 2 from generalized linear mixed-effects models. *Methods in Ecology and Evolution*, 4(2):133–142.

Nex, F. and Remondino, F. (2014). UAV for 3D mapping applications: a review. *Applied Geomatics*, 6(1):1–15.

Ni, W., Sun, G., Ranson, K. J., Pang, Y., Zhang, Z., and Yao, W. (2015). Extraction of ground surface elevation from ZY-3 winter stereo imagery over deciduous forested areas. *Remote Sensing of Environment*, 159:194–202.

Nyssen, J. and Vermeersch, D. (2010). Slope aspect affects geomorphic dynamics of coal mining spoil heaps in Belgium. *Geomorphology*, 123(1-2):109–121.

Penížek, V., Zádorová, T., Kodešová, R., and Vaněk, A. (2016). Influence of Elevation Data Resolution on Spatial Prediction of Colluvial Soils in a Luvisol Region. *PLOS One*, 11(11):e0165699.

Petras, V., Petrasova, A., Jeziorska, J., and Mitasova, H. (2016). Processing UAV and LiDAR point clouds in GRASS GIS. *ISPRS - International Archives of the Photogrammetry, Remote Sensing and Spatial Information Sciences*, XLI-B7:945–952.

Pfeifer, N., Stadler, P., and Briese, C. (2001). Derivation Of Digital Terrain Models In The Scop++ Environment. *OEEPE Workshop on Airborne Laserscanning and Interferometric SAR for Digital Elevation Models*, page 13.

Pingel, T. J., Clarke, K. C., and McBride, W. A. (2013). An improved simple morphological filter for the terrain classification of airborne

LIDAR data. *ISPRS Journal of Photogrammetry and Remote Sensing*, 77:21–30.

Pinton, D., Canestrelli, A., Wilkinson, B., Ifju, P., and Ortega, A. (2020). A new algorithm for estimating ground elevation and vegetation characteristics in coastal salt marshes from high-resolution UAV-based LiDAR point clouds. *Earth Surface Processes and Landforms*, 45(14):3687–3701.

Podobnikar, T. and Vrečko, A. (2012). Digital Elevation Model from the Best Results of Different Filtering of a LiDAR Point Cloud. *Transactions in GIS*, 16(5):603–617.

Polat, N. and Uysal, M. (2015). Investigating performance of Airborne LiDAR data filtering algorithms for DTM generation. *Measurement*, 63:61–68.

Popelková, R. and Mulková, M. (2018). The mining landscape of the Ostrava-Karviná coalfield: Processes of landscape change from the 1830s to the beginning of the 21st century. *Applied Geography*, 90:28–43.

Prošek, J. and Šímová, P. (2019). UAV for mapping shrubland vegetation: Does fusion of spectral and vertical information derived from a single sensor increase the classification accuracy? *International Journal of Applied Earth Observation and Geoinformation*, 75:151–162.

R Core Team (2018). R: A Language and Environment for Statistical Computing.

Rahman, M. M., McDermid, G. J., Strack, M., and Lovitt, J. (2017). A New Method to Map Groundwater Table in Peatlands Using Unmanned Aerial Vehicles. *Remote Sensing*, 9(10):1057.

Rashidi, P. and Rastiveis, H. (2017). Ground filtering LiDAR data based on multi-scale analysis of height difference threshold. *ISPRS - International Archives of the Photogrammetry, Remote Sensing and Spatial Information Sciences*, XLII-4/W4(4W4):225–229.

Reutebuch, S. E., McGaughey, R. J., Andersen, H.-E., and Carson, W. W. (2003). Accuracy of a high-resolution lidar terrain model under a conifer forest canopy. *Canadian Journal of Remote Sensing*, 29(5):527–535.

Ritter, B. (2014). *Use of unmanned aerial vehicles (UAV) for urban tree inventories.* PhD thesis, Clemson University.

Roggero, M. (2001). Airborne Laser Scanning: Clustering in Raw Data. *International Archives of Photogrammetry Remote Sensing and Spatial Information Sciences*, 34 (3/W4):227–232.

Roussel, J.-R., Caspersen, J., Béland, M., Thomas, S., and Achim, A. (2017). Removing bias from LiDAR-based estimates of canopy height: Accounting for the effects of pulse density and footprint size. *Remote Sensing of Environment*, 198:1–16.

Rupnik, E., Daakir, M., and Pierrot Deseilligny, M. (2017). MicMac – a free, open-source solution for photogrammetry. *Open Geospatial Data, Software and Standards*, 2(1):14.

Šálek, M. (2012). Spontaneous succession on opencast mining sites: implications for bird biodiversity. *Journal of Applied Ecology*, 49(6):1417–1425.

Sangireddy, H., Stark, C. P., Kladzyk, A., and Passalacqua, P. (2016). GeoNet: An open source software for the automatic and objective extraction of channel heads, channel network, and channel morphology from high resolution topography data. *Environmental Modelling & Software*, 83:58–73.

Sedlák, V., Hofierka, J., Gallay, M., and Kaňuk, J. (2018). Specific Solution of 3d Deformation Vector in Mine Subsidence: a Case Study of The Košice-Bankov Abandoned Magnesite Mine, Slovakia. *Archives of Mining Sciences*, vol. 63(No 2).

Serifoglu Yilmaz, C. and Gungor, O. (2018). Comparison of the performances of ground filtering algorithms and DTM generation from a UAV-based point cloud. *Geocarto International*, 33(5):522–537.

Serifoglu Yilmaz, C., Gungor, O., and Yilmaz, V. (2016). Performance evaluation of different ground filtering algorithms for UAV-based point clouds. *ISPRS - International Archives of the Photogrammetry, Remote Sensing and Spatial Information Sciences*, XLI-B1:245–251.

Serifoglu Yilmaz, C., Yilmaz, V., and Güngör, O. (2018). Investigating the performances of commercial and non-commercial software for ground filtering of UAV-based point clouds. *International Journal of Remote Sensing*, 39(15-16):5016–5042.

Shackelford, N., Miller, B. P., and Erickson, T. E. (2018). Restoration of Open-Cut Mining in Semi-Arid Systems: A Synthesis of Long-Term Monitoring Data and Implications for Management. *Land Degradation & Development*, 29(4):994–1004.

Shan, J. and Aparajithan, S. (2005). Urban DEM Generation from Raw Lidar Data. *Photogrammetric Engineering & Remote Sensing*, 71(2):217–226.

Silva, C. A., Klauberg, C., Hentz, Â. M. K., Corte, A. P. D., Ribeiro, U., and Liesenberg, V. (2018). Comparing the Performance of Ground Filtering Algorithms for Terrain Modeling in a Forest Environment Using Airborne LiDAR Data. *Floresta e Ambiente*, 25(2).

Simpson, J., Smith, T., and Wooster, M. (2017). Assessment of Errors Caused by Forest Vegetation Structure in Airborne LiDAR-Derived DTMs. *Remote Sensing*, 9(11):1101.

Sithole, G. and Vosselman, G. (2004). Experimental comparison of filter algorithms for bare-Earth extraction from airborne laser scanning point clouds. *ISPRS Journal of Photogrammetry and Remote Sensing*, 59(1-2):85–101.

Slatton, K. C., Carter, W. E., Shrestha, R. L., and Dietrich, W. (2007). Airborne Laser Swath Mapping: Achieving the resolution and accuracy required for geosurficial research. *Geophysical Research Letters*, 34(23).

Smith, M., Carrivick, J., and Quincey, D. (2016). Structure from motion photogrammetry in physical geography. *Progress in Physical Geography: Earth and Environment*, 40(2):247–275.

Snavely, N., Seitz, S. M., and Szeliski, R. (2008). Modeling the World from Internet Photo Collections. *International Journal of Computer Vision*, 80(2):189–210.

Sohn, G. and Dowman, I. (2002). Terrain Surface Reconstruction By the Use of Tetrahedron Model With the MDL Criterion. *International Archives of Photogrammetry Remote Sensing and Spatial Information Sciences*, 34 (3/A):336–344.

Spaete, L. P., Glenn, N. F., Derryberry, D. R., Sankey, T. T., Mitchell, J. J., and Hardegree, S. P. (2011). Vegetation and slope effects on accuracy of a LiDAR-derived DEM in the sagebrush steppe. *Remote Sensing Letters*, 2(4):317–326.

Steiakakis, E., Kavouridis, K., and Monopolis, D. (2009). Large scale failure of the external waste dump at the "South Field" lignite mine, Northern Greece. *Engineering Geology*, 104(3-4):269–279.

Stephenne, N., Frippiat, C., Veschkens, M., Salmon, M., and Pacyna, D. (2014). Use of a Lidar High Resolution Digital Elevation Model for Risk Stability Analysis. *EARSeL eProceedings*, 13(3):24–29.

Stereńczak, K., Ciesielski, M., Balazy, R., and Zawiła-Niedźwiecki, T. (2016). Comparison of various algorithms for DTM interpolation from LIDAR data in dense mountain forests. *European Journal of Remote Sensing*, 49(1):599–621.

Sulaiman, N. S., Majid, Z., and Setan, H. (2010). DTM generation from LiDAR data by using different filters in open-source software. *Geoinformation Science Journal*, 10(2):89–109.

Susaki, J. (2012). Adaptive Slope Filtering of Airborne LiDAR Data in Urban Areas for Digital Terrain Model (DTM) Generation. *Remote Sensing*, 4(6):1804–1819.

Svobodova, K., Sklenicka, P., Molnarova, K., and Salek, M. (2012). Visual preferences for physical attributes of mining and post-mining landscapes with respect to the sociodemographic characteristics of respondents. *Ecological Engineering*, 43:34–44.

Sweeney, C. (2016). Theia Multiview Geometry Library: Tutorial & Reference.

Szostak, M., Knapik, K., Wężyk, P., Likus-Cieślik, J., and Pietrzykowski, M. (2019). Fusing Sentinel-2 Imagery and ALS Point Clouds for Defining LULC Changes on Reclaimed Areas by Afforestation. *Sustainability*, 11(5):1251.

Tan, Y., Wang, S., Xu, B., and Zhang, J. (2018). An improved progressive morphological filter for UAV-based photogrammetric point clouds in river bank monitoring. *ISPRS Journal of Photogrammetry and Remote Sensing*, 146:421–429.

Tarolli, P. and Sofia, G. (2016). Human topographic signatures and derived geomorphic processes across landscapes. *Geomorphology*, 255:140–161.

Tinkham, W. T., Huang, H., Smith, A. M. S., Shrestha, R., Falkowski, M. J., Hudak, A. T., Link, T. E., Glenn, N. F., and Marks, D. G. (2011). A Comparison of Two Open Source LiDAR Surface Classification Algorithms. *Remote Sensing*, 3(3):638–649.

Toldo, R., Gherardi, R., Farenzena, M., and Fusiello, A. (2015). Hierarchical structure-and-motion recovery from uncalibrated images. *Computer Vision and Image Understanding*, 140:127–143.

Tomaštík, J., Mokroš, M., Saloň, Š., Chudý, F., and Tunák, D. (2017). Accuracy of Photogrammetric UAV-Based Point Clouds under Conditions of Partially-Open Forest Canopy. *Forests*, 8(5):151.

Tomaštík, J., Mokroš, M., Surový, P., Grznárová, A., and Merganič, J. (2019). UAV RTK/PPK Method—An Optimal Solution for Mapping Inaccessible Forested Areas? *Remote Sensing*, 11(6):721.

Tonkin, T. and Midgley, N. (2016). Ground-Control Networks for Image Based Surface Reconstruction: An Investigation of Optimum Survey Designs Using UAV Derived Imagery and Structure-from-Motion Photogrammetry. *Remote Sensing*, 8(9):786.

Tonkin, T., Midgley, N., Graham, D., and Labadz, J. (2014). The potential of small unmanned aircraft systems and structure-from-motion for topographic surveys: A test of emerging integrated approaches at Cwm Idwal, North Wales. *Geomorphology*, 226:35–43.

UN General Assembly (1986). Principles relating to Remote Sensing of the Earth from Outer Space : resolution / adopted by the General Assembly.

van Iersel, W., Straatsma, M., Addink, E., and Middelkoop, H. (2018). Monitoring height and greenness of non-woody floodplain vegetation with UAV time series. *ISPRS Journal of Photogrammetry and Remote Sensing*, 141:112–123.

Vojar, J., Doležalová, J., Solský, M., Smolová, D., Kopecký, O., Kadlec, T., and Knapp, M. (2016). Spontaneous succession on spoil banks supports amphibian diversity and abundance. *Ecological Engineering*, 90:278–284.

Vosselman, G. (2000). Slope based filtering of laser altimetry data. *International Archives of Photogrammetry and Remote Sensing*, 33 (B3/2):935–942.

Vosselman, G. and Mass, H.-G. (2010). *Airborne and Terrestrial Laser Scanning*. Whittles Publishing, Caithness, Scotland.

Vymazal, J. and Sklenicka, P. (2012). Restoration of areas affected by mining. *Ecological Engineering*, 43:1–4.

Wack, R. and Wimmer, A. (2002). Digital terrain models from airborne laser scanner data – a grid based approach. *International Archives of Photogrammetry Remote Sensing and Spatial Information Sciences*, 34 (3/B):293–296.

Wallace, L., Bellman, C., Hally, B., Hernandez, J., Jones, S., and Hillman, S. (2019). Assessing the Ability of Image Based Point Clouds Captured from a UAV to Measure the Terrain in the Presence of Canopy Cover. *Forests*, 10(3):284.

Wallace, L., Lucieer, A., Malenovský, Z., Turner, D., and Vopěnka, P. (2016). Assessment of Forest Structure Using Two UAV Techniques: A Comparison of Airborne Laser Scanning and Structure from Motion (SfM) Point Clouds. *Forests*, 7(12):62.

Wallace, L., Lucieer, A., Watson, C., and Turner, D. (2012). Development of a UAV-LiDAR System with Application to Forest Inventory. *Remote Sensing*, 4(6):1519–1543.

Wan, P., Zhang, W., Skidmore, A. K., Qi, J., Jin, X., Yan, G., and Wang, T. (2018). A simple terrain relief index for tuning slope-related

parameters of LiDAR ground filtering algorithms. *ISPRS Journal of Photogrammetry and Remote Sensing*, 143:181–190.

Wang, X., Ma, X., Yang, F., Su, D., Qi, C., and Xia, S. (2020). Improved progressive triangular irregular network densification filtering algorithm for airborne LiDAR data based on a multiscale cylindrical neighborhood. *Applied Optics*, 59(22):6540.

Wasowski, J., Bovenga, F., Nutricato, R., Nitti, D. O., and Chiaradia, M. T. (2018). Advanced satellite radar interferometry for deformation monitoring and infrastructure control in open-cast mines and oil/gas fields. *Innovative Infrastructure Solutions*, 3(1):68.

Wehr, A. and Lohr, U. (1999). Airborne laser scanning—an introduction and overview. *ISPRS Journal of Photogrammetry and Remote Sensing*, 54(2-3):68–82.

Westoby, M., Brasington, J., Glasser, N., Hambrey, M., and Reynolds, J. (2012). 'Structure-from-Motion' photogrammetry: A low-cost, effective tool for geoscience applications. *Geomorphology*, 179:300–314.

White, J., Wulder, M., Vastaranta, M., Coops, N., Pitt, D., and Woods, M. (2013). The Utility of Image-Based Point Clouds for Forest Inventory: A Comparison with Airborne Laser Scanning. *Forests*, 4(3):518–536.

Wickham, H. (2009). *ggplot2*. Springer New York, New York, NY.

Wortley, L., Hero, J.-M., and Howes, M. (2013). Evaluating Ecological Restoration Success: A Review of the Literature. *Restoration Ecology*, 21(5):537–543.

Wu, C. (2011). VisualSFM : A Visual Structure from Motion System.

Wężyk, P., Szostak, M., Krzaklewski, W., Pająk, M., Pierzchalski, M., Szwed, P., Hawryło, P., and Ratajczak, M. (2015). Landscape

monitoring of post-industrial areas using LiDAR and GIS technology. *Geodesy and Cartography*, 64(1):125–137.

Xiang, J., Chen, J., Sofia, G., Tian, Y., and Tarolli, P. (2018). Open-pit mine geomorphic changes analysis using multi-temporal UAV survey. *Environmental Earth Sciences*, 77(6):220.

Yan, W., Guan, H., Cao, L., Yu, Y., Li, C., and Lu, J. (2020). A Self-Adaptive Mean Shift Tree-Segmentation Method Using UAV LiDAR Data. *Remote Sensing*, 12(3):515.

Yang, M.-D., Chao, C.-F., Huang, K.-S., Lu, L.-Y., and Chen, Y.-P. (2013). Image-based 3D scene reconstruction and exploration in augmented reality. *Automation in Construction*, 33:48–60.

Yang, P., Ames, D. P., Fonseca, A., Anderson, D., Shrestha, R., Glenn, N. F., and Cao, Y. (2014). What is the effect of LiDAR-derived DEM resolution on large-scale watershed model results? *Environmental Modelling & Software*, 58:48–57.

Zalesky, J. and Capova, K. (2017). Monitoring and Assessment of Remedial Measures in Closed Open Cast Mine. In *Advancing Culture of Living with Landslides*, pages 597–605. Springer International Publishing, Cham.

Zalesky, M., Zalesky, J., Kuklik, P., and Hanek, P. (2008). Monitoring of a large slide and slope reclamation in a former Open-Pit Mine. In *Proceedings of 13th FIG International Symposium on Deformation Measurements and Analysis and 4th IAG Symposium on Geodesy for Geotechnical and Structural Engineering*.

Zeybek, M. and Şanlıoğlu, (2019). Point cloud filtering on UAV based point cloud. *Measurement*, 133:99–111.

Zhang, K., Chen, S.-C., Whitman, D., Shyu, M.-L., Yan, J., and Zhang, C. (2003). A progressive morphological filter for removing nonground

measurements from airborne LIDAR data. *IEEE Transactions on Geoscience and Remote Sensing*, 41(4):872–882.

Zhang, K., Gann, D., Ross, M., Robertson, Q., Sarmiento, J., Santana, S., Rhome, J., and Fritz, C. (2019). Accuracy assessment of ASTER, SRTM, ALOS, and TDX DEMs for Hispaniola and implications for mapping vulnerability to coastal flooding. *Remote Sensing of Environment*, 225:290–306.

Zhang, K. and Whitman, D. (2005). Comparison of Three Algorithms for Filtering Airborne Lidar Data. *Photogrammetric Engineering & Remote Sensing*, 71(3):313–324.

Zhang, W., Qi, J., Wan, P., Wang, H., Xie, D., Wang, X., and Yan, G. (2016). An Easy-to-Use Airborne LiDAR Data Filtering Method Based on Cloth Simulation. *Remote Sensing*, 8(6):501.

Zhang, Z., Gerke, M., Vosselman, G., and Yang, M. Y. (2018). Filtering photogrammetric point clouds using standard LiDAR filters towards DTM generation. *ISPRS Annals of Photogrammetry, Remote Sensing and Spatial Information Sciences*, IV-2(2):319–326.

Zhao, X., Guo, Q., Su, Y., and Xue, B. (2016). Improved progressive TIN densification filtering algorithm for airborne LiDAR data in forested areas. *ISPRS Journal of Photogrammetry and Remote Sensing*, 117:79–91.

Chapter 9

Curriculum Vitae
& List of Publications

Personal

Name: Petr Klápště
Date of birth: February 11th, 1989 (*Czech Republic*)
E-mail: pklapste@fzp.czu.cz
ORCID: orcid.org/0000-0002-8633-1788
RG: researchgate.net/profile/Petr-Klapste
LinkedIn: linkedin.com/in/petrklapste

Affiliations

2015 – present
Department of Spatial Sciences
Faculty of Environmental Sciences
Czech University of Life Sciences Prague
Member of *Spatial Science in Ecology and Environment* Leading
Research Group

Education

2015 – present
Department of Spatial Sciences
Faculty of Environmental Sciences
Czech University of Life Sciences Prague
PhD studies in Applied and Landscape Ecology
Thesis topic: Assessment of ground filtering algorithms of point clouds in complex artificial terrains

2017 – 2020
Institute of Education and Communication
Czech University of Life Sciences Prague
Certificate of completion in Study for Teaching Vocational Subjects
Thesis topic: Usage of m-learning in education

2012 – 2015
Faculty of Environmental Sciences
Czech University of Life Sciences Prague
Master's degree in Landscape and Land Management
Thesis topic: Landscape development in the borderland of the Czech Republic along the border with the former GDR and Poland

2009 – 2012
Faculty of Science, Humanities and Education
Technical University of Liberec
Bachelor's degree in Applied Geography
Thesis topic: Old plans of Liberec from 19th century to mid of 20th century

Participation in Research Projects

2021 – 2026
Center for Landscape and Biodiversity
Technology Agency of the Czech Republic
Co-investigator

2020 – 2023
Possibilities for updating map layers of NATURA 2000 biotopes using advanced remote sensing methods
Technology Agency of the Czech Republic
Co-investigator

2018 – 2022
Responsible water management in built-up areas in relation to the surrounding landscape
Ministry of Education, Youth and Sports of the Czech Republic
Co-investigator

2019 – 2021
Safety mapping of the vegetation along the transport infrastructure
Technology Agency of the Czech Republic
Co-investigator

2019 – 2021
Vegetation health monitoring under ongoing climate change using remote sensing
Ministry of Finance of the Czech Republic
Co-investigator

2019 – 2020
V4 communication platform for use of Earth Observation methods in biotic forest disturbances
Visegrad Fund
Co-investigator

2018 – 2019
Detection of infection forest bark beetle (*Ips typographus*) in advance using unmanned air vehicles
Technology Agency of the Czech Republic
Co-investigator

2017 – 2018
The impact of the resolution of remote sensing data for the assessment of ecological measures
Grant Agency of the Czech University of Life Sciences Prague
Co-investigator

2016 – 2018
New approaches to the use of geodata in habitat-species models
Internal Grant Agency of the Faculty of Environmental Sciences
Leader

2015 – 2016
The reduction of habitat fragmentation consequences in various types
of landscape in the Czech Republic
Ministry of Finance of the Czech Republic
Co-investigator

Internships

11/2019 – 11/2019
Department of Surveying and Cartography Engineering
School of Land Surveying, Geodesy and Mapping Engineering
Technical University of Madrid, Spain
Internship

4/2019 – 5/2019
Department of Forest Management, Geomatics and Forest Economics
Faculty of Forestry
University of Agriculture in Krakow, Poland
Internship

International Conferences

6/2018
Ground classification of UAV image-based point clouds through
different algorithms: open source vs commercial software
Petr Klápště, Rudolf Urban & Vítězslav Moudrý
*In: UAS4Enviro 2018 – 6th International Conference on "Small
Unmanned Aerial Systems for Environmental Research".*
Split, Croatia.

Publications in Journals with Impact Factor ($\mathbf{J}_{imp}$)

Sensitivity analysis of parameters and contrasting performance of ground filtering algorithms with UAV photogrammetry-based and LiDAR point clouds (2020). **Klápště P.**, Fogl M., Barták V., Gdulová K., Urban R. & Moudrý V. *International Journal of Digital Earth*, Taylor & Francis, vol. 13, p. 1672-1694.

Assessment of LiDAR ground filtering algorithms for determining ground surface of non-natural terrain overgrown with forest and steppe vegetation (2020). Moudrý V., **Klápště P.**, Fogl M., Gdulová K., Barták V. & Urban R. *Measurement*, Elsevier, vol. 150.

Comparison of leaf-off and leaf-on combined UAV imagery and airborne LiDAR for assessment of a post-mining site terrain and vegetation structure: Prospects for monitoring hazards and restoration success (2019). Moudrý V., Gdulová K., Fogl M., **Klápště P.**, Urban R., Komárek J., Moudrá L., Štroner M., Barták V. & Solský M. *Applied Geography*, Elsevier, vol. 104, p. 32-41.

Other Publications

Digital elevation models as predictors of yield: Comparison of an UAV and other elevation data sources (2017). Moravec, D., Komárek, J., Kumhálová, J., Kroulík, M., Prošek, J., & **Klápště, P.** *Agronomy Research*, vol. 15, p. 249–255.

Teaching Experience

2015 – present
Department of Spatial Sciences
Lecturer of GIS; Computer Technology Utilization; Unmanned Aerial Systems in Environmental Sciences; Remote Sensing with Unmanned Aerial Systems; Lidar Data Processing